2009

Seasonal variability in absorption and fluorescence properties of chromophoric dissolved organic matter in the Barataria Basin, Louisiana, USA

Shatrughan Singh
Louisiana State University and Agricultural and Mechanical College

SEASONAL VARIABILITY IN ABSORPTION AND FLUORESCENCE PROPERTIES OF CHROMOPHORIC DISSOLVED ORGANIC MATTER IN THE BARATARIA BASIN, LOUISIANA, USA

A Thesis

Submitted to the Graduate Faculty of the
Louisiana State University and
Agricultural and Mechanical College
in partial fulfillment of the
requirements for the degree of
Master of Science

in

The Department of Oceanography and Coastal Sciences

by

Shatrughan Singh
B.Sc., University of Allahabad, 2002
M.Sc. (Tech.), Banaras Hindu University, 2005
December, 2009

Dedication

In loving memory of my father,
Who taught me how to live your dreams by yourself.

Acknowledgements

I would like to gratefully acknowledge my advisor, Dr. Eurico J. D'Sa, for his invaluable support and guidance throughout this study and for help in preparing this manuscript. This work in its present form is due to his valuable comments and suggestions.

I would like to thank my committee members Drs. Nan Walker and John White for their useful comments and suggestions on this manuscript. The ultimate completion of this work is attributed to insightful comments and valuable suggestions from my committee members.

I am greatly indebted to Dr. Eugene Turner, Erick Swenson, Charles Milan, and Gary Peterson for their help with water sample collection from the study area and providing me the opportunity to exploit salinity, temperature, chlorophyll, and total organic carbon data for March, April, May, November, December, 2008, and January, 2009 which was actually processed in their laboratory. Their help with data collection is enormous and is greatly appreciated.

I am grateful to Dr. Colin Stedmon for introducing me to the wonderful world of PARAFAC analyses and his invaluable comments and suggestion during interpretation of my PARAFAC results. Thanks are also extended to Dr. Wade Sheldon for the fluorescence toolbox.

I would like to thank the faculty, staff and graduate students of the Department of Oceanography and Coastal Sciences at Louisiana State University for their contribution towards the success of this thesis.

I would like to thank the Mineral Management Services (MMS) – Coastal Marine Institute (CMI) Cooperative Agreement (M08AX12685) and to a NASA Grant (NNA07CN12A) to Dr. E. D'Sa for financial support to complete this work. Partial support from a Northern Gulf of Mexico Initiative (NGI) – Shell Grant is also acknowledged.

I would also like to thank my friends Mr. Padmanava Dash and Mr. Bibhudutta Panda for frequently reminding me of this awesome journey in my academic career.

It would be unfair if I do not mention the name of my lab mate and friend Ms. Puneeta Naik as she has helped me not only with water sample filtering, but also with analysis of data and with help in MATLAB programming.

At last, I would especially like to thank my mother, Mrs. Sonmati Singh for her constant support of love, motivation and encouragement throughout this study. Thanks are also extended to my family members including my two elder brothers, my two sister-in-laws and two sweet little nieces whom I missed everyday but I am sure this all hard work will go to benefit their future.

Preface

Chapter One is an introduction to chromophoric dissolved organic matter, excitation emission matrices, absorption and fluorescence spectroscopy, parallel factor analysis and description of study area.

Chapter Two deals with the fluorescence properties of chromophoric dissolved organic matter (CDOM) observed in the Barataria Basin, Louisiana, USA for the surface water samples collected in March, 2008 from an axial transect in the Barataria Basin. The use of excitation emission matrices (EEMs) using fluorescence spectroscopy is described here. Also discussed are CDOM properties and variability with physical parameters, such as salinity and temperature.

Chapter Three deals with the seasonal variability in absorption and fluorescence properties of CDOM observed in the Barataria Basin, Louisiana, USA for the surface water samples collected along the Barataria Basin transect during both high and low flow conditions. March, April, and May (2008) represent high flow conditions and November, December (2008), and January (2009) are considered low flow conditions on the basis of streamflow in the Mississippi River during these periods. The excitation emission matrices (EEMs) using fluorescence spectroscopy are employed here to characterize CDOM variability along the Barataria transect with physical parameters, such as salinity and temperature, as well with absorption properties of water samples. Fluorescence and humification indices and fluorescence peak ratios are introduced here to observe seasonal variability of CDOM.

Chapter Four elaborates on use of excitation emission matrices using fluorescence spectroscopy along with parallel factor analysis (PARAFAC). EEMs together with PARAFAC provide the opportunity to quantify the observed variability in different chemical components of CDOM in the study area. Humification Indices have also been used to characterize the CDOM variability in the Barataria Basin.

Chapter Five detailed the general conclusions drawn from these studies and future research implications which could be useful to identify the sources and sinks of dissolved organic matter in the Barataria Basin and should provide useful information for improved management of the drainage basin, especially for water quality and ecological purposes by reducing the negative human impacts.

Table of Contents

List of Tables

List of Figures

Abstract

Absorption and fluorescence measurements of chromophoric dissolved organic matter (CDOM) were examined along a transect containing 36 sampling stations in the Barataria Basin during high and low conditions to observe seasonal variation in these optical properties. The objectives of this study were (i) to observe CDOM variability in Barataria Basin in variable flow (high and low) conditions, and to characterize the CDOM, (ii) to identify the constituents of CDOM and to model CDOM compositional variability in the Barataria Basin using parallel factor analysis (PARAFAC). CDOM–salinity relationships were non-conservative in lower and upper part of the transect; however a conservative inverse relationship in the middle basin suggest that CDOM could be used as an useful indicator of salinity in the middle Barataria Basin. Larger variations in mean CDOM absorption and fluorescence values have been observed during low flow conditions than that during high flow conditions along the same transect. In general, mean CDOM absorption and fluorescence have shown linear inverse relation with salinity (r^2 = 0.5 for high flow; r^2 = 0.6 for low flow) and increased upstream along the stations. Using PARAFAC, four components could be identified in the Barataria Basin. Two humic, one non-humic, and one pedogenic component derived from PARAFAC modeling. These components showed the characteristics of the bulk fluorescence properties with an exception of component 3 (non-humic). Component 3 was found similar to autochthonous production of labile organic matter and was supported by elevated levels of chlorophyll-*a* between stations from 25 to 30. Fluorescence and humification indices along with peak ratios were calculated. In conclusion, CDOM variability in the Barataria Basin was characterized and modeled using the PARAFAC. The results obtained in this study are similar to previously reported results in estuarine environments. This study showed the potential application in characterizing CDOM variability in the Barataria Basin which explained over 99% variability of the water samples consisting of four major constituents. In future studies, water discharges from different water bodies in the Barataria Basin could be traced using CDOM compositional variability observed by EEM-PARAFAC technique.

Chapter 1

General Introduction

1.1. Background

Organic matter is ubiquitous in the environment in various forms, in particular, dissolved and particulate. The colored fraction of the dissolved organic matter (hereafter, DOM) which absorbs light in the ultraviolet (UV) and visible range of electromagnetic radiation is known as chromophoric/colored dissolved organic matter (CDOM). It is sometimes also called yellow substance, gilvin or colored dissolved organic matter (Coble, 2007; Kirk, 1994). The presence of colored dissolved organic matter (CDOM) in a water body yields color ranging from yellow to brown. CDOM represents 30-70 % of total dissolved organic matter in fresh and oceanic environments with higher values in fresh estuarine environments (Coble, 2007). It is important to understand the origin and fate of dissolved organic matter in an environment in order to characterize the sources and sinks of CDOM.

The abundance of dissolved organic matter in estuarine systems could be derived from decomposition of terrestrial plants and microbial activities. Degradation of dead phytoplankton and zooplankton by bacterial activity also contribute to the production of CDOM in natural waters. The production of CDOM could be autochthonous (in situ) or allochthonous (transport) depending on the characteristics of the environment. Transport processes, such as run-off due to precipitation or drainage release in watersheds could carry the dead plants and bacterial biomass from the origin and lead to production of CDOM by chemical alterations facilitated by living micro and macro-organisms moving throughout the extent of a water body (Stedmon et al., 2007). Resuspension of sediment particles is another potential source of CDOM either due to tidal mixing or wind generated in a natural water system (Burdige et al, 2004). Previous literature reviewed human induced anthropogenic effects which greatly influence the natural environment due to land use, drainage, sewage or industrial wastes by causing biogeochemical alterations in CDOM optical properties.

The loss of colored dissolved organic matter could be due to flocculation, photo or biological degradation, and particle adsorption or aggregation. Flocculation could be one important sink for CDOM as larger particles conjugate and could separate out into comparably larger molecules thereby reducing the optical properties associated with CDOM, primarily in low salinity regions where freshwater and saline waters meet. This process is frequent in an estuarine region or coastal waters causing a red shift in CDOM absorption as well fluorescence properties and in turn resulting in variable concentration and conformational change in dissolved organic matter. Particle adsorption is another means of release of CDOM from the water column, by the adsorption of larger molecules on clay materials (pronounced on the Louisiana shelf). It does not contribute much to the optical properties of CDOM along with flocculation, but is significant when estimating the carbon budget in sediments of an estuarine environment (Del Castillo, 2005). The most pronounced process of CDOM removal from the water column in a natural system is photodegradation. This mechanism occurs when the molecules absorb energy in the ultraviolet and visible range of the electromagnetic radiation causing photo-chemical alterations in the colored dissolved organic matter pool and thus its removal from a natural system (Del Vecchio and Blough, 2002). Microbial degradation is another probable sink of CDOM in the water column by bacterial consumption of low molecular weight labile dissolved organic matter produced after photodegradation and then respired as carbon dioxide into the atmosphere (Stedmon and Markager, 2005b).

The organic matter typically occurs in forms of humin, humic acids, and fulvic acids generally originating from dead plant humus and degraded materials in a watershed. These forms can be distinguished on the basis of their solubility in alkali (or bases) and acids. When humus is

treated with an alkali, humin does not dissolve in alkali, but humics separate out as a precipitate and are dissolved in high pH. The subsequent treatment of humics with acids separate out humics as a precipitate and the fulvics remain dissolved in low pH (Fig. 1.1). Humics are comprised of high conjugated molecules and high aromaticity with high molecular weight whereas fulvics are composed of aliphatic contents with low molecular weight. In general, terrestrially derived organic matter and coastal waters are influenced by humics while oceanic waters away from land are dominated by fulvic acids (Reddy and DeLaune, 2008).

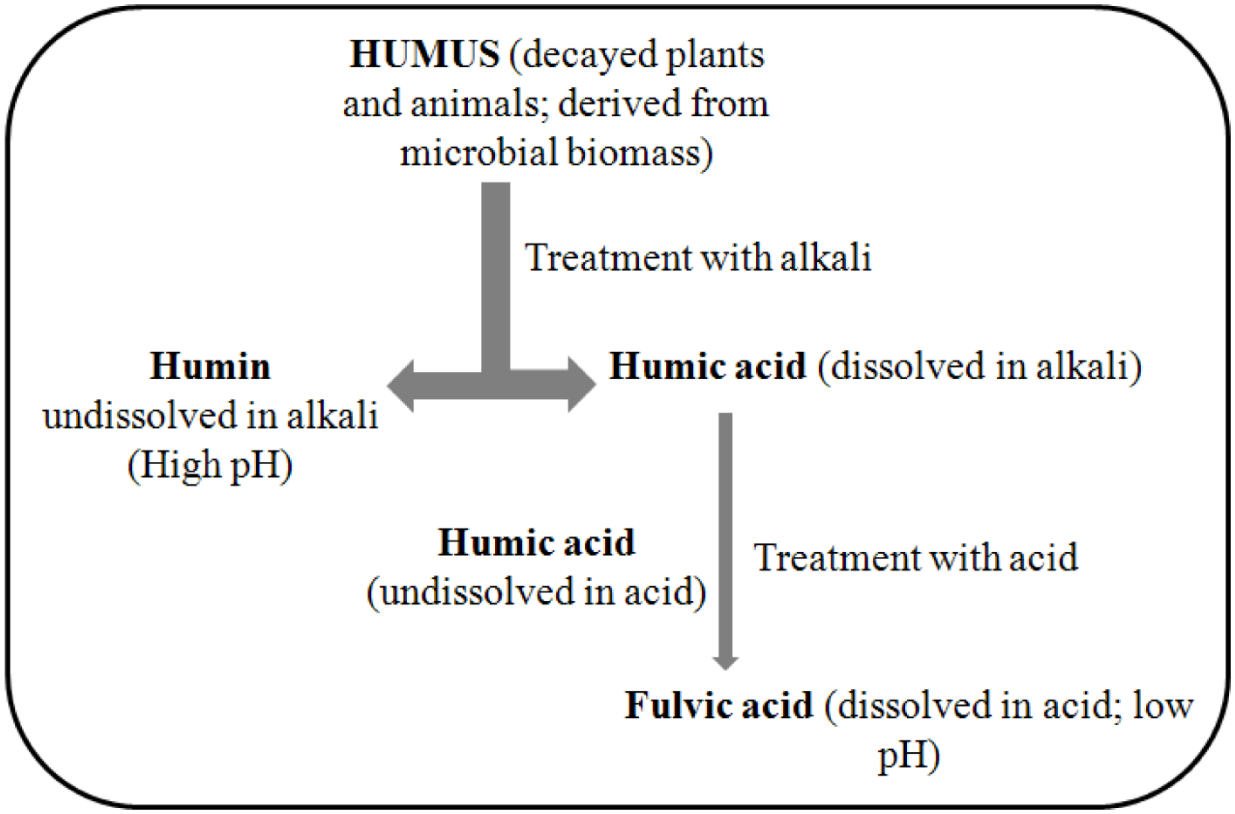

Figure 1.1 Classification of humic materials generally found in estuarine and oceanic environment (Modified from Reddy and DeLaune, 2008).

1.2. Absorption and Fluorescence Spectroscopy

The biogeochemical properties of CDOM can be traced by its optical properties allowing us to use relatively rapid and cheaper absorption and fluorescence properties as a proxy for DOM which can help in qualitative and quantitative estimation of CDOM characteristics in a natural system. The chemical nature of a molecule is responsible for its absorption and fluorescence properties. The aromaticity and conjugate bonds between molecules present in a solution are accountable for absorption of radiation in the UV and visible regions of the electromagnetic spectra. The absorption spectra of CDOM in an estuarine water sample represent the mix of different compounds in that sample. These spectra could be separated into different peaks representing individual chromophores (or fluorophores) using fluorescence spectroscopy.

Absorption spectroscopy aids in quantifying CDOM characteristics in the UV and visible ranges of the electromagnetic spectrum by modeling CDOM absorption curve characterized by an exponential equation (given below) at a wavelength (λ).

$$a\,(\lambda) = a\,(\lambda_0).exp^{\,[S(\lambda_0)-\lambda]}$$

where, λ_0 is a reference wavelength. S is spectral slope calculated to characterize CDOM.

However, the limitation of absorption spectroscopy in distinctly identifying the different fluorophores in given water sample presents an opportunity to use fluorescence spectroscopy to resolve a sample in its constituent fluorophores. Fluorescence spectroscopy by means of excitation emission matrices (EEMs) is used to characterize CDOM in fresh and oceanic environments (Coble et al., 1990, 2007). As CDOM consists of distinct fluorophores, it fluoresces when exposed to UV and visible light at different wavelengths according to the composition of constituent fluorophores. These different components can be traced at their origin either from terrestrially derived organic matter or marine derived organic matter. The origin and fate of anthropogenically derived organic matter can also be monitored using fluorescence technique of excitation emission matrices (EEMs). The EEMs are obtained from a combination of several excitation and emission spectra at different wavelengths. These EEMs can reveal information about the water sample constituents through the analysis of observed peaks corresponding to specific excitation and emission spectra. To interpret the wealth of information carried by EEMs, visual analysis and ratios of different fluorescence regions have been successfully used (e.g., fluorescence index and humification index) in recent years (McKnight et al., 2001; Zsolnay et al., 1999).

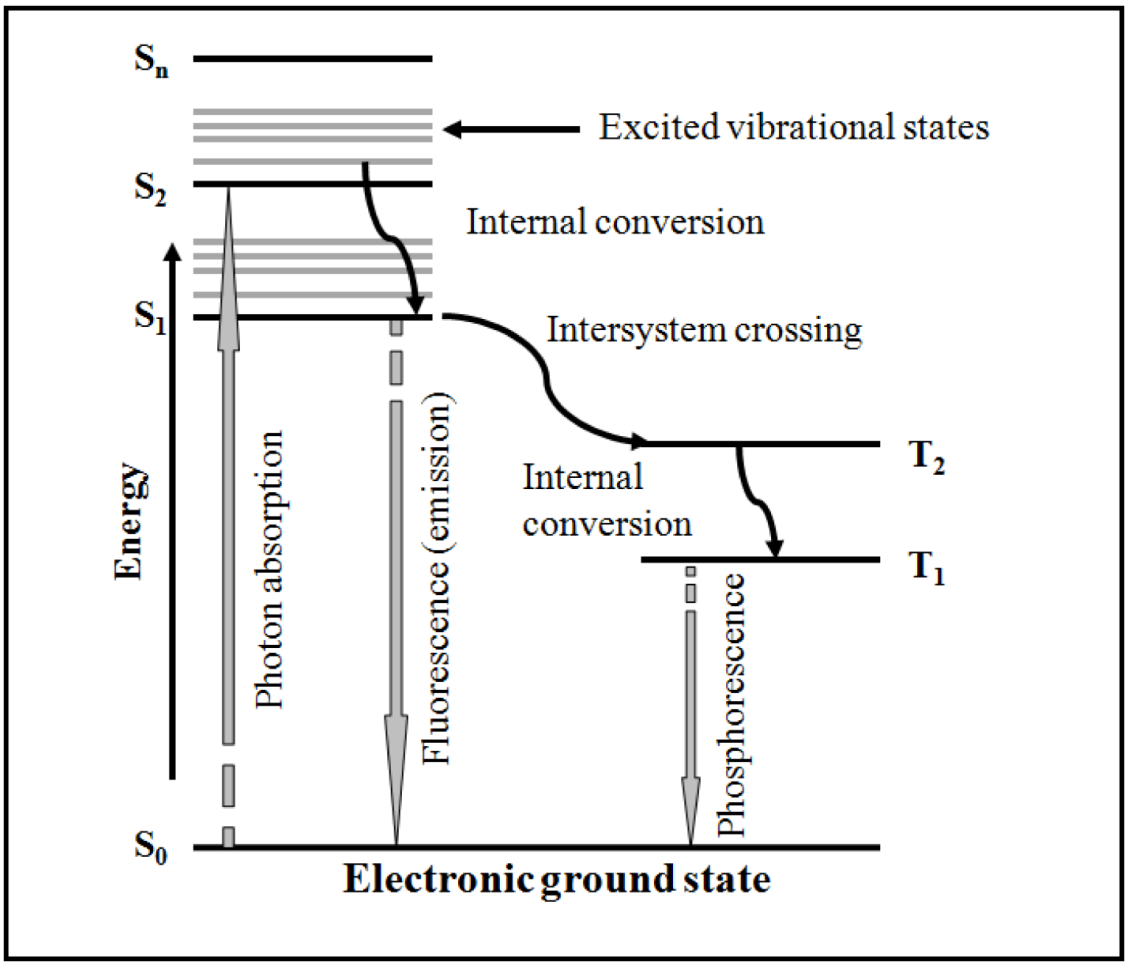

Figure 1.2 Jablonski diagram explaining the mechanism for absorption and fluorescence transition states of a fluorescent molecule (Modified from Lakowicz, 2006).

The basics of absorption and fluorescence spectroscopy are well defined using Jablonski diagram (Fig. 1.2). The light absorbed and emitted fluorescence due to a fluorescing molecule (or fluorophore) results in a change of state from ground level to excited levels and vice versa. When a fluorophore is irradiated with photon energy, it is excited to move from its ground state to upper excited energy level in a singlet state and return back to ground level while releasing the energy in the form of emission intensity (fluorescence) in a very short duration or an order of 10^{-15} to 10^{-8} s. Phosphorescence is a phenomena that occurs similarly to fluorescence but with a longer duration (10^{-4} to 10^{2} s) and during transition from triplet excited state to ground energy level (Lakowicz, 2006).

1.3. PARAFAC Analysis

The advent of parallel factor analysis (PARAFAC), a statistical tool, helped in effectively modeling the EEMs and in quantifying the concentration of individual components. The change in compositional variability in a water sample can be precisely quantified using PARAFAC in conjunction with EEMs. PARAFAC also aided in identifying the pedogenic (soil derived) humic component in this study which is an important budget of the DOM pool in study area. This thesis continues the use of PARAFAC technique along with EEMs for characterizing and monitoring CDOM sources and sinks in the Barataria Basin (Stedmon et al., 2003, 2008).

1.4. Study Area

Barataria Basin is a complex estuarine system enclosed by the Mississippi River in the north and east, Bayou Lafourche in the west and the Gulf of Mexico in the south (Fig. 1.3). It was deprived of its natural sediment and nutrient supply directly from the Mississippi River run off since the levee construction since 1930s (Madden et al., 1988; Mossa, 1996). Due to adverse impact of the river levee placement, the abandoned basin was later reconnected to the Mississippi River through a fresh water diversion called the Davis Pond Diversion. A few siphons (West Pointe a la Hache, Port Sulphur, and Naomi) were also constructed to release freshwater from the Mississippi River to the wetland. Swamps, freshwater, brackish, and marshes characterize this estuarine environment. Freshwater flow from the top of the basin to where it mixes with the Gulf of Mexico thereby producing physical, chemical, and biological gradients in the basin. Freshwater flow originating from runoffs due to precipitation, drainage, sewage, human activities (such as, agriculture and urban development), and industrial wastes affects the water quality of the lakes, ponds, and bayous of the basin system. Flow from freshwater point and non point sources control the biogeochemistry of this estuary in terms of organic and inorganic carbon release as well nutrient supply to the basin by changing the physicochemical properties of the constituents. The freshwater discharge regulates the changes in distribution of salinity in the wetland along with physical forcing, such as wind driven, tidal mixing and slope of land from swamps to the Gulf of Mexico. Several studies have been done in the past to qualitatively and quantitatively analyze the salinity variation with changes in nutrient supply and carbon budget (Castro et al., 2003; Happ et al., 1977).

1.5. Objectives

This study focuses on the use of recent techniques of fluorescence spectroscopy and PARAFAC for the characterization of CDOM, an indicator of water quality, in the Barataria Basin. Although

attempts have been made to quantify carbon transport through the basin to the Gulf of Mexico (Castro et al., 2003; Das et al., 2009; Feijtel et al., 1985; Happ et al., 1977), this study will provide a new approach using fluorescence spectroscopy derived EEMs and PARAFAC to analyze the organic fraction of dissolved carbon transport to the Gulf of Mexico and to quantify changes in its composition along the way through the basin.

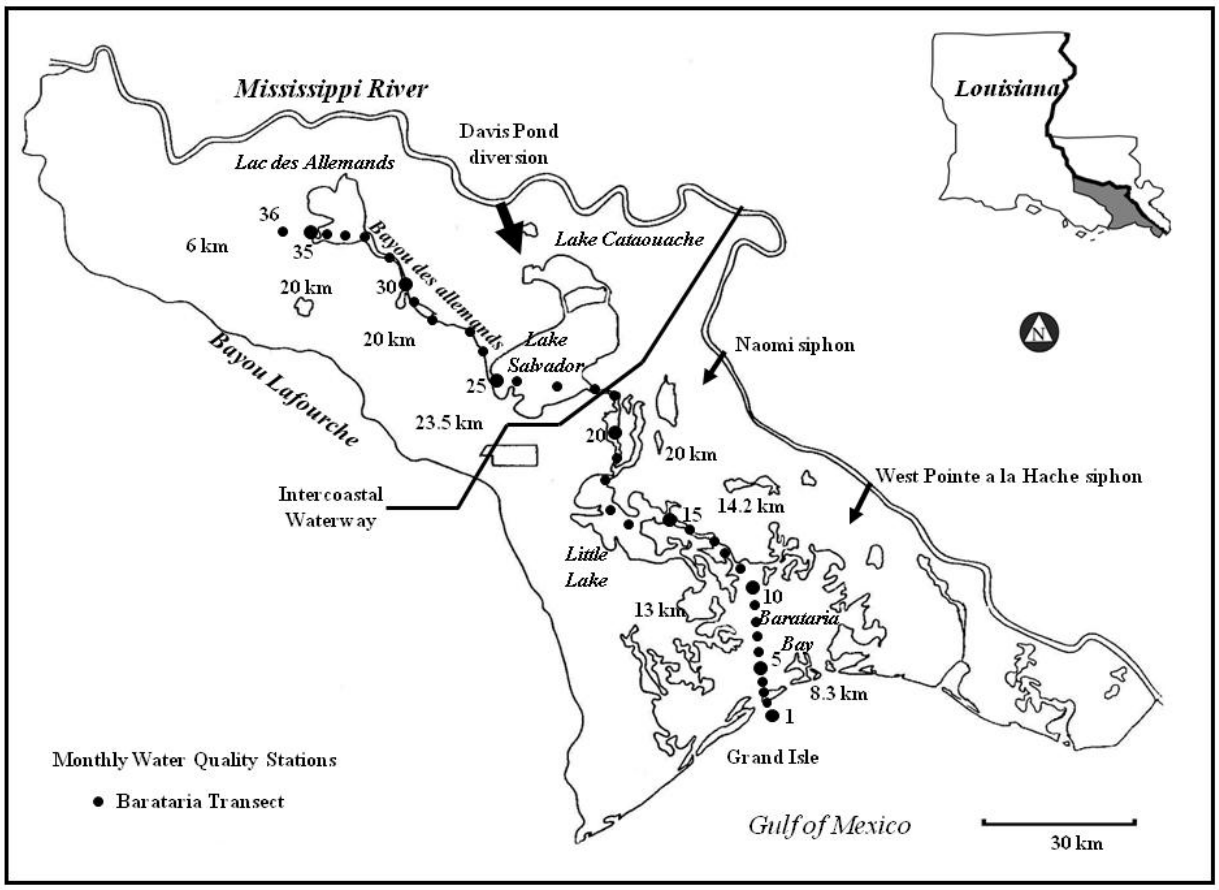

Figure 1.3 Location of Barataria Basin in Louisiana, USA near the Gulf of Mexico. Sampling stations are plotted with annotations at every five station along a 124 km axial transect. Distances between annotated stations are given in kms.

Chapter 2

Fluorescence Properties of Chromophoric Dissolved Organic Matter (CDOM) Along a Transect in the Barataria Basin, Louisiana, USA

2.1. Introduction

Chromophoric dissolved organic matter (CDOM) is defined as the light absorbing component of total dissolved organic matter (DOM) that absorbs light in the ultraviolet and visible range of the electromagnetic spectrum. It is also known as gelbstoff, gilvin, and yellow substance. (Coble, 1996, 2007; Del Vecchio and Blough, 2004; Zhang et al., 2007). CDOM together as humic and fulvic acids, represents 70% of the total dissolved organic material which contribute to light absorption and fluorescence by non-chlorophyllous material in coastal region (Nieke et al., 1997). Changes in the CDOM absorption and fluorescence can reflect the variations in CDOM composition from several autochthonous or allochthonous sources resulting from physical, biological, and chemical processes that occur in the water column (Coble, 1996; Del Castillo et al., 1999, Del Castillo and Coble, 2000; Stedmon et al., 2007). CDOM measurements are based on the intensity of absorption of light or fluorescence emission as a function of wavelength. CDOM shows a featureless absorption spectrum that increases exponentially from the visible to UV wavelengths (Del Vecchio and Blough, 2006). Spectral measurements of CDOM absorption and fluorescence provides useful information of CDOM sources and have been used to study water-mass mixing in bays (Chen et al., 2007; D'Sa et al., 1999; Rochelle-Newall and Fisher, 2002), estuaries (Boyd and Osburn, 2004; Hong et al., 2005; Nieke et al., 1997; Uher et al., 2001), rivers (Del Castillo et al., 1999), coastal waters (D'Sa and Miller, 2003; D'Sa et al., 2006; D'Sa, 2008; Ferrari and Dowell., 1998) and oceans (Coble et al., 1998; Kowalczuk et al., 2005) as CDOM serves as a tracer to examine transport and mixing processes.

Hoge et al. (1993) presented a linear relationship between CDOM absorption and fluorescence in a coastal region, whereas Green and Blough (1994) reported an exponential relationship between CDOM absorption and wavelength. These studies suggest a way to retrieve CDOM absorption coefficients from fluorescence measurements at a single excitation wavelength and were used by Nieke et al. (1997) to examine an estuarine region. Fluorescence spectroscopy using EEMs has been widely used to characterize CDOM in various water masses (Coble et al., 1990, 1996, 1998; Del Castillo et al., 1999; Del Castillo and Coble, 2000). The EEMs were acquired by using successive excitation wavelengths to obtain emission spectra. The excitation-emission spectra were then used to generate plots of fluorescence as a function of excitation-emission wavelengths, to differentiate between classes of fluorophores, changes in CDOM composition resulting from biogeochemical processes, and to trace different sources of CDOM. Further, EEM fluorescence spectroscopy was used to investigate natural waters in oceans and dynamic estuarine environments and to identify natural organic matter (Coble, 1996, 1998; McKnight et al., 2001). In order to determine the origin of CDOM, fluorescence maximum localization was used to obtain a qualitative information for some ubiquitous peaks such as A, C, M, B, and T (used in this study) referenced on their excitation-emission range (Coble, 1996), while similar peaks were defined with different notation as α', α, β, γ, and δ, to represent a number of different fluorescent components in a mix of total fluorescence (Parlanti et al., 2000) (Table 2.1). McKnight (2001) suggested use of an index, the Fluorescence Index, obtained from the ratio of fluorescence emission maximum at 470 and 520 nm excited at 370 nm, to trace the sources of dissolved organic matter.

Two primary fluorescing groups in dissolved organic matter studies have been identified as humic-like and protein-like substances. Humics are complex mixtures of aromatic and aliphatic compounds derived from decay of organic matter while protein-like substances are due to high biological activity. Humic substances are further characterized by humic acids and fulvic acids mainly differentiated on the basis of their solubility (Harvey et al., 1985). Humic acids are

dominated by aromatic compounds whereas fulvic acids are characterized by the dominance of aliphatic content. The A, C, and M peaks as defined by Coble (1996) are humic peaks and T peak is protein-like peak primarily representing the tryptophan-like component in the dissolved organic matter (Table 2.1). The EEMs have been used to trace photochemical and microbial reactions with organic matter (Del Vecchio and Blough, 2002; Stedmon and Markager, 2005b), as well as in water source categorization and correlation with water quality parameters (Holbrook et al., 2006). They have recently been applied to characterize CDOM in lakes (Zhang et al., 2007), estuaries (Hong et al., 2005; Uher et al., 2001), rivers (Baker et al., 2004; Clark et al., 2002), bays (Clark et al., 2002), waste water (Baker et al., 2004), and tidal marshes (Clark et al., 2008; Tzortziou et al., 2007, 2008).

Table 2.1 Previously defined fluorescence peak locations at excitation wavelength and maximum fluorescence emission intensity.

Fluorescence Peaks	Excitation (nm)	Emission (nm)	Coble's Designation (1996)	Parlanti's Designation (2000)
UV-C Humic like	260 (250 - 260)	380 - 460 (380 - 480)	A-peak	α'
UV-A Humic like	350 (330 - 350)	420 - 480 (420 - 480)	C-peak	α
Marine Humic like	312 (310 - 320)	380 - 420 (380 - 420)	M-peak	β
Tryptophan like, Protein like (or Phenol like)	275 (270 - 280)	340 (320 - 350)	T-peak	δ

[*] Values in brackets are denoted by Parlanti et al., (2000).

The Barataria Basin is a complex, well-mixed, and turbid water system characterized by high input of fresh water from different water bodies such as large lakes, bayous, streams and man-made river diversions. The Barataria Basin is located in southeast Louisiana, east of Bayou Lafourche and west of the Mississippi River delta and is separated from the Gulf of Mexico by the Grande Terre Islands (Fig. 1.3). Swamp forests and marshes characterize the Barataria Basin which has been isolated from the Mississippi River due to levee construction since the 1930s (Mossa, 1996). It has since been reconnected to the Mississippi River by the Davis Pond Diversion initiated in 2002. Previous studies of naturally occurring wetlands in the Barataria Basin have shown the impacts of modifications by artificial diversions (Swenson et al., 2006), discharge from Mississippi river (Wissel et al., 2005) and canal dredging (Sasser et al., 1986) which is altering the natural habitat (Craig et al., 1989; Jones et al., 2002) as well as water quality (Conner and Day Jr., 1987; Happ et al., 1977; Wissel et al., 2005) of the region. Few studies have addressed carbon and nitrogen flow in the Barataria Basin into the Gulf of Mexico (Castro et al., 2003; Feijtel et al., 1985; Happ et al., 1977). The objectives of the present study are to characterize the optical properties of CDOM in the Barataria Basin using field data collected during a period of high flow and to examine likely influences from different water sources (i.e., lakes and local runoff). To our knowledge, this is the first detailed study on the spatial variability of CDOM, and its spectrochemical characteristics. We have reported here the spatial variation of CDOM in the Barataria Basin, the causative factors for the observed distributions and the possible sources of CDOM.

2.2. Methods

2.2.1. Study Area

The Barataria Basin system is made up of biologically rich and productive habitats including swamps, fresh, brackish/intermediate, and saline marshes, bayous, bays, and barrier islands. Barataria Basin is an irregular shaped basin covering 1,673 km^2 surface area and 5,700 km^2 of drainage area with an average depth of two meter (Fig. 1.3). The average daily fresh water inflow into the basin is approximately 156 $m^3 s^{-1}$ with an average salinity of 13 psu. On the basis of climatological salinity mean values in different parts of the Barataria Basin which are covered by variable marsh types, it can be divided into three main regions: the upper basin (Station 24 to 36) mainly dominated by fresh marshes and mean salinity < 2 psu, the middle basin (Station 23 to 5) mainly dominated by brackish/intermediate marshes and a salinity range of 2 – 10 psu, and the lower basin (Station 4 to 1) lying in the saline marsh regions of the Barataria Basin with salinity range from 6 – 22 near the Gulf of Mexico (Conner and Day Jr., 1987). The main freshwater sources for the middle basin include rainfall, local run-off, and the Intracoastal Waterway that delivers water from the Atchafalaya River during high flow conditions to the Mississippi River. The Davis Pond Diversion, Port Sulphur, Naomi and West Pointe A la Hache siphons, numerous major and minor point discharges, septic tanks, sewage/storm water overflow, unsewered communities, drainage from pasturelands, and marshes all contribute to changes in water quality of the basin (Conner and Day Jr., 1987). The designed pumping rate for the Davis Pond Diversion is 300 $m^3 s^{-1}$ along with maximum pumping rates of 60 $m^3 s^{-1}$ for each Naomi and West Pointe A la Hache siphons, respectively. Although the salinity signals are highly coherent with Mississippi River discharge, these point sources can significantly contribute to a decrease in the average salinity of the basin region as reported in previous literature (Inoue et al., 2008; Swenson et al., 2006). The period of high river flow in spring, and high water residence time, typically 12 to 35 days (Wissel et al., 2005) could account for the variable CDOM concentrations in the study area.

2.2.2. Collection of Water Samples

The sampling for surface water was conducted at 36 stations (Fig. 1.3) along a 124 km transect which ran from South-East (SE) to North-West (NW) from the mouth of the basin (station 1) in the Gulf of Mexico to the north-west end of the upper basin (station 36) during a field trip taken on March 20, 2008. The surface water samples were brought back to the laboratory and immediately filtered using pre-rinsed 0.2 micron nucleopore membrane filters. The filtered samples were kept in a refrigerator for optical absorption and fluorescence analyses. The tap water was treated with a Barnstead Nanopure® Model D-50280 purification system. Temperature and salinity measurements were recorded in the field using a handheld YSI. Spatial pattern of surface salinity, temperature, CDOM absorption (measured at 355 nm and 412 nm), and CDOM fluorescence (measured as maximum emission fluorescence intensity obtained at excitation wavelength, λ_{ex} = 355 nm) are presented and discussed. Spectral slope, S was calculated in the range 350 to 500 nm. The Fluorescence Index (FI) was calculated as a ratio of maximum emission fluorescence intensities at 470 and 520 nm, with excitation at 370 nm (Tzortziou et al., 2008). The FI can be used to distinguish sources of dissolved organic matter containing humic substances in an aquatic environment (McKnight et al., 2001). FI values for

terrestrial originated humics (FI < 1.4) and marine originated materials (FI > 1.9) were suggested in McKnight's study.

2.2.3. Absorption Spectroscopy

The surface water samples were allowed to reach room temperature and the instrument was kept on for 30 minutes (to stabilize) before the samples were analyzed. Absorption spectra were obtained between 190 and 750 nm at 2-nm intervals using a Perkin Elmer Lambda 850 double-beam spectrophotometer equipped with a 1 cm path-length quartz cuvette (volume of 4 ml) and 150 mm spectralon coated integrating sphere. The data were corrected for scattering and baseline fluctuations by subtracting the average value of absorption between 700 and 750 nm from each spectrum (Green and Blough, 1994).The absorption coefficients (a) were calculated from the absorbances (A) obtained from the spectrophotometer using:

$$a(\lambda) = 2.303 \times \frac{A(\lambda)}{l}$$

where $A(\lambda)$ is the absorbance at a wavelength, λ, calculated as (Log (I_0/I), I is the intensity, and l is the path-length in meters. Spectral slope coefficients (S, nm^{-1}) were calculated by employing a non-linear least square regression of the plot $a(\lambda)$ versus wavelength over the range 350 to 500 nm using the equation of Markager and Vincent (2000).

$$a(\lambda) = a(\lambda_0)\exp[-S(\lambda - \lambda_0)]$$

where λ_0, the reference wavelength was set to 412 nm. Similar to other studies, the range from 350 to 500 nm for the calculation of S was selected with a limit at 500 nm as the values were close to zero. In this study, a_{CDOM} at 355 nm was selected to study the variability in absorption coefficients, their correlations with salinity and CDOM fluorescence in order to compare the results with previously reported studies (discussed later).

2.2.4. Fluorescence Spectroscopy

Surface water samples were treated in a similar manner as those from absorption measurements along an axial transect from the Barataria Basin. Samples having absorbance greater than 0.02 at 350 nm (A_{350} > 0.02) were diluted with particle free Nanopure Milli-Q water (also used as a blank) to account for the inner filter effects. Excitation Emission matrices (EEM) were generated using a Horiba Jobin Yvon Fluoromax-4 spectrofluorometer equipped with a 50 W ozone-free Xe arc lamp and a R928P photomultiplier tube as a detector. The spectroflurometer was set to collect the signal in ratio mode with dark offsets using a 5 nm bandpass on the excitation as well as emission monochromators. Factory supplied correction factors were applied to the scans to correct for instrument configuration. The EEM spectra were recorded for excitation spectra from 250 to 500 nm at every 5 nm intervals (Kowalczuk et al., 2005; Zepp et al., 2004) while the emission spectra ranged between 280 – 600 nm, with data saved for every 5 nm over an integration time of 0.1s. Milli-Q water blank EEM's were subtracted from the sample EEM's to eliminate Raman peaks and then EEM's were normalized to daily-determined water Raman integrated area maximum fluorescence intensity (350 ex/397 em, 5 nm bandpass) (Colin Stedmon, Pers. Comm.). Finally, the EEM's were multiplied with dilution factor derived from the fluorescence intensity at Ex/Em = 350/397 nm of water Raman scan to obtain the intensity for the original, undiluted sample (Coble et al., 1998). The fluorescence intensities measured were reported in Raman Units (RU) in this study. A 5% agreement was noted between replicate

scans in terms of intensity and within bandpass resolution in terms of peak location using Milli-Q water scans. Post processing and plotting of EEMs were done using FLToolbox (ver. 2.10b; February, 2007) developed by Wade Sheldon (University of Georgia) for MATLAB® (Zepp et al., 2004). FLToolbox allowed the quantification of the three-dimensional surface integration of EEMs over individual chromophore regions as well as integration of the total emission over the entire corrected fluorescence matrix using integration option (Zepp et al., 2004). The respective peaks, i.e., peaks A, C, M, and T could be seen by their integrated area shown by circles or ellipses centered over the maximum emission fluorescence intensity of that peak (later in Figs. 2.2 and 2.3). EEM spectra of the whole scan is also calculated for the integration area using the excitation ranges of 250-500 nm and emission ranges of 280-600 nm. Contribution by each peak to the total scanned integrated area is calculated as a ratio of a peak integration area divided by the summation of each peak contribution in order to estimate the percentage involvement of each chromophore to the total measured integrated area of the sample or total fluorescence intensity contributed by each chromophore of the sample (Kowalczuk et al., 2009).

2.3. Results

2.3.1. Spatial Distribution of Salinity, Temperature, a_{CDOM}, and F_{CDOM}

Figure 2.1 shows the variation of salinity, temperature, the absorption coefficient of CDOM at 355 nm and 412 nm, and the CDOM fluorescence excited at 355 nm and 412 nm and maximum fluorescence intensity emitted, along the axial transect of the Barataria Basin. The upper basin is characterized by low surface salinity gradient, with values ranging from 0.2 (station 24) to 0.1 (station 36) (Fig. 2.1a). Significant mixing between freshwater from the Mississippi River through the Davis Pond Diversion, the Gulf Intracoastal Waterway, and resident water in Lake Salvador is occurring, while in relatively stagnant water in Lake Des Allemands, the sources of fresh water are mostly from drainage and sewage. In between, there are connecting bayous to carry the fresh water through this transect. Temperatures decreased from 22 to 18°C from station 36 to station 24 along the axial transect (Fig. 2.1b). Stations 23 to 5 correspond to the middle basin and were characterized by higher salinity gradients. Salinity varied from 0.3 (station 23) to 11.4 (station 5), where fairly constant temperatures from 18.5 (station 23) to 17.3°C (station 5) have been recorded. In the lower basin region (station 4 to station 1), temperature varied from 18 (station 1) to 14°C (station 4), whereas salinity remained fairly constant at 15 with an exception at station 2 where it decreased to 13.6.

The distribution of CDOM absorption coefficient, $a_{CDOM,}$ at 355 and 412 nm along the transect is shown in Fig. 2.1c. CDOM absorption at 355 nm and 412 nm showed similar variation at all the stations along the transect. However, at 355 nm the observed CDOM absorption was higher as compared to 412 nm due to the exponential decrease of CDOM with increasing wavelength (Green and Blough, 1994). A seven-fold increase has been observed in a_{CDOM} at 355 nm along the transect from station 1 (3.56 m^{-1}) to station 36 (21.93 m^{-1}). The lower basin showed little variation in a_{CDOM} (355) with an increasing trend from station 1 (3.56 m^{-1}) to station 4 (4.16 m^{-1}); however a decrease at station 4 was seen as compared to station 2 (5.09 m^{-1}) and 3 (5.05 m^{-1}) that could be attributed to the possible tidal mixing in this region of the basin. The middle basin showed almost a two-fold increase in a_{CDOM} (355) from station 5 (5.86 m^{-1}) to station 23 (10.76 m^{-1}). Some exceptions were seen to the general increasing trend notably near the transition from the middle basin to the upper basin wherein a decrease (stations 20, 21, and 22) was followed by a rapid increase (stations 23 and 24) in a_{CDOM} (355). This shift could be

attributed to the fresh water input from Bayou Des Allemands which connects the Lake Des Allemands in south and at the northern part of Lake Salvador. The variation of a_{CDOM} (355) in the upper basin is characterized by a 1.5-fold increase from station 24 (14.19 m^{-1}) to station 36 (21.93 m^{-1}). A large number of exceptions to the increasing trend were seen in the upper basin as it is characterized by complex nature of sources (autochthonous production, sewage and agricultural discharge) or sinks (photodegradation and microbial activity) and the same may be reflected by a_{CDOM} (355).

The CDOM fluorescence, F_{CDOM}, increased along the transect with inflection points at a few stations likely representing point sources or sinks of CDOM. The F_{CDOM} measured at 355 nm was higher as compared to 412 nm with a trend similar to that observed for a_{CDOM}. For spatial distribution, F_{CDOM} (355) is described here in detail as similar trends have been observed for 412 nm (Fig. 2.1d). F_{CDOM} (355) increased by almost nine folds with station 1 showing 0.21 R.U. to 1.68 R.U. at station 36. The largest increase was seen in the middle basin with station 5 showing 0.35 R.U. to 0.72 R.U. at station 23. Generally F_{CDOM} (355) increased from station 1 to station 4 in lower basin, except at station 2 where F_{CDOM} (355) was higher compared to all the other stations in lower basin. This corresponds to the large decrease in salinity at station 2 (discussed later). In the middle basin, this increasing trend of F_{CDOM} (355) was seen to a lesser extent with many exceptions indicating potential sources and sinks of CDOM. A large shift in F_{CDOM} (355) was seen at the transition between the middle and upper basin; station 23 (0.72 R.U.) to station 24 (1.03 R.U.) that was also observed in a_{CDOM} (355). The general increasing trend of F_{CDOM} (355) was observed in the upper basin from station 24 (1.03 R.U.) to station 36 (1.68 R.U.). Similar to that observed in a_{CDOM} (355), a large number of exceptions to the increasing trend were also seen in F_{CDOM} (355) in the upper basin (Fig. 2.1d). These distributions of a_{CDOM} (355) and F_{CDOM} (355) in the transect indicate that measurements of CDOM absorption and fluorescence generally complement each other, however marked differences were observed at some stations, especially in the upper basin. From station 34 onwards, a_{CDOM} (355) decreased whereas F_{CDOM} (355) increased greatly. This contrasting observation shows that some deviation can occur between F_{CDOM} and a_{CDOM} measurements at higher CDOM concentrations could be due to inner filter effects (Green and Blough, 1994). Although these samples were diluted to the limit to remove inner filter effects, but there lie a possibility of remained inner filter effects in samples at these locations.

2.3.2. Quantitative Distribution of CDOM Fluorescence and Absorption

EEM spectroscopy was utilized to classify the constituent fluorophores present along the transect stations of the Barataria basin. The EEM spectra at station 1 (near the mouth of the basin) and station 36 (at the end of the transect) are shown in Fig. 2.2, that characterizes the end members of the transect. The high salinity member (station 1) shows a prominent ‘T’ peak (tryptophan-like or protein-like), while the low salinity member (station 36) shows a prominent ‘A’ peak (humic-like). The ‘A’ peak represents the humic substances excited at lower wavelengths, $\lambda_{ex} \leq 250$ nm and emitted at longer wavelengths, λ_{em} = 420-480 nm (Coble, 1996). CDOM fluorescence increases for humic substances in land water due to high terrestrial inputs with few exceptions in our study. Stations 9, 14, 20, and 28 were chosen as they deviated from the general increasing trend (Fig. 2.3).

The marine originated material is characterized at station 1 by the dominance of ‘T’ and ‘M’ peaks, whereas the terrestrially originated humic materials of CDOM is predominant at station 36 by the representation of ‘A’ and ‘C’ (humic like and terrestrial fulvic substances) peaks

influenced by the nearby freshwater source such as Bayou Chevreuil (Fig. 1.3). The broader peak 'A' at all stations along the transect indicates higher terrigeneous sources of CDOM in this region. The 'M' peak is more prominent than the 'C' peak that could be attributed to anthropogenic inputs from wastewater and agricultural runoff (Coble, 2007) or to resuspension in coastal sediments (Komada et al., 2002).

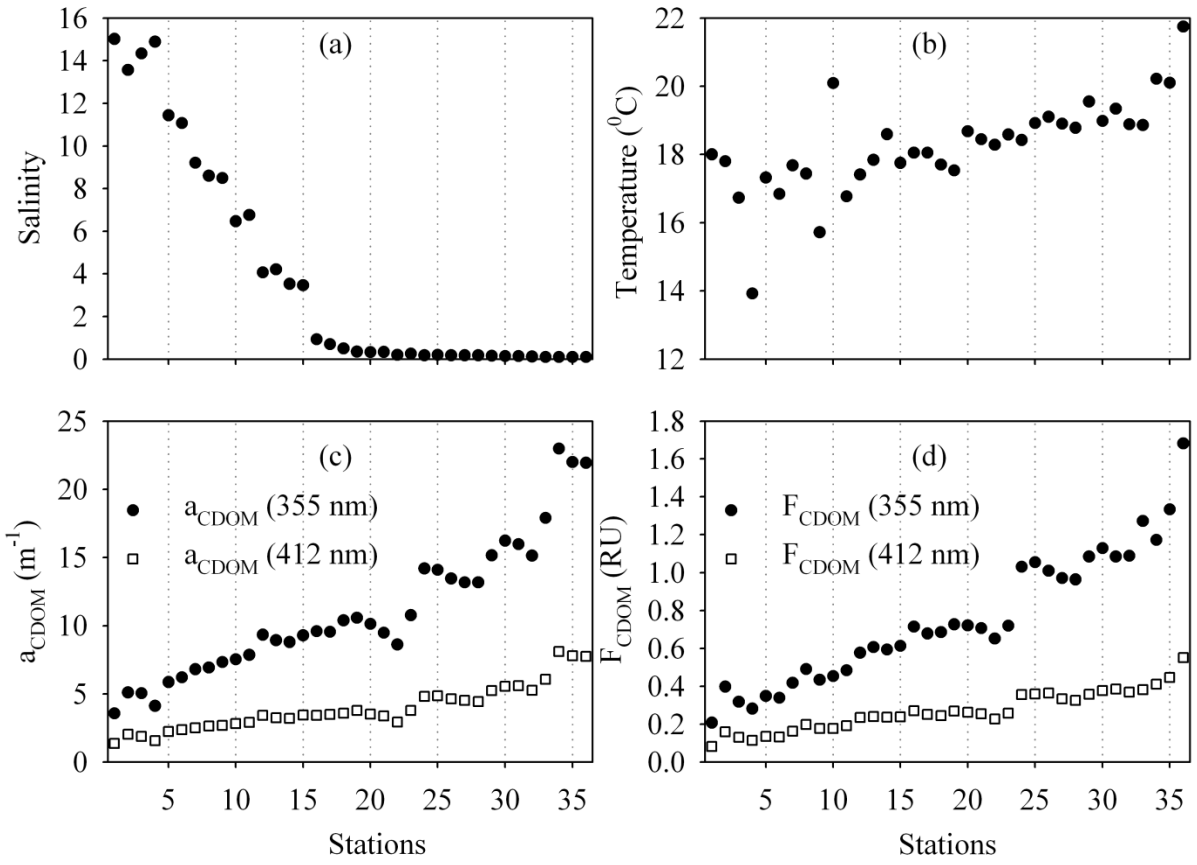

Figure 2.1 Distribution of (a) salinity, (b) temperature, (c) absorption coefficient of CDOM at 355 and 412 nm, and (d) CDOM fluorescence at 355 and 412 nm along the axial transect.

The integration of peak areas of EEM spectra provide a way to calculate the percent contribution of each peak that is used to quantify and characterize CDOM along the transect (Kowalczuk et al., 2005). The ratios of each peak to total EEM intensity (calculated by summation of A, C, M, and T peak at each station) in percent obtained from integrated area scans at station 1 were: A/Total = 48%, C/Total = 18.86%, M/Total = 21.98% and T/Total = 11.15%. In contrast, these peak ratios at station 36 were as follows: A/Total = 50.59%, C/Total = 21.39%, M/Total = 23.59% and T/Total = 4.42%. The variation in percent contribution of 'A', 'C', and 'M' peaks are little as compared to variation of percent contribution of 'T' peak along the transect as shown in Table 2.2. The 'T' peak contribution at station 1 is almost three times of the contribution of 'T' peak at station 36.

The absorption coefficients and the logarithm of absorption coefficient as a function of wavelength are presented in Fig. 2.4. The absorption plot shows the exponential decrease of CDOM absorption with increase in wavelength, while the spectral slope calculated over the 350 – 500 nm range indicate station 2 with lowest spectral slope (0.0153 nm^{-1}) and significantly higher slope at station 24 (0.0196 nm^{-1}). The average spectral slope variation in the lower basin,

middle basin, and upper basin were 0.0159 ± 0.0005 nm^{-1}, 0.0178 ± 0.0010 nm^{-1}, and 0.0190 ± 0.0003 nm^{-1}, respectively. With reduced tidal influences and greater residence time in the middle and upper basins, the greater spectral slopes in these waters suggest potential effects of photobleaching. The observed variation of CDOM absorption spectra in different regions of the basin suggests CDOM sources or loss of CDOM by mixing, tidal influence, freshwater discharge from various streams and basins that influence CDOM concentration and composition along the transect.

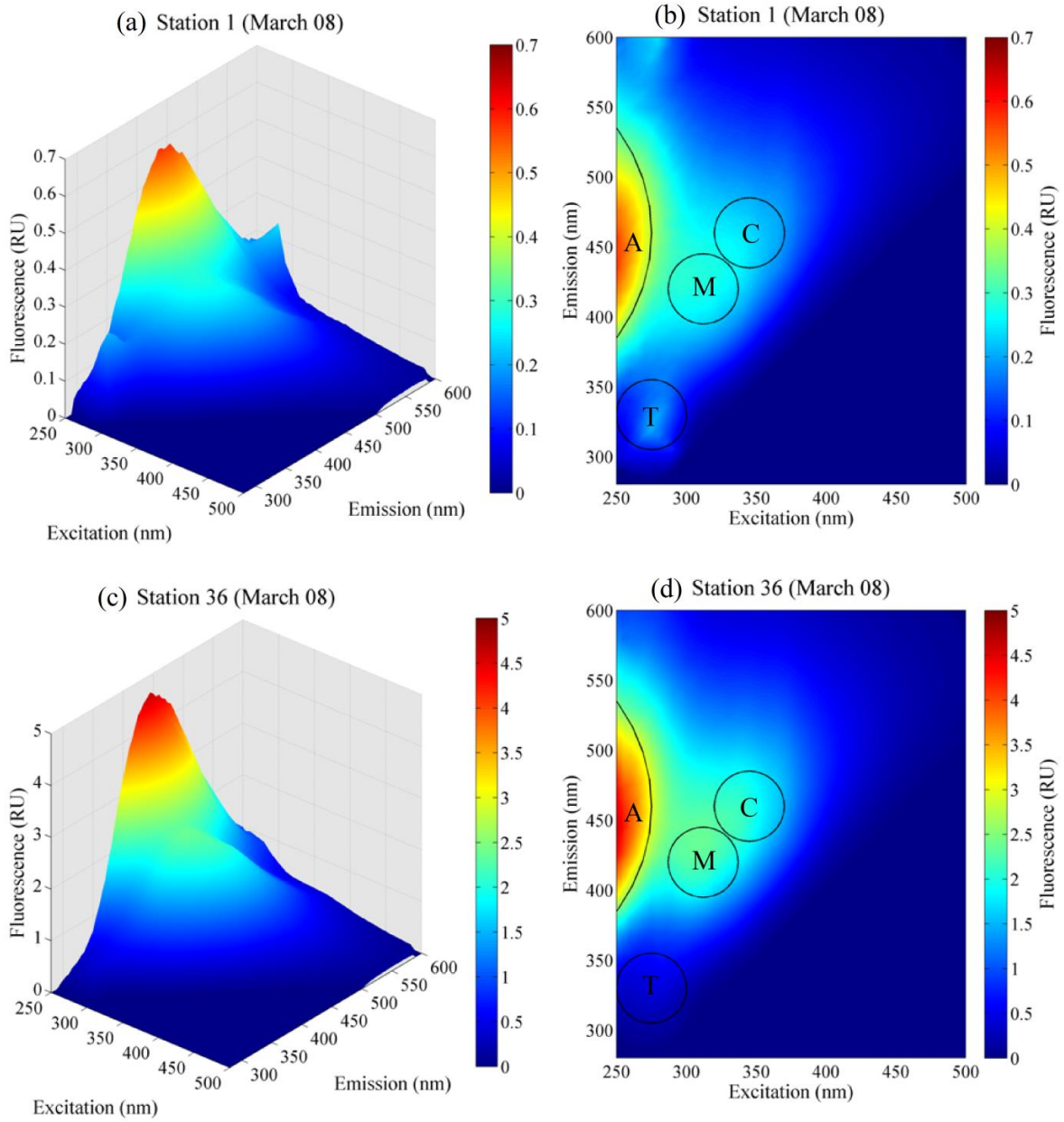

Figure 2.2 (a). 3D-EEM spectra of station 1 (b) Contour plot of EEM spectra of station 1 represents high salinity end member of the Barataria Basin transect (c) 3D-EEM spectra of station 36 (d) Contour plot of EEM spectra of station 36 represents low salinity end member of Barataria Basin transect. The A, C, M, and T peaks are fluorescence peaks according to Coble (1996). The integration cross-section area is shown by circles at peak maxima (note the scale change).

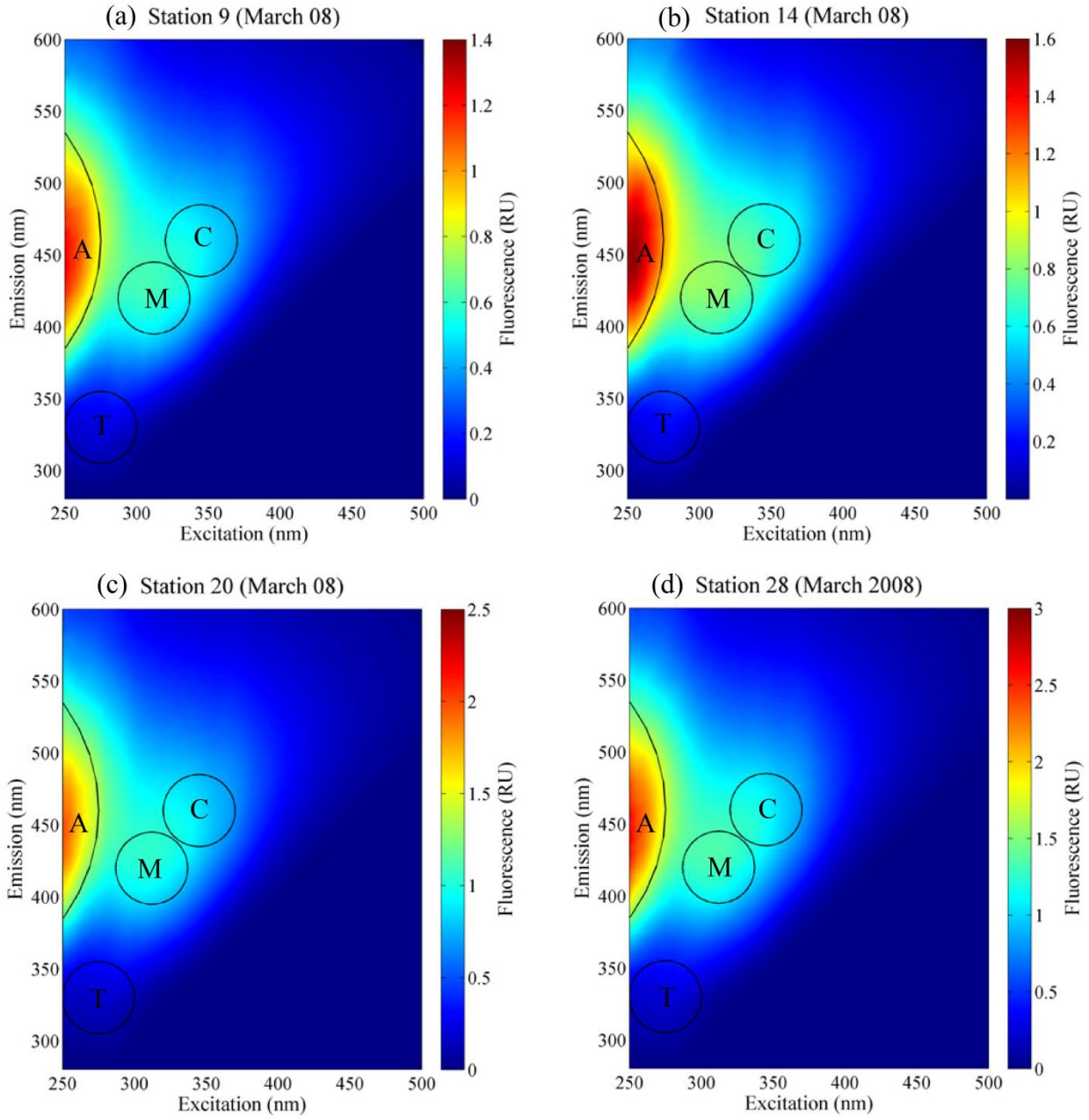

Figure 2.3 Contour plots of EEM spectra of (a) station 9 (b) station 14 (c) station 20, and (d) station 28 of the Barataria Basin transect. The labeled peaks are fluorescence peaks in accordance with Coble (1996) and the circles represent integrated cross-section area at peak maxima (note the scale change).

Table 2.2 Variation in percentage of distinctive peak ratios to the total integrated scanned area along the transect.

Station Name	A/TOT (%)	C/TOT (%)	M/TOT (%)	T/TOT (%)
Station 1	48.00	18.86	21.98	11.15
Station 2	49.37	19.41	22.03	9.19
Station 3	51.60	19.92	22.95	5.53
Station 4	50.55	19.68	22.81	6.96
Station 5	51.21	19.73	22.99	6.08
Station 6	51.25	19.76	23.07	5.92
Station 7	51.21	19.94	23.17	5.68
Station 8	51.61	20.42	23.07	4.90
Station 9	51.86	20.06	23.07	5.02
Station 10	50.99	20.03	23.04	5.93
Station 11	52.04	20.08	22.98	4.91
Station 12	52.20	19.69	23.16	4.95
Station 13	51.35	20.26	23.33	5.06
Station 14	51.52	20.19	23.15	5.14
Station 15	51.49	20.29	23.21	5.01
Station 16	51.37	20.48	23.32	4.84
Station 17	51.56	20.51	23.27	4.65
Station 18	50.46	20.94	23.73	4.87
Station 19	49.49	21.02	24.49	5.00
Station 20	50.41	21.01	24.19	4.40
Station 21	51.27	20.61	23.26	4.86
Station 22	50.87	20.44	23.37	5.33
Station 23	50.79	20.82	23.63	4.76
Station 24	50.85	20.79	23.80	4.57
Station 25	50.50	21.13	23.71	4.65
Station 26	50.37	20.66	24.30	4.68
Station 27	51.38	20.76	23.37	4.50
Station 28	50.85	20.79	23.76	4.60
Station 29	50.78	21.12	23.78	4.32
Station 30	50.62	21.15	23.68	4.55
Station 31	50.71	20.50	24.36	4.44
Station 32	50.35	21.07	24.12	4.46
Station 33	47.18	24.35	24.23	4.24
Station 34	50.77	20.44	23.41	5.38
Station 35	51.73	21.20	22.68	4.39
Station 36	50.59	21.39	23.59	4.42

* Peaks A, C, M, and T are humic-like and protein-like peaks as discussed in the text. (Coble, 1996).

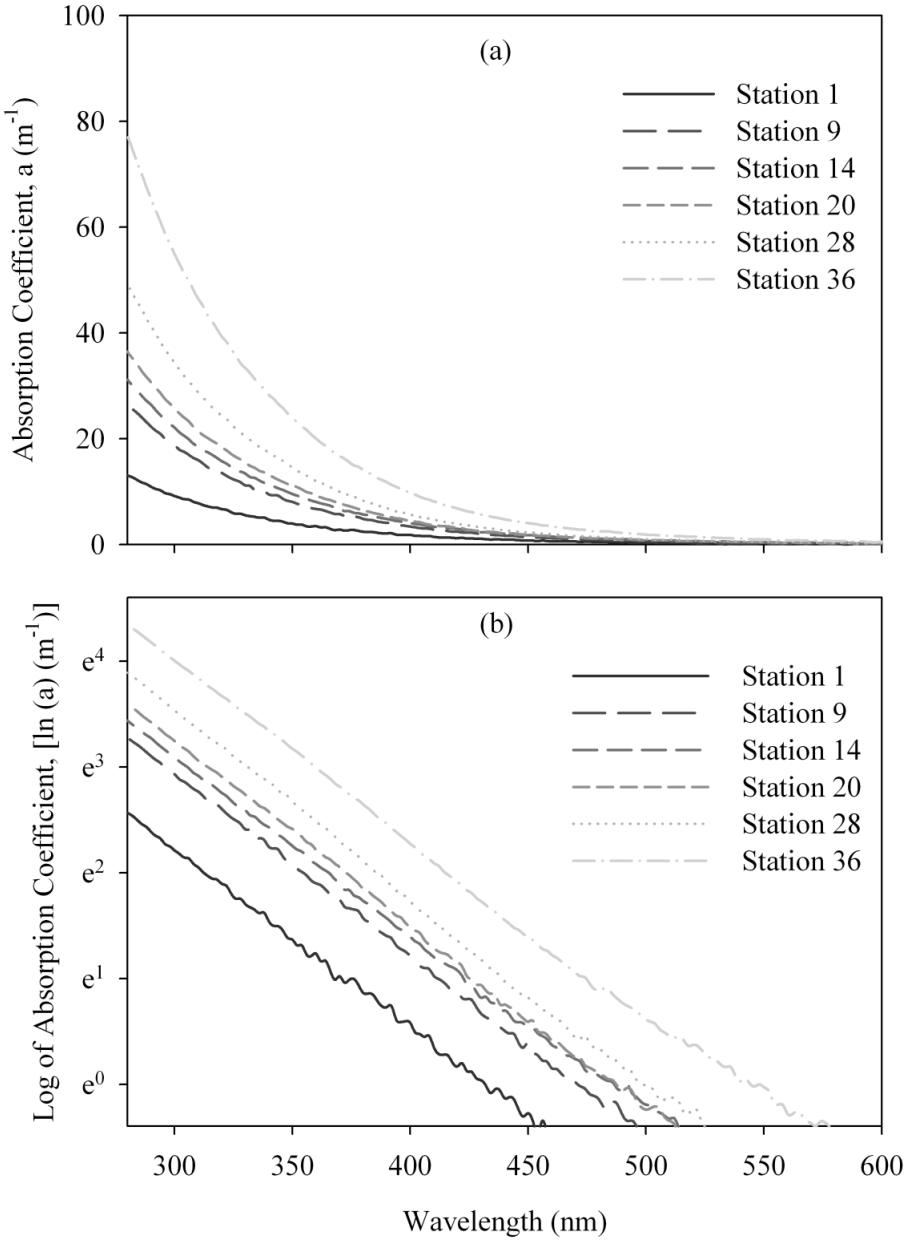

Figure 2.4 (a) CDOM absorption coefficient, a_{CDOM} (m^{-1}) (b) a_{CDOM} in logarithmic scale plotted against the wavelength; measured with a 1 cm pathlength cuvette.

2.3.3. Relationship between CDOM Fluorescence, Absorption and Spectral Slope with Salinity and Temperature

Figure 2.5 shows the CDOM absorption, measured at 355 nm, the fluorescence maximum intensity calculated at excitation wavelength, λ_{ex} = 355 nm, and the spectral slope variation with salinity along the transect. A decrease in CDOM absorption and fluorescence in the transect of the Barataria Basin with increase in salinity is observed and the overall negative relationship is established. The regression equations are obtained only for middle basin as the upper and lower basin showed very little variation with salinity (Figs. 2.5a and 2.5b). The middle basin stations from 5 to 23 follow the trend of decreased CDOM fluorescence with increase in salinity and

showing conservative mixing (D'Sa et al., 2006), while in lower basin (from stations 1 to 4), a slight upward curvature is observed which suggests non-conservative mixing. This may be due to increased CDOM in this part of the basin from freshwater discharge from nearby sources or to resuspension due to strong tidal mixing (Boyd and Osburn, 2004; Del Vecchio and Blough, 2006; Komada et al., 2002; Stedmon et al., 2003). In the upper basin (from stations 24 to 36), CDOM fluorescence showed no dependence to salinity with non-conservative mixing occurring in this portion of the transect. The CDOM absorption spectral slope (350 to 500 nm range) plotted against salinity show an inverse relationship in 0.0153 to 0.0196 nm^{-1} range (Fig. 2.5c). The variation seen in spectral slope measurements throughout the transect suggests that there is a significant chemical alteration in CDOM during its transport along the basin (Boyd and Osburn, 2004). These structural changes in allochthonous CDOM as observed by spectral slope variation for higher wavelength (412 nm) may reflect photobleaching and estuarine mixing.

The CDOM fluorescence plotted against temperature (Fig. 2.6) shows a positive correlation with only a few dispersed data points primarily revealing different water mass sources influencing the study area. This could be due to the shallow depths of the estuarine region and effects of solar radiation over the water bodies. The observed positive relationship as opposed to previously reported results suggests the complexity of the study area (several fresh water point sources) as well as transport of dissolved organic matter through fresh, brackish, and saline marshes of the transect stations. Similar result has been observed for the CDOM absorption coefficient plotted against temperature (not shown).

2.4. Discussion

2.4.1. CDOM Transect Variability

The variation of CDOM absorption along the transect at 355 nm and 412 nm (Fig. 2.1c) and fluorescence spectra in Raman Units (R.U.) at two different excitation wavelengths (355 nm and 412 nm) show similar trends except at station 34 in the upper basin (Fig. 2.1d). CDOM optical properties depend partly on its sources and composition. A drop in salinity at station 2 in comparison to stations 1, 3 and 4 accompanied by a large increase in CDOM absorption suggest freshwater influences and tidal mixing as possible factors influencing CDOM absorption and fluorescence (Fig. 2.1). Stations 5 to 11 follow the trend of increased CDOM absorption and fluorescence with salinity decrease and variable temperature suggesting some point sources from nearby emergent herbaceous wetlands. Station 12 is located in the herbaceous wetlands and the increased CDOM absorption and fluorescence is possibly due to the flow from the nearby brackish and estuarine marshes. An increase in CDOM observed at stations 15 and 16 located in Little Lake could be due to flushing from nearby small bayous while stations 17 to 23 suggest influences from Lake Salvador and the Gulf Intracoastal Waterway with CDOM absorption varying between 9.5-10.8 m^{-1}. A sharp increase to 14.2 m^{-1} is observed from station 24 onwards located in Lake Salvador and under the influence of discharge from Bayou Des Allemands which enters Lake Salvador from the northwest through a narrow bayou stream (Fig. 1.3). This increase at the transition zone of the middle basin and upper basin is mainly due to terrestrial humic substances resulting in a large increase in EEM integral area of 'A' peak (from 3749.9 R.U. nm^2 at station 23 to 5460.5 R.U. nm^2 at station 24). The drainage flow from agricultural fields, farms, and nearby pasture might have caused the increased CDOM at stations 29 and 30. Further increases at stations 33 and 34 could be due to flows from nearby fresh marshes or discharge through Bayou Boeuf. Waters flowing through shallow bayous and swamps might have caused

the high CDOM absorption (~21.9 m^{-1}) at stations 35 and 36. Drainage and sewage from nearby minor communities, agricultural land and farms could be reasonable sources for the high CDOM at these locations.

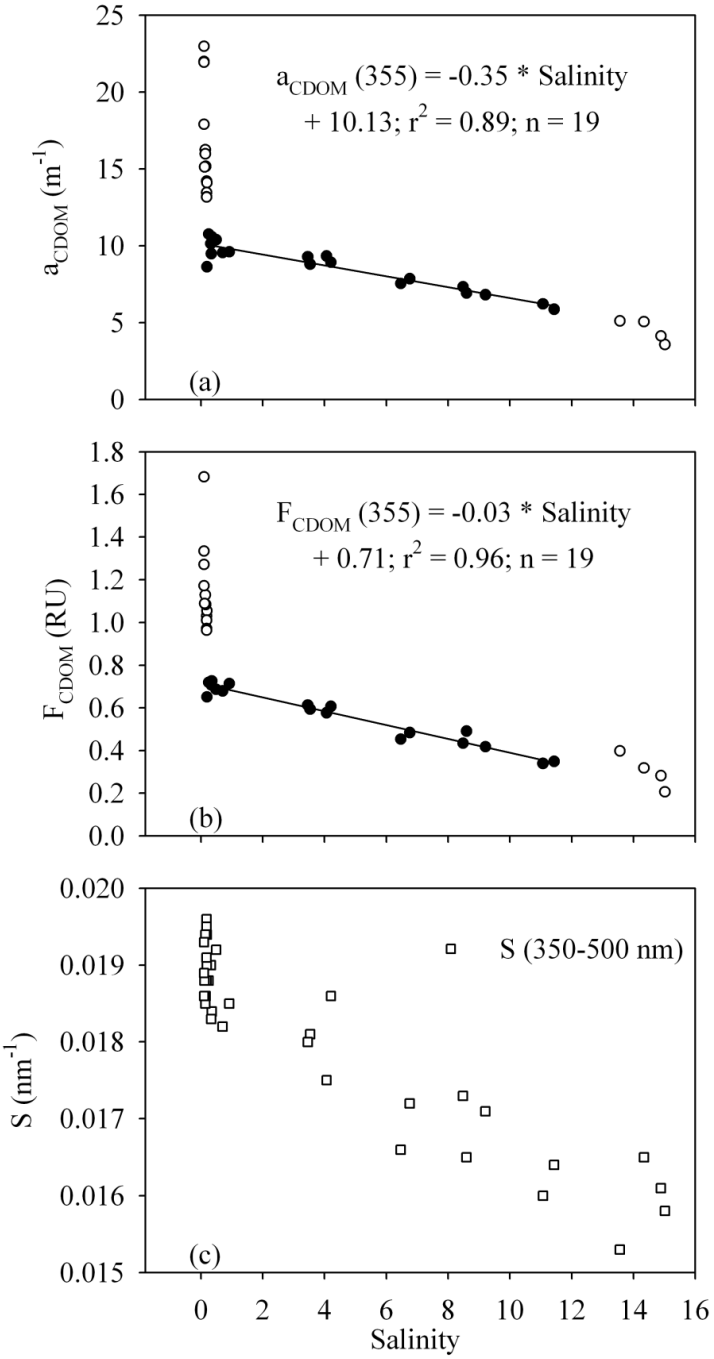

Figure 2.5 (a) Variation of CDOM absorption measured at λ = 355 nm, (b) fluorescence maximum intensity calculated at excitation wavelength, λ_{ex} = 355 nm, and (c) CDOM spectral slope calculated (350 - 500 nm range), plotted against salinity from the surface water along the transect. All the samples have been plotted, but samples with filled circles only (middle basin) were considered for the regression analyses.

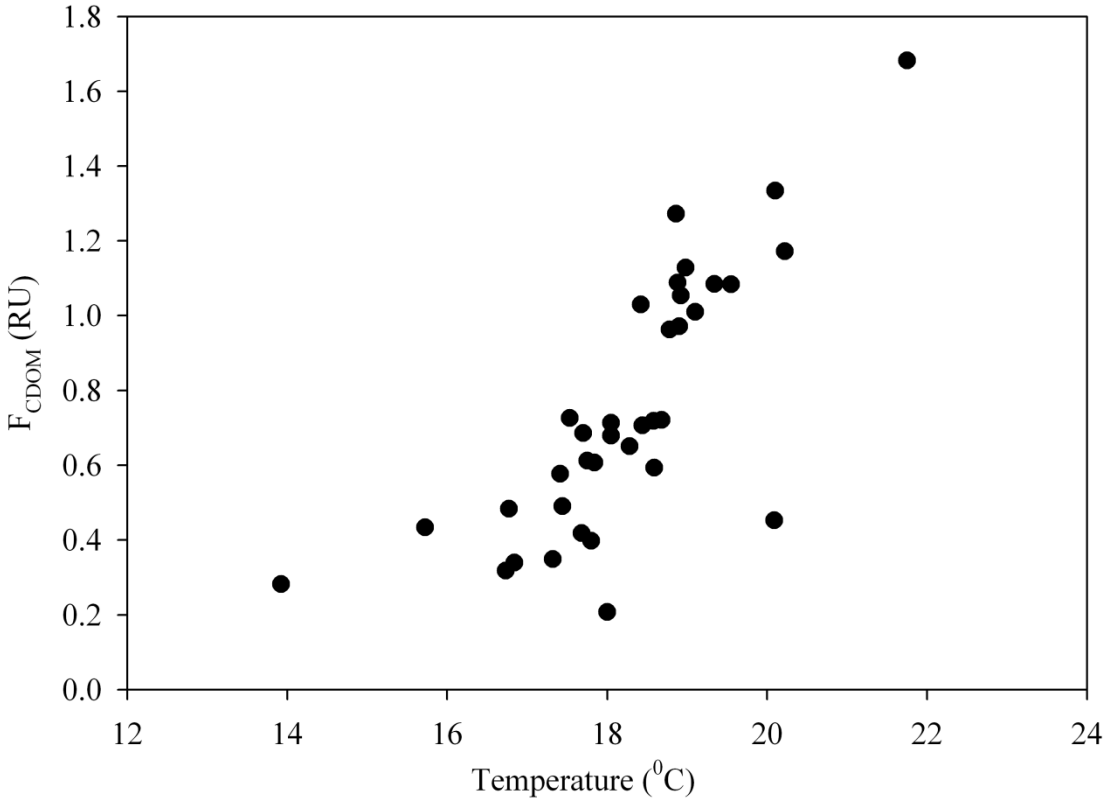

Figure 2.6 Distribution of CDOM fluorescence, F_{CDOM}, measured at excitation wavelength, λ_{ex} = 355 nm against temperature (°C) along the transect.

The range of CDOM absorption at 355 and 412 nm and the spectral slope (S) in the Barataria Basin were observed to be similar to other estuarine, coastal and inland regions such as the Pearl River estuary (China) (Chen et al. 2004; Hong et al., 2005) or coastal regions of the Southern Baltic Sea (Ferrari and Dowell, 1998). Variability in CDOM absorption reported by Chen et al. (2004) ranged from 0.34 to 1.4 m^{-1} at 355 nm for a study in the Pearl River Estuary, China during a one month period in July, 1999. A similar study performed in the same region reported CDOM absorption varying from 0.24 to 1.93 m^{-1} in November, 2002 at 355 nm (Hong et al., 2005) whereas Green and Blough (1994) have recorded CDOM absorption values of 33.7 m^{-1} during a study in Tamiami River (Florida, USA). In our study, CDOM absorption variability ranged from 3.6 to 22.9 m^{-1} at 355 nm and 1.4 to 8.1 m^{-1} at 412 nm which suggests the influence of the different water bodies within the Barataria Basin. Spectral slope coefficients, S in this study were ranging from 0.015 to 0.019 nm^{-1} for the interval 350 to 500 nm while S reported by Hong et al. (2005) for a similar interval (300-500 nm) for Pearl River Estuary, China, ranged between 0.014 to 0.018 nm^{-1}. Ferrari (2000) recorded S values ranging from 0.011 to 0.028 nm^{-1} in the interval 350 to 480 nm in a study in Gulf of Lions, near the coastal regions of Rhone River, France.

Fluorescence Index (calculated as a ratio of maximum emission intensity measured at 470 nm to the maximum emission intensity measured at 520 nm; both at excitation wavelength of 370 nm) which provides a measure of distinct sources of aquatic humic-fulvic acids, did not show any significant difference in the sources of CDOM and was similar to the tidal marshes in Chesapeake Bay (Tzortziou et al., 2008). The values were mostly close to 1.4 and could only be

representative of terrigeneous CDOM sources from the saline and brackish marshes (in middle and lower basin) and fresh marshes and swamps (in upper basin).

2.4.2. Peak Variations along the Transect

The peak ratios to the total integrated scanned area (Table 2.2) are estimated. The variation in 'A', 'C', and 'M' peak ratios to the total fluorescence intensity is not significantly varying, but the 'T' peak ratio to the total fluorescence intensity is almost one-third at station 36 than that at station 1. There is an observed decrease in 'A' peak ratio at station 33, at southern end of Lac Des Allemands (Fig. 1.3) due to increased load of suspended particles derived from anthropogenic and terrestrial inputs from nearby fresh marshes through Lake Boeuf (Conner and Day Jr., 1987). 'C' peak ratio has increased from 6.6 at station 32 to 7.7 at station 33 and again decreased to 6.7 at station 34. This increased inflection is possibly due to the resuspension of suspended organic particles at the location or the remineralization of relatively fresh particulate organic matter (Coble et al., 1998). The 'M' peak ratio to total has not shown any significant variation as the inputs derived from terrigeneous origin, anthropogenic and agricultural wastes are probably in equilibrium throughout the basin during study period. The 'T' peak ratio at station 1 (11.15%) is almost three times the value at station 36 (4.42%) (Table 2.2) that suggests the increased aromaticity going upstream along the transect.

We have also calculated a ratio of 'A' peak to 'C' peak to distinguish for CDOM origination from terrestrial sources depending on the lower values of this ratio. Coble (1996) defined that ratio of A/C peak could provide information about the terrigeneous origin of humic matter which otherwise could not be explained using single peak values. It was observed that if the samples are from far ocean, they have higher A/C ratio indicating low values of C peaks that in turn implies reduced influence of terrestrial humic sources whereas if the sample from inland or near coastal region is considered, higher terrestrial influence could be observed with increase in C peak values which eventually lower the A/C peak ratio (plots not shown here). In this study, we have observed A/C peak ratio ranging from highest value of 2.54 at station 1 to lowest value 1.94 at station 33 which suggest high terrestrial influence upstream in the transect. The mean values of 1.08 (± 0.25) in rivers to a mean value of 1.34 (± 0.25) in transitional marine water has been reported (Coble et al., 1996). Similarly, Sierra et al., (2005) have calculated this peak ratio for a study in southern coastal areas of Brazil with varying water samples and found a range of ratios varying from 1.35 for a fulvic acid sample to 3.16 for a humic acid sample. We have not observed a large variability in peak ratios but distinguishable differences can be observed between terrestrial and marine sources.

2.4.3. Empirical Relationship between CDOM Fluorescence and Absorption

The high correlation between CDOM fluorescence and absorption enables the use of fluorescence as a proxy for absorption (Hoge et al., 1993). Except for the three stations (34, 35 and 36) with very high CDOM absorption (Fig. 2.7), high correlation between fluorescence and absorption were observed for the Barataria Basin. The regression equations obtained in this study are F_{CDOM} (355) = 0.08 * a_{CDOM} (355) – 0.07; r^2 = 0.98 and F_{CDOM} (412) = 0.07 * a_{CDOM} (412) – 8.51; r^2 = 0.96 (Fig. 2.7). Hoge et al. (1993) reported the absorption and fluorescence relationship using regression equations in several water bodies ranging from bays to oceans for 355 nm. The regression equation for Gulf of Mexico reported as a_{CDOM} (355) = 0.192 (± 0.003) * F_{CDOM} (355) + 0.075 (± 0.048) in a study performed in a wide geographic range from Pacific

Ocean water samples to Atlantic Ocean water sample by Hoge et al. (1993). Recently, Chen et al. (2007) have performed a similar study in Tampa Bay, Florida, USA at 400 nm and have found a regression equation for Alafia river in Tampa Bay as F_{CDOM} (400) = 12.02 * a_{CDOM} (400) + 5.95; r^2 = 0.91, but with only six samples which seems to be inadequate to report a general regression equation. In our, study, we have taken 33 samples and assumed that this should be enough to arrive at a conclusion in terms of a general regression equation obtained for the Barataria Basin for 355 nm.

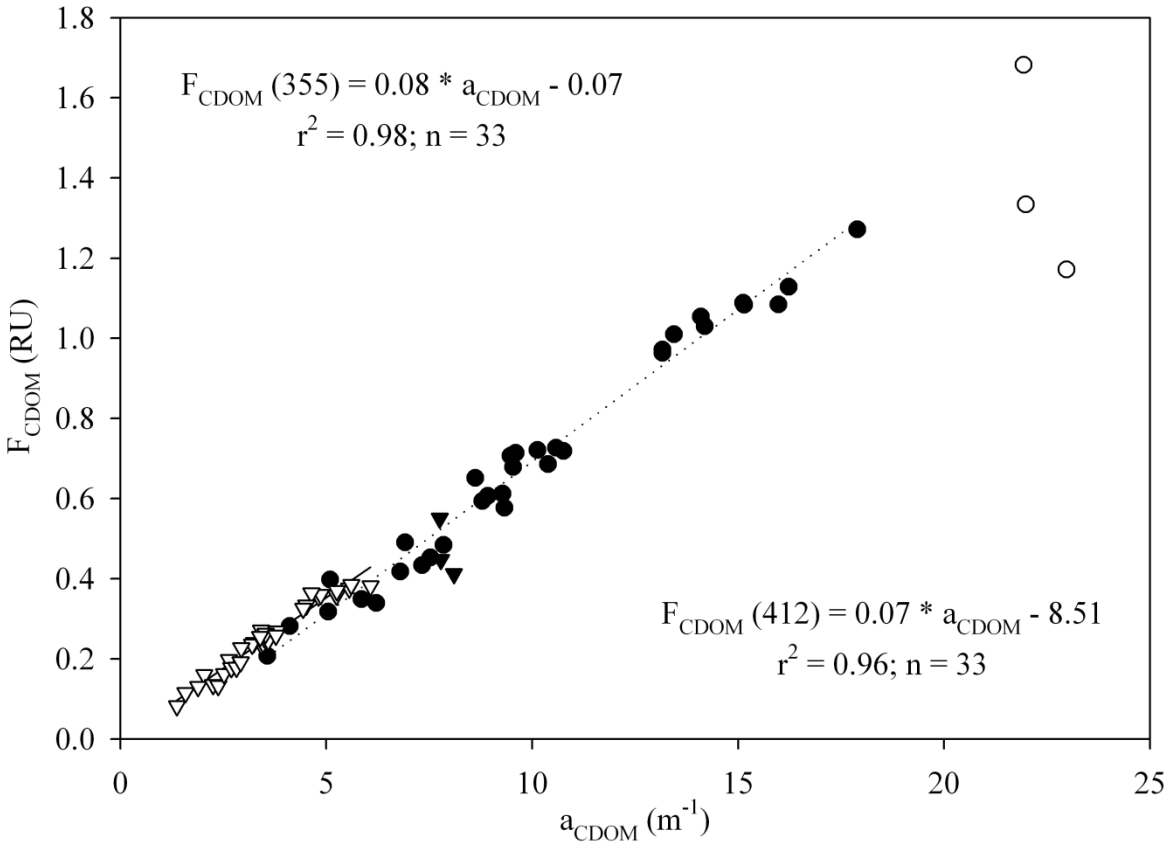

Figure 2.7 Correlation between CDOM absorption and fluorescence measured at 355 and 412 nm. The regression equations, correlation coefficients (r^2), and the number of samples (n) are given in the plot. The empty circles (355 nm) and filled triangles (412 nm) were not considered for the regression analyses.

2.5. Summary

CDOM abundance, its spatial variability, and spectrochemical characteristics were investigated using measurements of absorption and fluorescence in the Barataria Basin, a complex estuarine system. The CDOM optical properties and their distribution in the Barataria Basin were strongly influenced by the inputs from freshwater point sources. The higher CDOM absorption and fluorescence associated with low salinity values in the study area indicated increased sources of terrigeneous substances. The CDOM absorption-salinity and CDOM fluorescence-salinity inverse relationship showed conservative mixing in the middle basin (station 5 – 23), whereas they showed non-conservative mixing in the lower basin (station 1 – 4), and no relation in the upper basin (station 24 – 36). In the 15.02 – 0.1 salinity range, CDOM absorption coefficients at

355 and 412 nm ranged from 3.6 – 22.9 m^{-1} and 1.4 – 8.1 m^{-1} respectively, and the CDOM fluorescence at excitation wavelengths, λ_{ex} = 355 and 412 nm, ranged from 0.2 – 1.6 and 0.1 - 0.6 Raman Units (RU), respectively. These values are found to be close to the reported values in previous literature in coastal or estuarine regions.

The relationship between CDOM absorption and fluorescence can be used as a tracer for water mass identification and as a surrogate measure of salinity in the middle basin region of the Barataria Basin, where it has shown a conservative mixing relationship. The application of EEM technique allowed us to differentiate between fractions of CDOM in the Barataria Basin. The analyses of percent contribution of four principal peaks and total integrated fluorescence along the salinity gradient supported the increasing contribution by T peak in the marine environment. The observed high CDOM fluorescence in the Barataria Basin could be indicative of various physical, chemical, and biological processes in the study area. This study provided a general understanding of CDOM sources, distribution, and sinks in the Barataria Basin. Further studies may help to clarify the observed causes of increased sources of CDOM such as local streams, bayous, ground water influence, and bottom sediment resuspension and to understand the processes changing the CDOM composition while transporting the freshwater towards the oceanic end of the transect in the Barataria Basin.

Chapter 3

Seasonal Variability in Optical Properties of Chromophoric Dissolved Organic Matter (CDOM) in the Barataria Basin, Louisiana, USA

3.1. Introduction

Chromophoric dissolved organic matter (CDOM) is an important constituent of total dissolved organic matter (DOM) pool and operationally defined as the colored portion of DOM. It represents 20 – 70% of total DOM with highest values in coastal areas and lowest in deep oceanic environments (Coble, 2007; Nieke et al., 1997). The CDOM is primarily derived from degradation of dead plants and animal matter and is yellowish to brown in color. CDOM characteristics vary depending on its source (autochthonous and allochthonous) in an aquatic environment and its dynamics are mainly controlled by flow conditions in a natural ecosystem (Coble, 2007; Kowalczuk et al., 2009). The important role of CDOM lies in cycling of carbon (Ågren et al., 2008), transport of trace metals (Hong et al., 2005), and trace gases (Vodacek et al., 1997).

Absorption and fluorescence properties of CDOM and their distribution depends on environment specific physical, chemical, and biological conditions. CDOM absorption and fluorescence properties can change with its constituent chemical components during its course of flow through different water bodies such as streams, bays, ponds, lakes, and coastal estuarine environments. The optical characteristics of CDOM have been a topic of attention for many decades by researchers due to its importance in identifying the sources and sinks of autochthonous (in situ production) and allochthonouos (transport) sources of CDOM and thereby influencing water quality of the environment in question (Coble et al., 1996; Ferrari and Dowell, 1998; Kowalczuk et al., 2009; McKnight et al., 2001). Many researchers have succesfully employed the absorption and fluorescence techniques to identify CDOM distribution and characteristics in natural aquatic systems (Ågren et al., 2008; Coble et al., 1996; Fellman et al., 2009; Hoge et al., 1993; Vodacek et al., 1997).

Absorption studies of CDOM have been recognized for a long time and have been used in a range of natural sytems such as bays (Sasaki et al., 2005), coastal areas (D'Sa and Miller, 2003), and oceanic waters (Bricaud et al., 1981). Further, CDOM fluorescence using EEMs provided a new avenue in characterization and distribution of CDOM in natural aquatic environments such as estuarine and marine environments (Chen et al., 2004; Chen et al., 2007; Coble et al., 1996; Kowalczuk et al., 2009; McKnight et al., 2001; Zhang et al., 2007). EEMs analysis have been found to be useful in identifying the interactions between distinct fluorophores/chromophores in a water sample which has provided a wealth of information in terms of CDOM constituents, their distribution and characteristics in a given water sample.

The absorption and fluorescence characteristics of CDOM have been applied to study Barataria Basin a highly productive and complex estuarine region, with a large level of expected CDOM variability along a transect extending from the mouth of the basin (near the Gulf of Mexico) to Lake Des Allemands upstream and to the northwest (Fig. 1.3). Barataria Basin consists of streams, ponds, and small to large lakes that are influenced from adjacent saline to fresh marshes. In particular, due to high complexity and variability in physico-chemical properties as well as high biological productivity of the Barataria Basin, the region has been of particular interest to the researchers for a long time (Conner and Day Jr., 1992; Das et al., 2009; Hatton et al., 1983; Hopkinson et al., 1978; Kirby and Gosselink, 1976; Madden et al., 1988; Nyman and DeLaune, 1991; Swenson et al., 2006).

The Barataria Basin is located east of Bayou Lafourche (a deserted Mississippi River channel several thousand years ago) and west of the Mississippi River delta and is separated from the Gulf of Mexico in the south by the Grande Terre Islands. Swamp forests, saline, brackish/intermediate, and fresh marshes characterize the nature of the Barataria Basin which is

isolated from the Mississippi River due to channelization and levee construction since the 1930s (Mossa, 1996). Later in 2002, Barataria Basin was reconnected to Mississippi River through Davis Pond Diversion to supplement sediment and nutrient supply in order to achieve former ecological conditions. Previous studies of naturally occurring wetlands in the Barataria Basin have shown the impacts of modifications by artificial diversions (Swenson et al., 2006), discharge from Mississippi River (Wissel et al., 2005) and canal dredging (Sasser et al., 1986) which has altered the natural habitat (Craig et al., 1989; Jones et al., 2002) as well as water quality (Conner and Day Jr., 1987; Happ et al., 1977; Wissel et al., 2005) of the region. Principle hydrologic inputs for the Barataria Basin were altered by channelization, dredging, and artificial constructions that changed the sediment, carbon and nutrient budget in the basin. Precipitation, urban runoff, and agricultural and industrial wastes are the main hydrologic inputs in the basin in present days which in turn are changing the marsh characteristics as well as testing the existence of several flora and fauna due to controlled flow of sediments and nutrient supply to the basin. The dominant vegetation in fresh marshes are *Panicum hermitoman, Eleocharis Spartina,* and *Sagittaria Falcata*, whereas brackish marshes have plenty of *Spartina Patens* with little *Spartina Alterniflora*. The saline marshes in the lower Barataria Basin near the gulf are primarily dominated by *Spartina Alterniflora*. Low rate of sedimentation and high rate of subsidence are causing these marshes to change their inherited properties. The low rate of sedimentation or accretion is usually supported by reduced rate of vertical aggregation of produced organic matter (Hatton et. al, 1983).

A few studies have examined carbon and nitrogen flow in the Barataria basin (Castro et al., 2003; Das et al., 2009; Feijtel et al., 1985; Happ et al., 1977) in order to estimate the carbon and nitrogen inputs through the basin to the Gulf of Mexico. The variability in organic matter inputs to the Barataria Basin have been discussed by a few researchers. For instance, Madden (1988) examined the effects of fresh and marine water coupling in the Barataria Basin in terms of variable organic matter loading and found the impact of anthropogenic inputs over the upper Barataria Basin while the lower Barataria Basin was observed in its natural state during the study (Fig. 1.3). A similar study carried out by Cahoon (1994) to observe organic matter accumulation in a managed and an unmanaged site in the Barataria Basin has reported a higher accumulation rate of organic matter in an unmanaged site rather than a managed site with shorter life expectancy for managed sites in the Barataria Basin marshes.

The present study characterizes the seasonal variability in absorption and fluorescence optical properties of CDOM in the Barataria Basin (Fig. 1.3) using field data during a high flow (spring and early summer, 2008) and low flow season (winter, 2008-09). In addition, the effects of flow through different water bodies downstream such as lakes and local runoff were examined. To our knowledge, this is the first detailed study of the seasonal variability of CDOM, and its spectrochemical characteristics in the Barataria Basin. We have reported here the seasonal variation and distribution of CDOM during different flow conditions (low and high flow) in the Barataria Basin. Also, reported here is a relationship of CDOM absorption and fluorescence during high and low flow season. Seasonal variability of CDOM fluorescence and its constituents have been discussed and supported with observed variability in fluorescence and humification indices (discussed later). In this study, we have employed both absorption and fluorescence analysis techniques to identify CDOM variability during low and high flow conditions. The hypothesis set in this study is to observe statistically significant variability in CDOM absorption and fluorescence characteristics in the Barataria Basin during low and high flow conditions.

3.2. Methods

3.2.1. Study Area

The Barataria Basin system is made up of biologically rich and productive habitats including swamps, fresh, brackish/intermediate, and saline marshes, bayous, bays, small to large lakes, ponds, and barrier islands. It is an irregular shaped basin covering 1,673 km^2 surface area and 5,700 km^2 of drainage area with an average depth of 2.0 meter (Fig. 1.3). The average daily fresh water inflow into the basin is approximately 156 $m^3 s^{-1}$ with an average salinity of 13. The seasonal variation in salinity value is characterized by a peak during low flow conditions (late fall and winter) while salinity pattern fall down during high flow conditions due to increased surface runoff over the wetland as well as increased Mississippi River discharge at plume area near the mouth of the basin in gulf (Conner and Day Jr., 1987).

The main freshwater sources for the basin include precipitation, local urban runoff, agricultural and industrial runoff, Intracoastal Waterway that delivers water from the Atchafalaya River during high flow conditions to the Mississippi River, and diversions from the Davis Pond with a design-pumping rate of 300 $m^3 s^{-1}$, Naomi and West Pointe A la Hache with a maximum pumping rate of 60 $m^3 s^{-1}$ at each site, and Port Sulphur. Apart from these freshwater sources, numerous major and minor point discharges, septic tanks, sewage/stormwater overflow, unsewered communities, pasturelands, and marshes contribute to changes in water quality of the basin (Conner and Day Jr., 1987). Although the salinity signals are highly coherent with Mississippi River discharge, these point sources can significantly contribute to a decrease in the average salinity of the basin region as reported in previous literature (Inoue et al., 2008; Swenson et al., 2006). The period of high river flow in spring and early summer, and high water residence time, typically 12 to 35 days (Wissel et al., 2005) could account for the variable CDOM concentrations in the study area. During low flow conditions, presumably increased tidal influence, prolonged inundation of sea water, and rainfall associated with cold front passage, mostly occurring during low flow conditions (or winter), could alter the sheet flow pattern in the basin which could account for observed CDOM variability at station locations (Fig. 1.3) for the low flow season.

Student's paired t-test was performed (SigmaPlot ver. 10.0, Systat Software Inc. © 2006; at a significance level, p-value = 0.05) to assess whether mean salinity and temperature values determined for both, high and low flow conditions in this study were found to be significantly correlated. P-values obtained from these analyses showed significant differences in mean salinity and temperature calculated for high and low flow conditions (p-value < 0.0001 for both salinity and temperature). These results indicated that mean salinity and temperature values were significantly different over two different flow conditions, i.e., high and low flow conditions. This supported our basis to analyze and treat the high and low flow conditions separately for absorption and fluorescence studies of CDOM in the Barataria Basin.

3.2.2. Collection of Water Samples

The sampling for surface water was conducted at 36 stations (Fig. 1.3) located along a 124 km transect (South-East to North-West) from the mouth of the basin (station 1) in the Gulf of Mexico to the north-west end of the upper basin (station 36) in Barataria Basin during regular monthly field trips taken in March, April, May, November, December (2008), and January (2009). The monthly mean streamflow ($m^3 s^{-1}$) during the period of one year ranging from

January 2008 to January 2009 in the Mississippi River at Baton Rouge, Louisiana (Lat: 30.445667 °N, Lon: 91.191556 °W) is obtained from USGS (United States Geological Survey) water database to produce a representative plot for high and low flow conditions in the Barataria Basin (Fig. 3.1). High flow conditions show a peak during March, April, and May (2008) while a fall in mean streamflow curve can be seen during low flow conditions in November, December (2008), and January (2009).

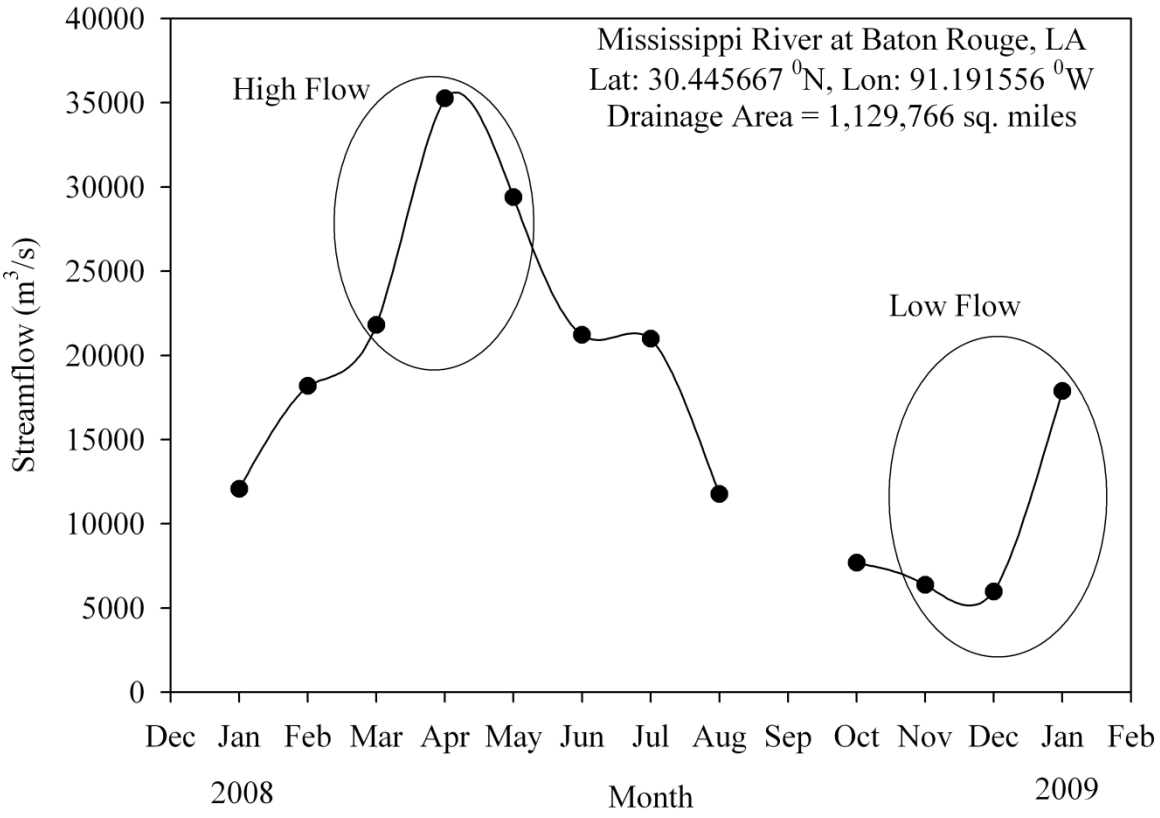

Figure 3.1 Mean monthly streamflow (m^3s^{-1}) of the Mississippi River measured at Baton Rouge, Louisiana for one year period ranging from January, 2008 to January, 2009.

The surface water samples collected at 36 sampling stations in the Barataria Basin were brought back to the laboratory and immediately filtered using pre-rinsed 0.2 micron nucleopore membrane filters. The filtered samples were kept in a refrigerator for optical absorption and fluorescence analyses. The tap water was treated with a Barnstead Nanopure® Model D-50280 purification system with a purity level of 18.2 MΩ. Temperature and salinity measurements were recorded using a handheld YSI. Distributions of mean surface salinity, temperature, CDOM absorption measured at 355 nm and CDOM fluorescence measured as maximum emission fluorescence intensity obtained at excitation wavelength, λ_{ex} = 355 nm are also reported (Table 3.1). Fluorescence Index was calculated as a ratio of maximum emission fluorescence intensities calculated at 470 and 520 nm, with excitation at 370 nm (Tzortziou et al., 2008). Fluorescence index can be used to distinguish sources of dissolved organic matter containing humic substances in an aquatic environment (McKnight et al., 2001) with suggested range for terrestrial originated humics of 1.4 and for marine originated materials of 1.9. Humification Index (HIX) (Zsolnay et al., 1999) was calculated by dividing the integrated area of fluorescence intensity measured

between emission wavelength of 435 and 480 nm by the integrated area of fluorescence intensity measured between emission wavelength of 300 and 345 nm with excitation at 254 nm.

3.2.3. Absorption Spectroscopy

The surface water samples were allowed to reach room temperature and the instrument was kept on for 30 minutes before the sample analysis. Absorption spectra were obtained between 190 and 750 nm at 2-nm intervals using Perkin Elmer Lambda 850 double-beam spectrophotometer equipped with 1 cm path-length quartz cuvette (volume of 4 ml) and 150 mm spectralon coated integrating sphere. The data were corrected for scattering and baseline fluctuations by subtracting the average value of absorption between 700 and 750 nm from each spectrum (Green and Blough, 1994). The absorption coefficients (a) were calculated from the absorbances (A) obtained from the spectrophotometer using:

$$a(\lambda) = 2.303 \times \frac{A(\lambda)}{l}$$

where $A(\lambda)$ is the absorbance at a wavelength, λ, calculated as (Log (I_0/I), I is the intensity, and l is the path-length in meters. Spectral slope coefficients (S, nm^{-1}) were calculated by employing a non-linear least square regression of the plot $a(\lambda)$ versus wavelength over the range 300 to 500 nm using the equation of Markager and Vincent (2000).

$$a(\lambda) = a(\lambda_0)\exp[-S(\lambda - \lambda_0)]$$

where λ_0, the reference wavelength was set to 400 nm. Range from 300 to 500 nm for the calculation of S was selected based on similar studies and beyond 500 nm values were close to zero. Here, a_{CDOM} (355 nm) was selected to study the variability in absorption coefficients, their correlations with salinity and CDOM fluorescence in order to compare the results with previously reported studies (discussed later).

3.2.4. Fluorescence Spectroscopy

Surface water samples were treated in a similar manner as those from absorption measurements along an axial transect from the Barataria Basin. Samples having absorbance greater than 0.02 at 350 nm (A_{350} > 0.02) were diluted with particle free Nanopure Milli-Q water (also used as a blank) to account for the inner filter effects. Excitation Emission matrixes (EEM) were generated using a Horiba Jobin Yvon Fluromax-4 spectrofluorometer equipped with a 50 W ozone-free Xe arc lamp and a R928P photomultiplier tube as a detector. The spectroflurometer was set to collect the signal in ratio mode with dark offsets using a 5 nm bandpass on the excitation as well as emission monochromators. Factory supplied correction factors were applied to the scans to correct for instrument configuration. The EEM spectra were recorded for excitation spectra from 250 to 500 nm at every 5 nm intervals (Kowalczuk et al., 2005; Zepp et al., 2004) while the emission spectra ranged between 280 – 600 nm, with data saved for every 5 nm over an integration time of 0.1s. Milli-Q water blank EEM's were subtracted from the sample EEM's to eliminate Raman peaks and then EEM's were normalized to daily-determined water Raman integrated area maximum fluorescence intensity (350 ex/397 em, 5 nm bandpass) (Colin Stedmon, Pers. Comm.). Finally, the EEM's were multiplied with dilution factor derived from the fluorescence intensity at Ex/Em = 350/397 nm of water Raman scan to obtain the intensity for the original, undiluted sample (Coble et al., 1998). The fluorescence intensities measured were reported in Raman Units (RU) in this study. A 5% agreement was noted between replicate

scans in terms of intensity and within bandpass resolution in terms of peak location using Milli-Q water scans. The EEM plots were prepared using FLToolbox (ver. 2.10b; February, 2007) developed by Wade Sheldon (University of Georgia) for MATLAB® (Zepp et al., 2004). A detailed description of FLToolbox can be found in Zepp et al., 2004. In addition, it also allowed the quantification of the three-dimensional surface integration of EEMs over individual chromophore regions as well as integration of the total emission over the entire corrected fluorescence matrix using integration option (Zepp et al., 2004). Later in Figs. 3.3 and 3.4, the respective peaks, i.e., peaks A, C, M, and T could be seen by their integrated area shown by circles or ellipses centered over the maximum emission fluorescence intensity of that peak. EEM spectra of the whole scan is also calculated for the integration area using the excitation ranges of 250-500 nm and emission ranges of 280-600 nm. Contribution by each peak to the total scanned integrated area is calculated as a ratio of peak integration area divided by the integrated fluorescence intensities of each peak in the scanned area in order to estimate the percentage involvement of each chromophore to the total measured integrated area of the sample or total fluorescence intensity of the sample (Kowalczuk et al., 2009).

3.3. Results

3.3.1. Distribution of Salinity, Temperature, a_{CDOM}, and F_{CDOM}

The variation in mean salinity, temperature, absorption coefficient of CDOM at 355 nm and CDOM fluorescence (when surface water samples were excited at 355 nm and maximum fluorescence intensity were recorded at emission wavelength) as a function of stations (near the mouth of the basin to upstream in land) along a 124 km axial transect of the Barataria Basin is shown in Fig. 3.2. The observed variability of these parameters are shown here for high flow season as well as for a low flow season. Barataria Basin is characterized by a surface salinity gradient, ranging from mean value of 16.07 (± 5.78) at station 1 (near the mouth of the basin; Fig. 1.3, Table 3.1) to mean value of 0.10 (± 0.005) at station 36 (end of the transect; Fig. 1.3, Table 3.1) in the high flow season whereas the surface salinity gradient for the low flow season is reported as ranging from mean value of 22.34 (± 7.46) at station 1 (Fig. 1.3, Table 3.1) to mean value of 0.10 (± 0.015) at station 36 (end of the transect; Fig. 1.3, Table 3.1). In general, the variability for salinity in low flow season is found to be greater than that observed in high flow season (Fig. 3.2a) which may be due to frequent inundation of sea water into the estuarine region during low flow conditions. Standard deviations are not shown in the Table 3.1 to avoid confusion over too many values in the table.

Temperature variability is greater in high flow season with observed variability ranging from mean value of 21.97°C (± 3.45) at station 1 (near the mouth of the basin; Fig. 1.3, Table 3.1) to mean value of 24.29°C (± 2.26) at station 36 (end of the transect; Fig. 1.3, Table 3.1). During low flow season, observed mean value at station 1 (near the mouth of the basin; Fig. 1.3, Table 3.1) was 15.87°C (± 0.91) and at station 36 (end of the transect; Fig. 1.3, Table 3.1) was 15.10°C (± 0.76) (Fig. 3.2b). The higher mean values of temperature for the high flow season is expected due to longer duration of days and greater insolation during later spring and summer months in the area of study.

Figures 3.2c and 3.2d shows the variability in CDOM absorption and fluorescence measured at 355 nm (excitation wavelength of 355 nm in case of CDOM fluorescence) respectively for both high and low flow seasons. Mean value for CDOM absorption (Fig. 3.2c) in high flow season is recorded as 3.25 ± 0.56 m^{-1} at station1 (near the mouth of the basin; Fig. 1.3, Table 3.1)

and 20.76 ± 2.43 m^{-1} at station 36 (end of the transect; Fig. 1.3, Table 3.1) whereas for low flow season, the mean value for CDOM absorption ranged from 1.48 ± 1.08 m^{-1} at station 1 (near the mouth of the basin; Fig. 1.3, Table 3.1) to 25.45 ± 7.03 m^{-1} at station 36 (end of the transect; Fig. 1.3, Table 3.1). During low flow season, there was greater variability in CDOM absorption in the lower part likely due to tidal effects whereas the upper part of the transect appeared to be unaffected by tidal influence. The decreased precipitation and runoff also likely contributed to the mean higher values in CDOM absorption during the low flow season in the upper Barataria Basin.

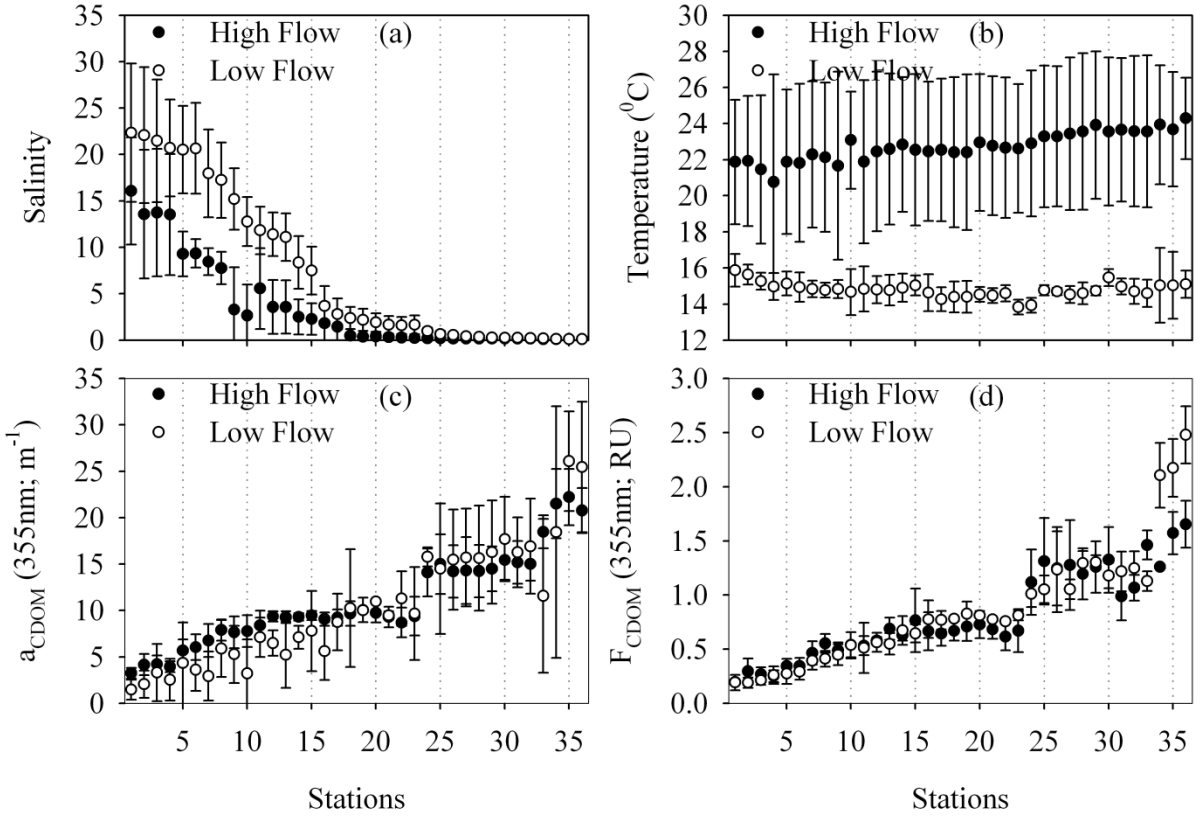

Figure 3.2 Distribution of mean (a) salinity, (b) temperature, (c) absorption coefficient of CDOM at 355, and (d) CDOM fluorescence maximum emission intensity excited at 355 nm along the axial transect for both, high and low flow, conditions.

CDOM fluorescence in high flow season (Fig. 3.2d) varied from mean value of 0.20 ± 0.02 RU at station 1 (near the mouth of the basin; Fig. 1.3, Table 3.1) to 1.65 ± 0.22 RU at station 36 (end of the transect; Fig. 1.3, Table 3.1) whereas in low flow season, it ranged from 0.19 ± 0.07 RU at station 1 (near the mouth of the basin; Fig. 1.3, Table 3.1) to 2.48 ± 0.27 RU at station 36 (end of the transect; Fig. 1.3, Table 3.1). Fluorescence measurements of CDOM showed the similar trend shown by CDOM absorption (Figs. 3.2c and 3.2d) with increase in mean values from station 1 (near the mouth of the basin; Fig. 1.3, Table 3.1) to station 36 (end of the transect; Fig. 1.3, Table 3.1). CDOM fluorescence appear similar during both seasons with lower variability in the lower Barataria Basin and higher in the upper basin.

Table 3.1 Summary of surface samples collected during monthly field trips for March, April, and May (2008) in high flow season and during November, December (2008), and January (2009) in low flow season from an axial transect in the Barataria basin.

Stations	Mean Salinity		Mean Temperature (°C)		Mean a_{CDOM} (355 nm)		Mean F_{CDOM} (355 nm)		Mean S (300-500 nm)		Mean Fluorescence Index (Ex=370; Em=470/520)	
	HF	LF	HF	LF	HF	LF	HF	LF	HF	LF	HF	LF
Station 1	16.07	22.34	21.87	15.87	3.25	1.48	0.20	0.19	0.0172	0.0357	1.4148	1.3999
Station 2	13.57	22.08	21.92	15.63	4.16	2.07	0.30	0.19	0.0173	0.0194	1.4172	1.3970
Station 3	13.74	21.48	21.45	15.27	4.21	3.32	0.27	0.21	0.0170	0.0184	1.4070	1.3932
Station 4	13.52	20.70	20.76	14.97	3.94	2.53	0.25	0.26	0.0172	0.0118	1.4223	1.3900
Station 5	9.29	20.51	21.88	15.13	5.67	4.36	0.34	0.27	0.0171	0.0127	1.3697	1.3734
Station 6	9.34	20.65	21.82	14.93	6.04	3.60	0.34	0.29	0.0171	0.0204	1.3695	1.3723
Station 7	8.45	17.96	22.29	14.83	6.75	2.93	0.47	0.39	0.0172	0.0192	1.3595	1.3783
Station 8	7.76	17.24	22.13	14.77	7.90	5.91	0.55	0.41	0.0172	0.0186	1.3520	1.3713
Station 9	3.30	15.20	21.66	14.83	7.65	5.29	0.49	0.45	0.0169	0.0180	1.3352	1.3816
Station 10	2.66	12.76	23.08	14.67	7.77	3.22	0.54	0.54	0.0171	0.0205	1.3582	1.3828
Station 11	5.56	11.82	21.88	14.83	8.40	7.12	0.53	0.51	0.0169	0.0418	1.3492	1.3723
Station 12	3.58	11.40	22.45	14.80	9.36	6.48	0.58	0.56	0.0168	0.0183	1.3612	1.3908
Station 13	3.57	11.09	22.59	14.77	9.28	5.23	0.69	0.55	0.0167	0.0192	1.3489	1.3557
Station 14	2.49	8.37	22.83	14.90	9.31	7.11	0.63	0.67	0.0168	0.0178	1.3504	1.3863
Station 15	2.27	7.50	22.54	15.03	9.47	7.80	0.77	0.65	0.0169	0.0184	1.3505	1.3770
Station 16	1.83	3.68	22.46	14.63	9.08	5.63	0.67	0.78	0.0170	0.0177	1.3556	1.3841
Station 17	1.44	2.81	22.54	14.27	9.23	8.76	0.64	0.77	0.0171	0.0182	1.3689	1.3774
Station 18	0.49	2.38	22.41	14.40	9.67	10.26	0.67	0.78	0.0169	0.0166	1.3645	1.3745
Station 19	0.36	2.18	22.41	14.40	10.05	10.03	0.71	0.83	0.0171	0.0171	1.3464	1.3848
Station 20	0.40	1.90	22.95	14.53	9.76	10.97	0.73	0.81	0.0169	0.0171	1.3579	1.3803
Station 21	0.32	1.65	22.77	14.47	9.30	9.49	0.68	0.78	0.0171	0.0172	1.3732	1.3982
Station 22	0.26	1.59	22.66	14.60	8.71	11.29	0.62	0.76	0.0170	0.0170	1.3640	1.3935
Station 23	0.22	1.65	22.62	13.83	9.38	9.67	0.67	0.81	0.0172	0.0244	1.3710	1.3629

Table 3.1 continued…

Stations	Mean Salinity		Mean Temperature (°C)		Mean a_{CDOM} (355 nm)		Mean F_{CDOM} (355 nm)		Mean S (300-500 nm)		Mean Fluorescence Index (Ex=370; Em=470/520)	
	HF	LF	HF	LF	HF	LF	HF	LF	HF	LF	HF	LF
Station 24	0.18	0.96	22.90	13.93	14.10	15.78	1.12	1.01	0.0171	0.0167	1.3700	1.3819
Station 25	0.18	0.64	23.28	14.77	14.99	14.50	1.31	1.05	0.0172	0.0172	1.3721	1.3931
Station 26	0.17	0.54	23.28	14.70	14.21	15.47	1.25	1.23	0.0174	0.0168	1.3655	1.3817
Station 27	0.17	0.42	23.43	14.53	14.30	15.70	1.28	1.05	0.0174	0.0166	1.3637	1.3965
Station 28	0.17	0.34	23.56	14.60	14.24	15.65	1.20	1.29	0.0175	0.0171	1.3648	1.3841
Station 29	0.16	0.27	23.92	14.73	14.49	16.29	1.26	1.30	0.0176	0.0168	1.3717	1.3999
Station 30	0.16	0.25	23.56	15.47	15.44	17.70	1.33	1.18	0.0174	0.0168	1.3647	1.3858
Station 31	0.15	0.24	23.65	14.97	15.17	16.27	0.99	1.22	0.0175	0.0167	1.3580	1.3873
Station 32	0.14	0.21	23.58	14.70	15.01	16.92	1.07	1.25	0.0176	0.0171	1.3706	1.3953
Station 33	0.11	0.19	23.56	14.60	18.48	11.58	1.46	1.13	0.0175	0.0175	1.3440	1.3809
Station 34	0.11	0.12	23.93	15.03	21.52	18.45	1.26	2.10	0.0168	0.0169	1.3639	1.4000
Station 35	0.11	0.11	23.68	15.03	22.22	26.09	1.57	2.17	0.0168	0.0167	1.3488	1.3962
Station 36	0.10	0.10	24.29	15.10	20.76	25.45	1.65	2.48	0.0170	0.0166	1.3568	1.3994

*HF is High Flow season during March, April, and May months.

#LF is Low Flow season during November, December, and January months.

3.3.2. EEMs Transect Seasonal Variability

EEM plots have been used to characterize the fluorescence variability in the transect for high and low flow seasons (Figs. 3.3 and 3.4). Typical EEM plots for station 1 (Fig. 3.3) (near the mouth of the basin; Fig. 1.3) and station 36 (Fig. 3.4) (end of the transect; Fig. 1.3) are shown. For the month of May-08 (Fig. 3.4c), station 36 could not be processed due to unavailability of instrument, EEM plot of station 30 (Fig. 3.4c) is chosen as representative of the last station since station 30 lies in upper part of the transect and close to station 36 (Fig. 1.3). Station 1 for both, high and low flow, season are plotted on same scale to compare the results and for visual observation to distinguish between features observed in EEMs of different season for station 1. Similarly the EEMs are plotted for station 36 (or last station) of the transect to observe the features for visual distinctions in both, high and low flow season (Fig. 3.4).

The dominant A-peak is visibly present in greater concentration in high flow season than that in the low flow season with an exception in Jan-09 for station 1 EEM plot (Fig. 3.3f). The concentration as observed is lowest in Dec-08 (Fig. 3.3e) for the low flow season whereas it is highest in Mar-08 (Fig. 3.3a) for the high flow season. C and M-peaks are visually missing from station 1 EEM plot for Dec-08 (Fig. 3.3e) which suggests tidal inundation during low flow season at the lower Barataria Basin and dilution at station 1 by tidal mixing. It is also revealed by the loss of A-peak at this location for Dec-08. The prominent visualization of peaks in Jan-09 (Fig. 3.3f) could be due to receeding tidal inundation or runoff from the upper Barataria Basin which is also supported by decreased salinity at this location in Jan-08 (14.38) than salinity values at station 1 during Nov-08 (29.18) and Dec-08 (23.46).

During the low flow season, the observed visual peak characteristics for station 36 (Fig. 3.4) are more pronounced than the same observed for high flow season. The highest concentrations of peaks are observed during Nov-08 (Fig. 3.4d) in visual analysis for low flow season while the lowest concentrations are visually observable for Apr-08 (Fig. 3.4b) during high flow season. The higher concentration at station 36 for all the respective peaks could be attributed to the lack of runoff and precipation during low flow conditions at this location which causes the increased humification at this location. Also, it could be due to unaffected tidal influence at this location which in turn causes the humic matter to be fairly stable at station 36.

The absorption spectra versus wavelength for station 1 and 36 for both, high and low flow, conditions are plotted in Fig. 3.5 that shows an exponentially increasing trend with decreasing wavelength (D'Sa, 2008). In general, the higher CDOM concentrations were noted for station 36 (Fig. 1.3) during both high and low flow conditions whereas lower CDOM concentrations were recorded for both high and low flow conditions at station 1 (Fig. 1.3). The CDOM concentrations were found to be increasing from station 1 to station 36 during both high and low flow conditions with greater variability in low flow conditions for station 36 and during high flow conditions for station 1. The observed higher CDOM absorption at station 1 during high flow than that during low flow could be due to runoff and precipitation of organic matter from upland to the mouth of the basin or due to more pronounced terrestrial influence during high flow conditions. During low flow conditions, the observed CDOM concentration at station 36 is more pronounced than that in high flow conditions. This may again be attributed to the low runoff and precipitation during low flow conditions at station 36 and fairly static humic material at this location causing increased absorption.

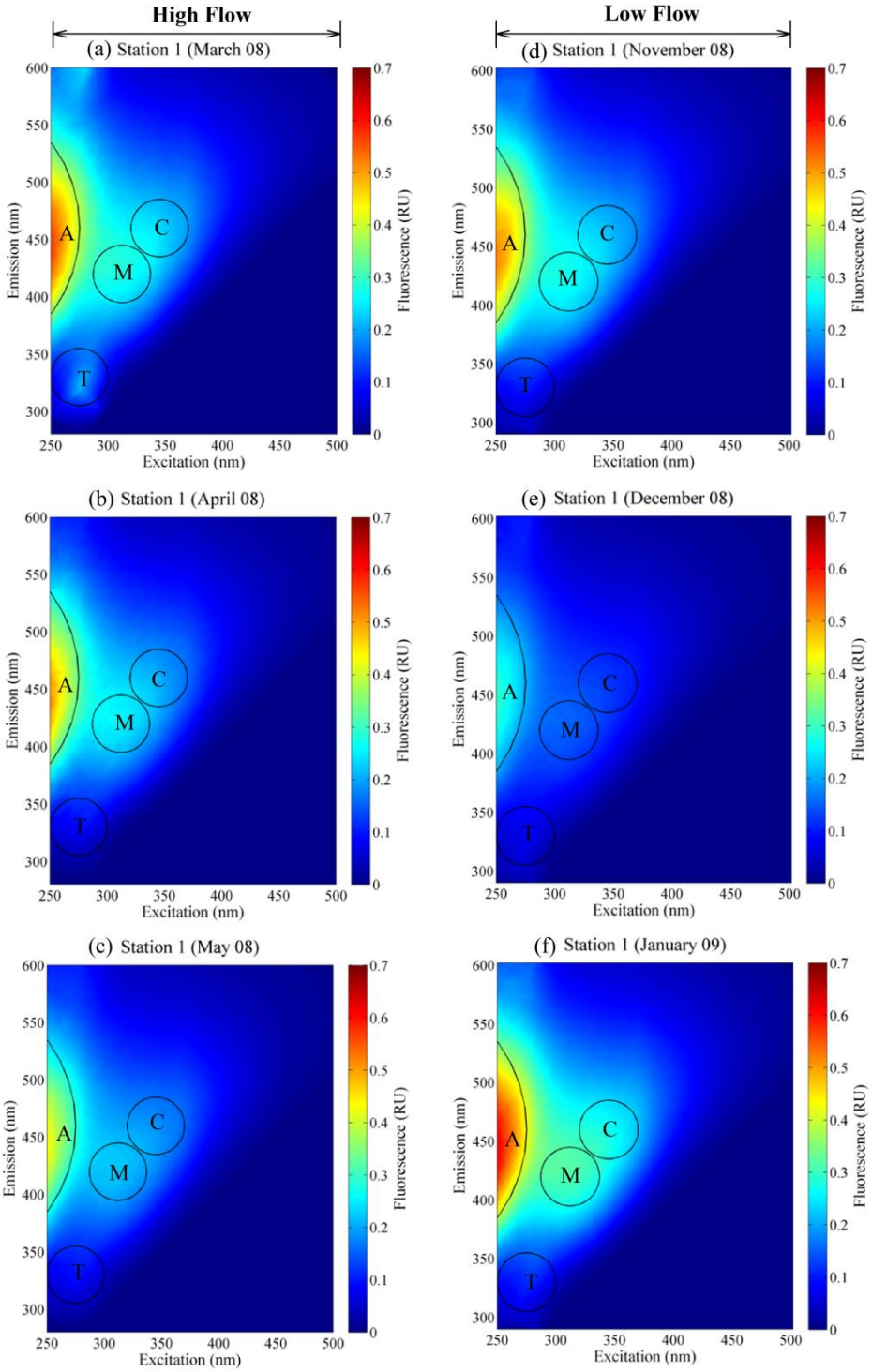

Figure 3.3 Contour plot of EEM spectra of station 1 during high flow conditions (a) March, 2008 (b) April, 2008, and (c) May, 2008; representing high salinity end member of the Barataria basin transect, and contour plot of EEM spectra of station 1 during low flow conditions (d) November, 2008 (e) December, 2008, and (f) January, 2009; representing high salinity end member of the transect, at the mouth of the basin near the Gulf of Mexico. The A, C, M, and T peaks are fluorescence peaks according to Coble (1996). The integration cross-section area is shown by circles at peak maxima.

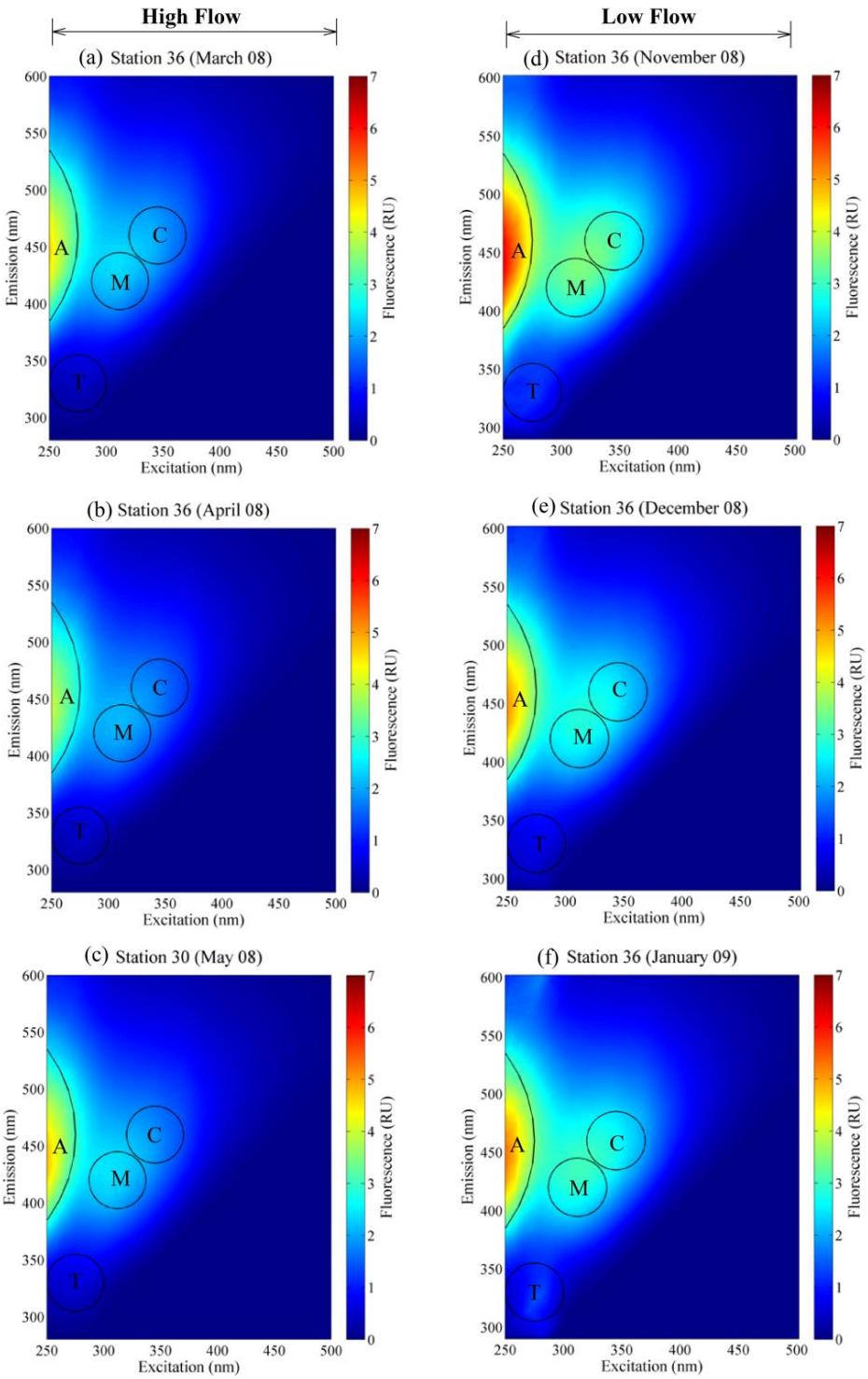

Figure 3.4 Contour plot of EEM spectra of station 36 during high flow conditions (a) March, 2008 (b) April, 2008, and station 30 in (c) May, 2008; representing freshwater end member of the Barataria basin transect, and contour plot of EEM spectra at station 36 during low flow conditions (d) November, 2008 (e) December, 2008, and (f) January, 2009; representing freshwater end member upstream in the transect. The A, C, M, and T peaks are fluorescence peaks according to Coble (1996). The integration cross-section area is shown by circles at peak maxima.

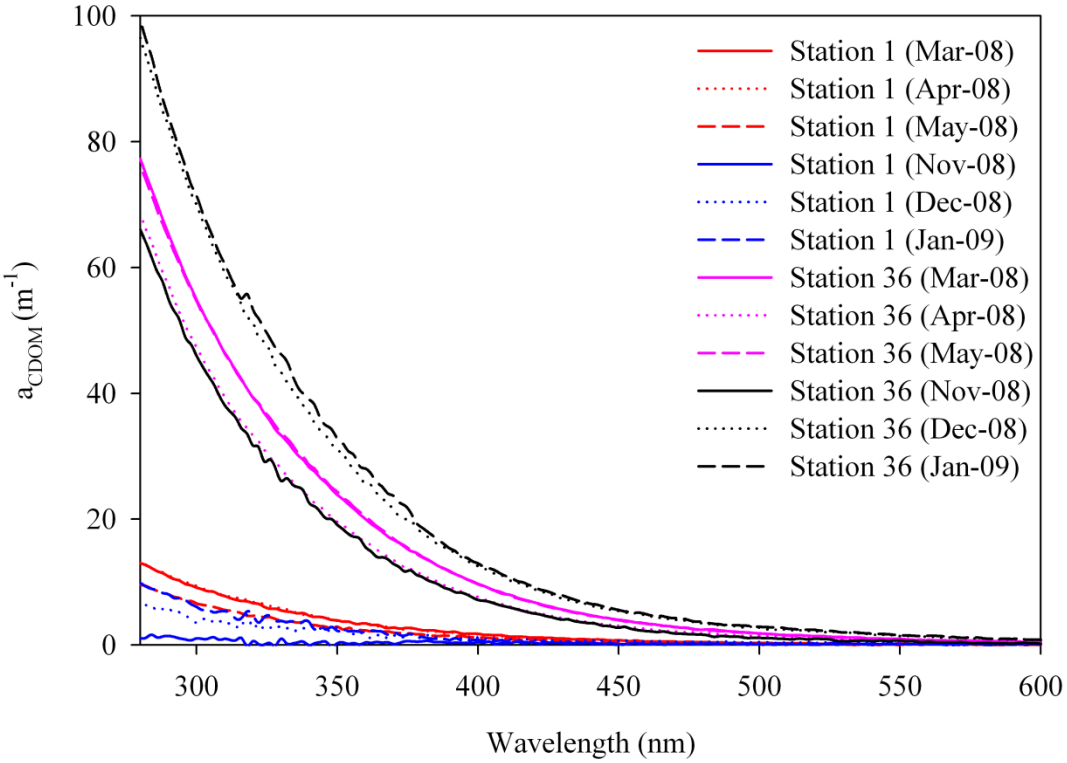

Figure 3.5 CDOM absorption coefficient, a_{CDOM} (m^{-1}) plotted against the wavelength (in nm); measured with a 1 cm pathlength cuvette for extreme stations, i.e., stations 1 and 36 of the Barataria basin transect during high flow and low flow conditions.

3.3.3. Variability of a_{CDOM}, F_{CDOM}, and Spectral Slope with Salinity

Seasonal variability of a_{CDOM}, F_{CDOM} and spectral slope, S against salinity is shown in Fig. 3.6. CDOM absorption and fluorescence showed a general decreasing trend with increasing salinity for both high and low flow seasons while spectral slope, S has shown a general increasing trend with salinity for low flow conditions. There is no observable trend during high flow conditions for spectral slope with salinity (Fig. 3.6c). Few data points for low flow conditions were not considered in the plotting and analysis as they were treated as outliers (Fig. 3.6f), there were total 7 such points at stations 1, 4, 5, 6, 10, 11, and 23 (Fig. 1.3). The increased CDOM values near stations 34, 35, and 36 are similar to those observed in the Lake Des Allemands area in a separate study (Dash, Pers. Comm.). The regression equations obtained for CDOM absorption and fluorescence against salinity for both, high and low flow, conditions are shown in Figs. 3.6a, 3.6b, 3.6d, and 3.6e. Generally, absorption and fluorescence both show a linear conservative relationship with salinity throughout the transect with exceptions at a few stations in the upper part of the transect (Figs. 3.6a, 3.6b, 3.6d, and 3.6e). Fairly good correlation between absorption and fluorescence with salinity respectively have been observed with slightly better results for low flow conditions than that for high flow conditions. In brief, the observed results for a_{CDOM}, F_{CDOM}, and S against salinity are fairly better in low flow conditions than those observed in high flow conditions.

Moreover, plots between S and a_{CDOM} is shown in Fig. 3.7 to observe the relationship between S variability against the abosorption coefficient of CDOM in the transect for both high and low flow conditions. During low flow conditions, S varied with observed a_{CDOM} fairly

smoothly, but during high flow conditions, this variability was not observed. The variation in S values with a_{CDOM} generally decreased toward higher mean a_{CDOM} values and vice-versa in low flow conditions whereas in high flow conditions, a scattered pattern for S variation with a_{CDOM} is observed. Few stations (stations 1, 11, and 23; Fig. 1.3) during low flow conditions were not considered in Fig. 3.7 as they were treated as outliers due to quite high sporadic S values.

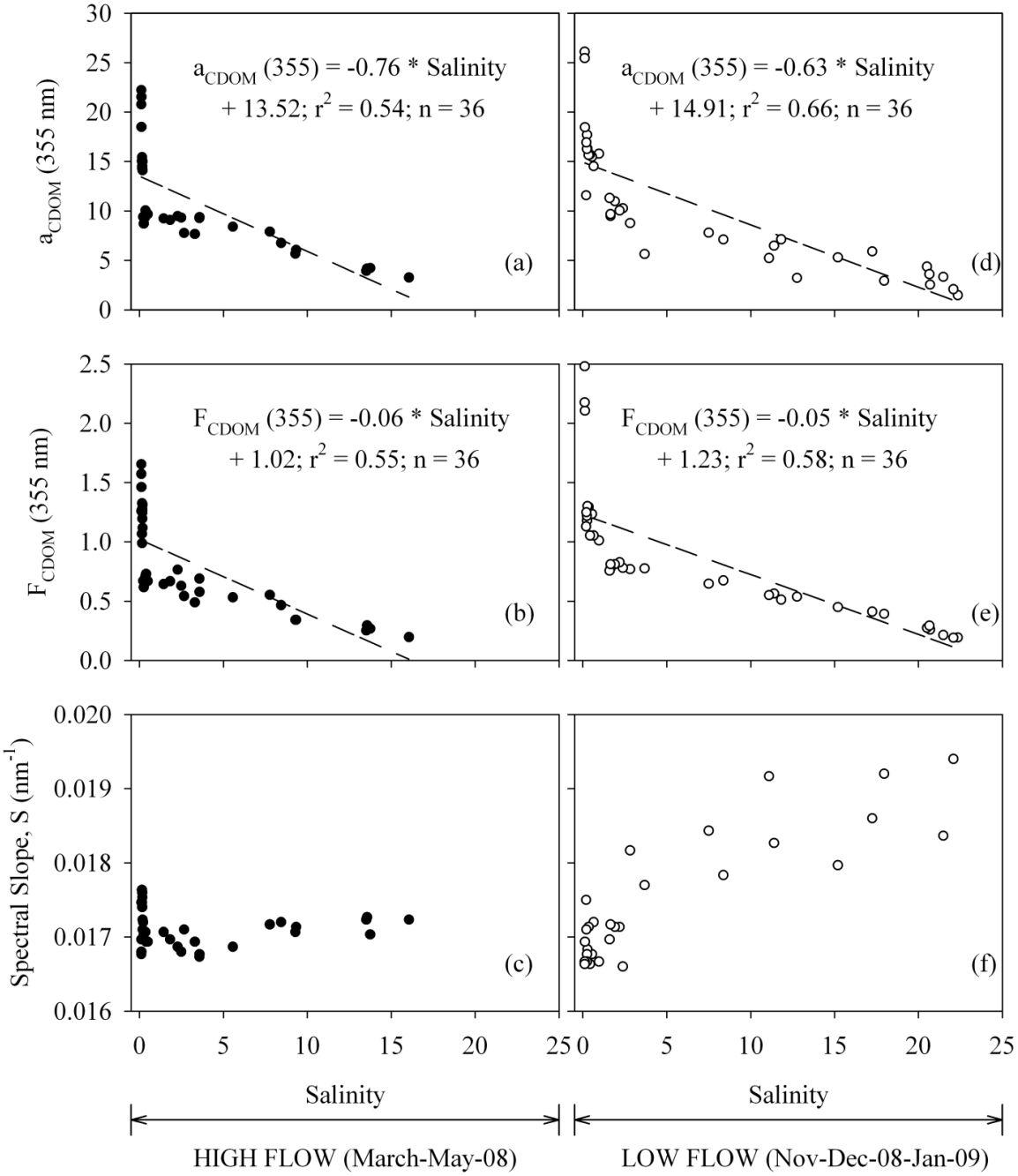

Figure 3.6 (a) Mean variation in March, April, and May 2008 of (a) CDOM absorption (m^{-1}) measured at λ = 355 nm, (b) Mean CDOM fluorescence (RU) maximum emission intensity calculated at excitation wavelength, λ_{ex} = 355 nm, (c) Mean CDOM spectral slope, S (nm^{-1}) during high flow conditions. (d), (e), and (f) are corresponding mean variations during low flow conditions plotted against salinity.

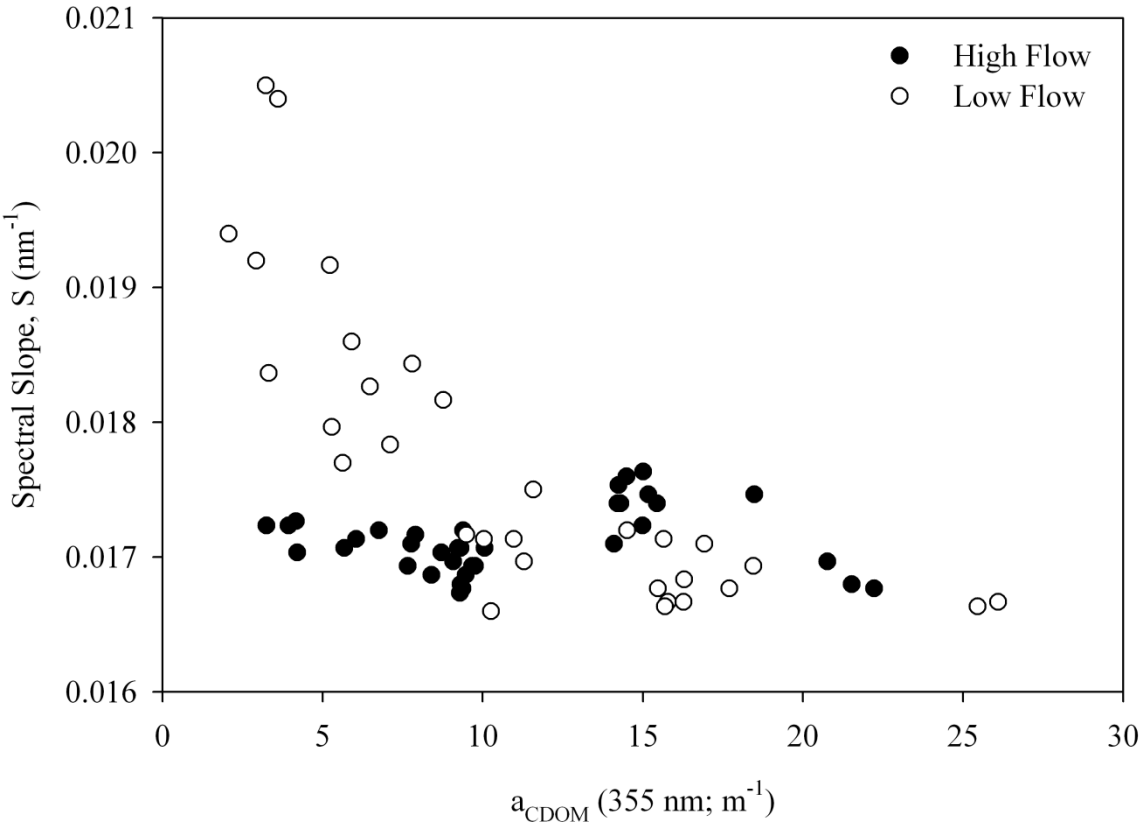

Figure 3.7 Mean Spectral slope coefficients, S (nm^{-1}) calculated in the range 300-500 nm, during high flow and low flow conditions plotted against mean CDOM absorption (m^{-1}) values. Filled circles denote high flow data points while empty circles are representative of low flow conditions.

3.3.4. Fluorescence Peaks Transect Variability

The seasonal variation of peaks (A-peak, C-peak, M-peak, and T-peak) along the transect have been plotted in Figs. 3.8a and 3.8b and shown in Table 3.2. These peaks were calculated by integrated area calculation using the FLToolbox and plotted against the transect stations. A-peaks were observed as having highest concentrations during both high and low flow conditions while T-peaks were having lowest concentrations. C and M-peaks are closely following each other and are showing similar trend of increasing concentrations from station 1 to station 36 (Fig. 1.3). Differences in peaks concentrations were observed during the two seasons with higher variability in high flow conditions for A-peak (Fig. 3.8a; Table 3.2). In the upper Barataria Basin, the variability of peaks concentration is more pronounced than that observed for the lower Barataria Basin during both high and low flow conditions. During low flow conditions, a small increasing trend in T-peak is observed in the upper part of the transect suggesting some kind of algal productivity at these locations (stations 34, 35, and 36; Fig. 1.3) (Fig. 3.8b; Table 3.2).

Peak ratios of A/C have been calculated for high and low flow seasons and were found to be generally decreasing upstream along the transect. The observed decrease in peak A/C ratio suggests the influence of terrestrial sources with increase in C-peak (also a terrestrial humic peak) upstream and lower values of A-peak upstream which is usually more prominent with distance from terrestrial influences. Although, A-peaks are ubiquitous in every environment, its

correlation with C-peaks is a good precursor to examine terrestrial impacts in a region. In this study, the A/C ratio reported during low flow season is found to be fairly correlated with station locations ($r^2 = 0.56$) while it is insignificant to report for high flow conditions ($r^2 = 0.39$) (plots not shown here).

3.4. Discussion

3.4.1. Seasonal Variability of CDOM Absorption and Fluorescence

CDOM absorption and fluorescence were found to be similar during both seasons, i.e., increasing concentration from station 1 to station 36 (Figs.1.3, 3.2c, and 3.2d) with some expected trends in different parts of the transect. The upper Barataria Basin showed high variability in CDOM absorption during low flow season while the lower Barataria Basin during high flow season. This difference may be due to the high runoff and precipitation in the upper part of the transect during high flow conditions which lowered the CDOM concentration in the upper part. Moreover, the tidal influence at these locations is also minimal (Kirby and Gosselink, 1976) during high flow conditions. In high flow conditions, the excess water of Mississippi River during high stages is flushed through discharge from Davis Pond Diversion above Lake Cataouache (Fig. 1.3) that could cause the sheet flow in the upper Barataria Basin and hence a reduction in the concentration of CDOM in the upper Barataria Basin. Due to larger surface area, this flow could be distributed over larger areal extent and thereby reduced CDOM concentration.

CDOM fluorescence values observed in the transect during both, high and low flow seasons also showed similar variability as observed for the CDOM absorption. An increasing trend of CDOM fluorescence is observed from station 1 to station 36 (Fig. 3.2d) during the two flow seasons. In the lower Barataria Basin, CDOM fluorescence varied similarly in both, high and low flow conditions, with slightly higher values for high flow conditions (similar to CDOM absorption).

The CDOM fluorescence variability during high and low flow conditions is also shown by Figs. 3.3 and 3.4. The observed values for CDOM fluorescence are higher in the lower Barataria Basin during high flow conditions as shown for station 1 and are lower in the lower Barataria Basin during low flow conditions (Fig. 3.3). During low flow conditions, the observed CDOM fluorescence variability in the upper Barataria Basin (station 36) is higher in comparison to CDOM fluorescence variability observed at station 36 during high flow conditions (Fig. 3.4).

The calculated CDOM absorption is compared with few other studies performed in similar environments and are shown in Table 3.3. CDOM absorption estimated for the Barataria Basin during high flow conditions at station 1 (3.25 ± 0.56 m^{-1}) are similar to lowest reported value in the study of Lake Taihu (2.20 m^{-1}) (Zhang et al., 2007) and at station 36 (20.76 ± 2.43 m^{-1}) close to 33.70 m^{-1} reported by Green and Blough (1994) for the Amazon River Estuary measured at 355 nm. The lowest value (1.48 ± 1.08 m^{-1}) observed in low flow conditions at station 1 is close to the lowest reported by Ferrari and Dowell (1998) in coastal areas of the Southern Baltic Sea (1.40 m^{-1}) to 25.45 m^{-1} ($\pm$ 7.03) at station 36 which is again close to the Amazon River Estuary reported value (33.70 m^{-1}) by Green and Blough (1994) (Table 3.3).

This study also compared the CDOM absorption reported by several authors in Table 3.3 and found that on the basis of this variability, we may conclude the observed diversity in the Barataria estuarine region. This large variability in CDOM absorption values also suggests the highly complex nature of the Barataria Basin water bodies ranging from small lakes to estuarine region with influence of the Gulf waters on its coastal boundaries.

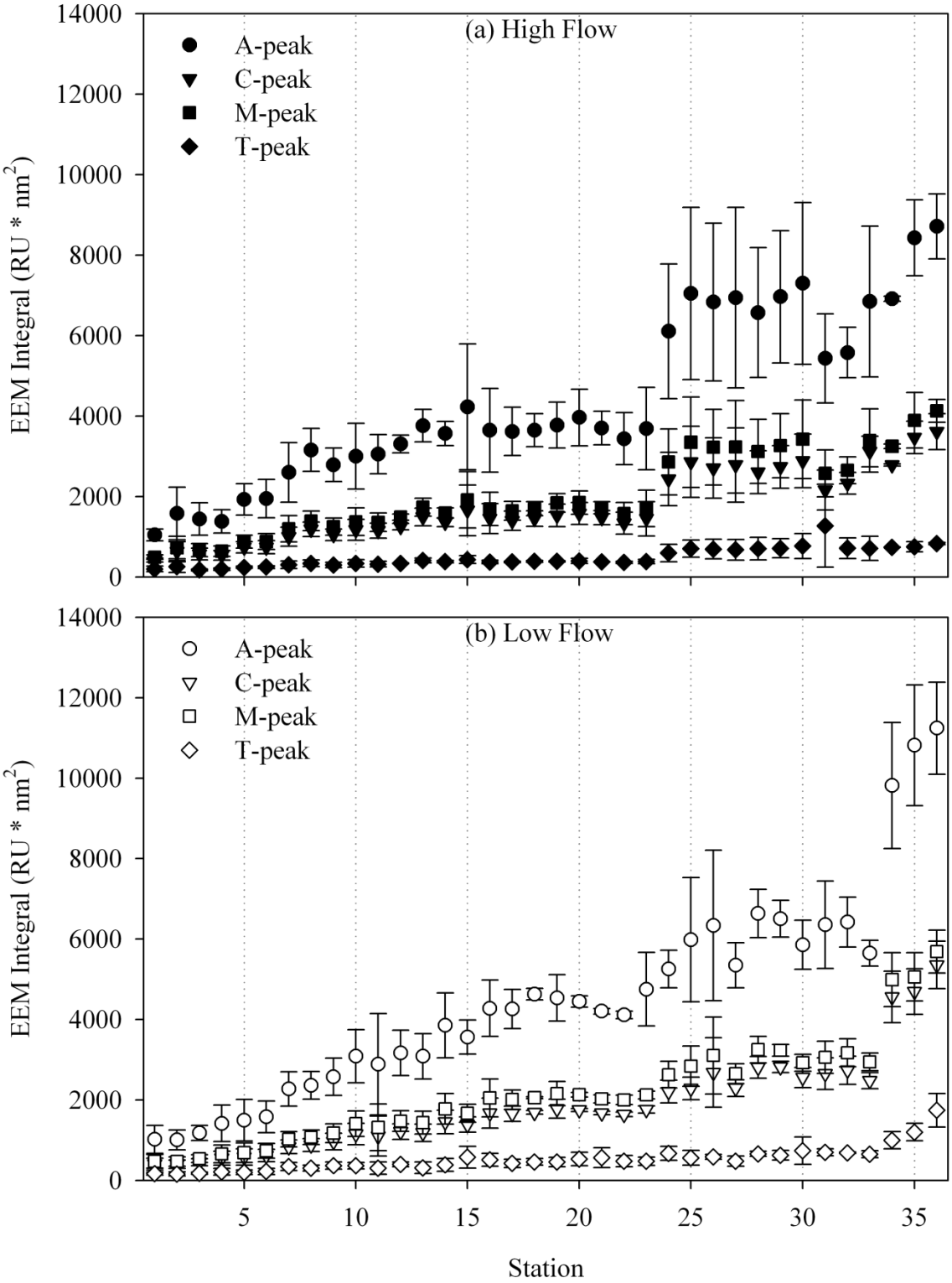

Figure 3.8 Mean integrated area (RU*nm^2) calculated using FLToolbox for respective fluorescence peak values during (a) high flow conditions, and (b) low flow conditions; along the stations in the Barataria Basin transect. Filled circles represent A-peaks, empty circles represent C-peak, filled inverted triangle represents M-peak, and empty triangle represent T-peak. Standard deviations from the mean values are shown by bars in plots.

Table 3.2 Mean fluorescence peaks variation measured from the total integrated scanned area under respective peaks using FLToolbox along the Barataria Basin transect during high and low flow conditions. Here, peak designations are as same defined by Coble (1996) (refer text).

	Mean A-peak		Mean C-peak		Mean M-peak		Mean T-peak	
Stations	**HF**	**LF**	**HF**	**LF**	**HF**	**LF**	**HF**	**LF**
Station 1	1043.24	1020.74	414.21	405.68	490.21	478.19	196.88	168.68
Station 2	1576.05	1007.92	625.93	403.98	727.58	472.83	253.46	162.07
Station 3	1438.56	1183.14	568.15	454.35	666.00	543.96	173.48	181.63
Station 4	1376.33	1419.18	535.49	553.71	636.46	661.34	192.25	214.08
Station 5	1925.64	1497.63	738.64	582.77	877.35	691.25	239.36	201.92
Station 6	1943.52	1582.50	737.04	621.67	878.10	736.27	244.07	225.08
Station 7	2597.67	2274.32	999.90	835.90	1194.03	1024.64	300.45	349.39
Station 8	3155.58	2362.76	1182.77	878.40	1390.88	1073.38	337.94	306.87
Station 9	2784.93	2578.28	1045.27	966.96	1248.88	1176.21	297.01	370.41
Station 10	2999.69	3088.46	1169.23	1155.66	1369.82	1412.14	335.49	369.57
Station 11	3053.28	2887.86	1147.55	1101.32	1355.22	1317.69	319.93	307.37
Station 12	3303.32	3169.94	1249.07	1213.32	1484.60	1474.86	337.34	400.20
Station 13	3758.99	3085.73	1489.91	1186.09	1732.13	1438.68	411.41	315.81
Station 14	3565.45	3856.76	1356.30	1453.10	1587.72	1777.86	380.04	388.99
Station 15	4225.54	3561.64	1652.48	1389.50	1915.17	1671.57	431.49	579.41
Station 16	3645.95	4279.29	1446.89	1674.54	1688.37	2050.86	371.85	513.24
Station 17	3613.02	4261.46	1394.70	1658.18	1641.25	2010.62	373.51	425.09
Station 18	3645.59	4629.98	1447.56	1691.30	1695.72	2059.89	385.64	462.23
Station 19	3773.37	4537.17	1527.86	1783.27	1839.67	2160.60	385.69	458.99
Station 20	3960.20	4446.54	1573.77	1752.29	1845.37	2130.96	396.94	533.69

Table 3.2 continued….

	Mean A-peak		Mean C-peak		Mean M-peak		Mean T-peak	
	HF	**LF**	**HF**	**LF**	**HF**	**LF**	**HF**	**LF**
Station 21	3699.35	4204.11	1469.60	1675.42	1718.05	2026.66	374.80	564.60
Station 22	3435.71	4115.47	1334.57	1643.78	1572.75	2003.03	363.19	481.70
Station 23	3687.33	4751.15	1445.40	1763.42	1701.50	2124.29	383.72	478.11
Station 24	6102.39	5254.66	2430.46	2210.21	2856.31	2627.41	592.74	674.31
Station 25	7043.58	5982.97	2857.60	2288.46	3344.69	2840.38	700.82	563.05
Station 26	6831.09	6338.09	2706.99	2683.15	3223.66	3106.34	690.66	589.58
Station 27	6939.94	5345.21	2780.37	2294.45	3230.20	2653.25	672.01	480.95
Station 28	6567.81	6635.44	2602.47	2811.29	3117.52	3250.09	702.54	661.83
Station 29	6961.28	6502.30	2733.98	2822.11	3260.40	3235.00	711.71	625.83
Station 30	7296.35	5859.20	2884.68	2558.29	3421.00	2924.08	765.84	742.43
Station 31	5428.93	6355.42	2159.61	2653.95	2572.28	3060.64	1271.65	698.71
Station 32	5575.28	6420.85	2327.99	2739.04	2648.33	3173.29	714.98	690.01
Station 33	6842.62	5646.86	3117.48	2480.06	3388.05	2946.54	709.07	654.34
Station 34	6912.53	9814.47	2781.61	4557.59	3246.61	4991.24	739.50	1003.33
Station 35	8427.98	10814.05	3466.66	4694.18	3891.06	5059.79	747.00	1203.70
Station 36	8712.48	11240.13	3611.01	5355.83	4127.47	5685.55	830.55	1744.85

*HF is High Flow season during March, April, and May months.

#LF is Low Flow season during November, December, and January months.

Table 3.3 Absorption coefficients (m^{-1}) and spectral slopes (nm^{-1}) of CDOM calculated in some estuarine and coastal waters in the world and from this study (extended from Hong et al., 2005). In this study, the absorption and spectral slope coefficients were obtained from mean values during high and low flow conditions (refer text).

Region	Salinity Range	a_{CDOM} (355 nm)	S (nm^{-1})	Reference
Amazon River Estuary	15.10 – 36.40	0.14 – 3.12	0.0150 – 0.0330	Green and Blough (1994)
Tamiami River	-	33.70	0.0170	Green and Blough (1994)
Southern Baltic Sea (coastal areas)	2.00 – 8.00	1.40 – 12.80	0.0186 – 0.0200 (355 - 420 nm)	Ferrari and Dowell (1998)
Gulf of Lions (near Rhone river mouth)	33.50 – 38.20	0.05 – 1.71 (350 nm)	0.0110 – 0.0280 (350 – 480 nm)	Ferrari (2000)
Chesapeake Bay (April)	~ 13.00 – 33.00	0.40 – 2.20	0.0175 – 0.0208 (350 – 400 nm)	Rochelle-Newall and Fisher (2002)
Chesapeake Bay (October)	~ 5.80 – 27.00	0.70 – 2.10	0.0194 – 0.0217 (350 – 400 nm)	Rochelle-Newall and Fisher (2002)
Pearl River Estuary, China (July)	0.00 – 34.96	0.34 – 1.40	-	Chen et al. (2004)
Pearl River Estuary, China (November)	0.00 – 32.49	0.24 – 1.93	0.0138 – 0.0184 (300 – 500 nm)	Hong et al. (2005)
Lake Taihu, China	-	2.20 – 8.60	0.0127 – 0.0190 (280 – 500 nm); 0.0122 – 0.0174 (360 – 440 nm)	Zhang et al. (2007)
Doubtful Sound, New Zealand (May)	4.70 – 25.90	1.00 – 12.90	0.0150 – 0.0160 (280 -700 nm)	Gonsior et al. (2008)
Barataria Basin, USA	0.10 (± 0.005) – 16.07 (± 5.78) (High Flow)	3.25 (± 0.56) – 20.76 (± 2.43)	0.0167 (± 0.0000) – 0.0176 (± 0.0008) (300 – 500 nm)	This Study
Barataria Basin, USA	0.10 (± 0.015) – 22.34 (± 7.46) (Low Flow)	1.48 (± 1.08) – 25.45 (± 7.03)	0.0118 (± 0.0003) – 0.0205 (± 0.0111) (300 – 500 nm)	This Study

*Standard deviations from mean values are given in brackets.

3.4.2. CDOM Absorption and Fluorescence Variability with Salinity

The CDOM absorption and fluorescence with salinity appear conservative during both, high and low flow, conditions in most part of the transect with few exceptions at stations in the upper Barataria Basin (Figs. 3.6a, 3.6b, 3.6d, and 3.6e). The regression equations obtained for CDOM absorption [a_{CDOM} (355 nm) = -0.76 * salinity + 13.52; r^2 = 0.54] and fluorescence [F_{CDOM} (355 nm) = -0.06 * salinity + 1.02; r^2 = 0.55] during high flow conditions are fairly consistent with the observed regression equations during low flow conditions for CDOM absorption [a_{CDOM} (355 nm) = -0.063 * salinity + 14.91; r^2 = 0.66] and fluorescence [F_{CDOM} (355 nm) = -0.05 * salinity + 1.23; r^2 = 0.58] with slightly better correlations obtained during low flow conditions. This also suggests the acceptable use of fluorescence measurements over absorption measurements for CDOM analysis which discussed later (Fig. 3.9). This study supported the reported results relating to the accuracy and preciseness of fluorescence measurements over absorption which could provide more information in terms of variability of constituents of water sample in question and should be more adaptable for CDOM analysis in the study of complex estuarine environments such as the Barataria Basin.

During low flow conditions, the results obtained for spectral slope, S variation with salinity (Fig. 3.6f) and with a_{CDOM} (355 nm) (Fig. 3.7) are better than those obtained during high flow conditions (Figs. 3.6c and 3.7). This also suggest that during low flow conditions the natural pattern of S variability is observed in this study in which S is increasing upstream (wetland areas) away from the coastal region. This is also consistent with increase of S with increasing salinity as reported by previous researchers in similar estuarine or coastal environments (Table 3.3). The lowest values for S reported in this study during low flow conditions (0.0118 ± 0.0003 nm^{-1}) is similar to the lowest value reported by Ferrari (2000) in Gulf of Lions (near Rhone River mouth) with S calculated in the range of 350-480 nm whereas, the interval range in this study for S calculation is chosen as 300-500 nm (Table 3.3). The highest S value reported in this study for low flow conditions (0.0205 ± 0.0111 nm^{-1}) are close to the highest reported value by Ferrari and Dowell (1998) for coastal areas of Southern Baltic Sea calculated in the interval of 355-420 nm. Although the S value varies with the choice of wavelength interval selection, it is assumed for comparisons of values to other regions that change in S values are not significant in Table 3.3. Results of spectral slope calculated in this study is comparable to the values obtained by Hong et al., (2005) as having same spectral slope calculation range in a study done for Pearl River estuary, China.

In this study, during high flow conditions, S computation does not show a specific pattern. Moreover, the S values are scattered during the high flow conditions and ranged between (0.0167 ± 0.0000 nm^{-1}) to (0.0176 ± 0.0008 nm^{-1}) with slight variation in lowest and highest values and less pronounced variation observed during low flow conditions ranging from (0.0118 ± 0.0003 nm^{-1}) to (0.0205 ± 0.0111 nm^{-1}) (Figs. 3.6c, 3.6f, and 3.7; Table 3.3).

3.4.3. Seasonal Fluorescence Peak Variability along the Transect

The fluorescence peaks A, C, M, and T also showed results similar to fluorescence calculated at 355 nm, during high flow and low flow conditions at stations 1 and 36, respectively. Peaks observed at station 1 are having more prominent visible features during high flow conditions whereas peaks observed during low flow conditions at station 36 are visibly more pronounced (Figs. 3.3 and 3.4). The M and C peaks responsible for terrestrial influence from urban runoff and agricultural wastes are clearly distinguishable for low flow conditions at station 36 whereas

they are visibly absent in high flow conditions at station 36. Figs. 3.8a and 3.8b also support the differences observed for seasonal variations in respective peaks with high variability in the upper Barataria Basin for A-peak during high flow conditions and a small observable peak variation for T-peak in the upper Barataria Basin during low flow conditions. This variability could be attributed to the degree of humification and increased algal productivity in the upper Barataria Basin mainly comprised of the eutrophic Lake Des Allemands (Fig. 1.3). Also, the sources primarily derived from lowland swamp forests and fresh marshes in this part of the transect could contribute to the elevated levels of humic materials during high flow conditions.

The observed good correlation for A/C peak ratio during low flow conditions could be explained by increased C peak intensities relative to the increase in A peak intensities along the transect from station 1 (near the mouth of the basin) to station 36 (end station upstream). This supports the increased terrestrial influence in the upper Barataria Basin during low flow conditions due to urban runoff or runoff from nearby agricultural farms adjacent to marsh areas upstream. However, the observed lower varibility in A/C peak ratios during high flow season could well be explained by high runoff from discharge that could be flushing out the terrestrial mateerial in downstream part of the transect and the organic matter that could be transported along the transect with the flow. Moreover, increased precipitation could be another hydrographic input causing to lower the peak ratio variability during high flow season.

3.4.4. CDOM Absorption and Fluorescence Relationship

Seasonal relationship between mean absorption coefficient and fluorescence intensity values for CDOM at 355 nm wavelength are shown in Fig. 3.9 during both, high and low flow conditions. The observed high correlation between CDOM absorption and fluorescence during both, high and low flow conditions suggests the use of more precise fluorescence measurements as a better proxy for CDOM concentrations in the Barataria Basin over absorption measurements. The correlation between CDOM absorption and fluorescence is slightly better in high flow (r^2=0.93) conditions than that obtained for low flow (r^2=0.90) conditions. In both, high and low flow conditions this relationship is more acceptable in the lower Barataria Basin than in upper part of the Barataria transect. The regression equations for CDOM absorption and fluorescence during high and low flow conditions are given in Fig. 3.9 and are independent of CDOM sources whether autochthonous origin or allochthonous sources and their chemical characteristics. There are some scattered points in low flow conditions in regression analysis while during high flow conditions much better regression values are observed.

In earlier studies, Vodacek and Blough (1997) have examined a relationship between CDOM absorption and fluorescence measurements done for surface water samples collected from Delaware bay and Sargasso Sea and have found a positive linear relationship with regression equation as a_{CDOM} (355) = 0.243 * F_{CDOM} (355) + 0.055; r^2=0.94. They indicated that the relationship could not be affected by distinct sources as well as variable chemical characteristics of the water samples. Later on, to establish an useful relationship between CDOM absorption and fluorescence measurement which could lead to increased use of fluorescence measurements in comparison to absorption, Ferrari and Dowell (1998) made an attempt to successfully acquire a regression equation as a_{CDOM} (355) = 0.124 (± 0.005) * F_{CDOM} (355) + 0.46 (± 0.059) (r^2 = 0.97) in a study of coastal regions of Southern Baltic Seas. They not only derived the equation for the coastal regions, but also worked in several other environments using two different forms of the regression equations. Recently, Zhang et al. (2007) conducted a similar study to examine a relationship between CDOM absorption and fluorescence at 355 nm in a shallow subtropical lake

Taihu, China and found a positive relationship with a regression equation as a_{CDOM} (355) = 3.72 (± 0.43) * F_{CDOM} (355) + 2.12 (± 0.33) (r^2=0.66) irrespective of sources of CDOM in the study region. Our study also supports the use of fluorescence measurements over absorption that could explain more variability in CDOM concentrations with increased sensitivity and precision.

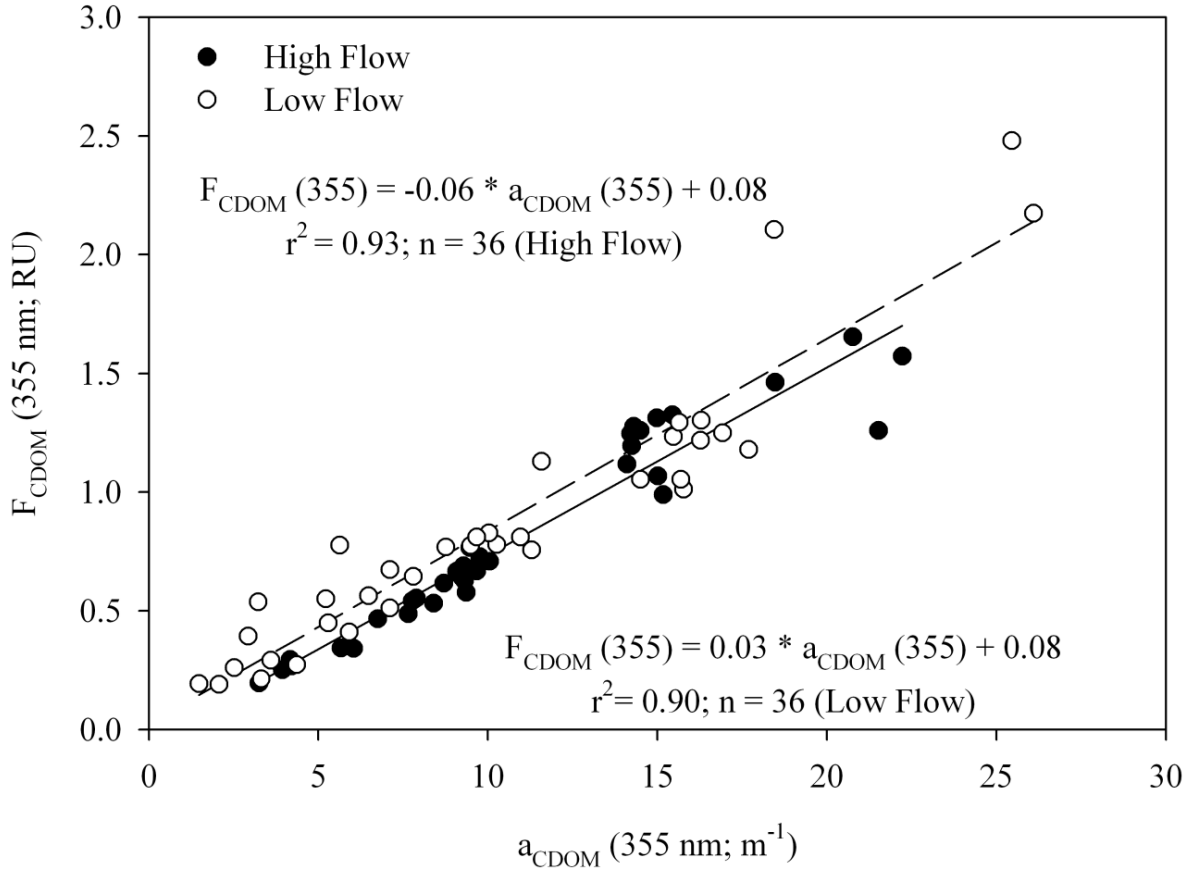

Figure 3.9 Correlations between mean CDOM absorption (m^{-1}) and fluorescence (RU) measured at 355 nm are plotted for all the stations during high and low flow conditions. The regression equations, correlation coefficients (r^2), and the number of samples (n) are shown in the plot. The filled circles represent high flow conditions, and empty circles represent low flow conditions.

3.4.5. Fluorescence and Humification Indices

The fluorescence and humification indices were calculated for high and low flow seasons along the transect according to previously described methods (see method section). In general, a negative relationship between fluorescence index (FI) and humification index (HIX) is observed along the stations upstream from the mouth of the basin at station 1 (Fig. 1.3). The FI and HIX were plotted against the stations noticed during both high and low flow conditions (plots not shown here). Mean values for FI during low flow conditions were calculated ranging from 1.35 (lowest at station 13) to 1.40 (highest at stations 1 and 34) while for HIX, the mean values were varying from 7.01 (lowest at station 1) to 13.63 (highest at station 27). Similarly, during high flow conditions, mean values calculated for HIX ranged from 7.35 (lowest at station 1) to 13.99

(highest at station 35) in comparison to FI calculated during high flow conditions varies from 1.34 (lowest at station 33) to 1.42 (highest at station 4).

The observed general trend for both, FI (decreasing trend along the stations upstream) and HIX (increasing trend along the stations upstream) were better during high flow conditions than that during low flow conditions, especially in the upper Barataria Basin where unexpected reduced humification is observed during low flow conditions. Similarly, increased FI mean values were observed in the upper Barataria Basin during low flow conditions suggesting the occurrence of microbial activity in this part of the transect which could be lowering the degree of humification at these locations. During high flow conditions, the general increasing trend for HIX and an expected decreasing trend of FI were observed supporting an increase in degree of humification as well as a decrease in microbial activity in the upper Barataria Basin. Briefly, HIX were more consistent than FI values during both high and low flow conditions and should be more suitable to study a complex estuarine environment similar to the Barataria Basin. Further, statistical analyses using student's paired t-test (using SigmaPlot ver. 10.0, Systat Software Inc. © 2006; at a significance level, p-value = 0.05) were done to identify whether FI and HIX were significantly different during the flow conditions and were found statistically significantly different for different flow conditions (p-value < 0.0001; for both FI and HIX) which also supported the observed difference in HIX during low flow conditions in the upper Barataria Basin with reduced degree of humification.

3.5. Conclusion

CDOM absorption and fluorescence properties have been analyzed in this study during high and low flow conditions to observe the seasonal variability and have not been found significantly different even though the hydrographic variables, (i.e., salinity and temperature) were significantly different during the flow conditions. These results suggest that there was no observed seasonal variability in humic material constituents in the Barataria Basin during various flow conditions. Further, these findings show that transport of organic material from upstream to downstream varies along the transect. Flushing of organic matter downstream during high flow conditions and intrusion of highly saline water during low flow conditions could be responsible for the observed variability in the organic matter budget in the Barataria Basin. The upper Barataria Basin might show more seasonal variability than the lower Barataria Basin if analyzed separately over a longer period which could be an extension of this work in future studies. This is evident from the estimation of humification and fluorescence indices; however, fluorescence index may not provide a better understanding in characterizing CDOM sources than humification indices in such complex estuarine environments as Barataria Basin. The peak ratios obtained for two humic like fluorophores (peaks A and C) to verify terrestrial influence along the transect, were found to give better results during low flow conditions. Further, an empirical relationship between CDOM absorption and fluorescence were developed for both high and low flow conditions in the Barataria Basin which could be used to trace organic matter sources using rapid and sensitive fluorescence measurements in comparison to absorption measurements.

Chapter 4

Chromophoric Dissolved Organic Matter (CDOM) Variability in Barataria Basin (USA) Using Excitation-Emission Matrix (EEM) Fluorescence and Parallel Factor Analysis (PARAFAC)

4.1. Introduction

Chromophoric dissolved organic matter (CDOM) is defined as the light absorbing component of total dissolved organic matter (DOM) that absorbs light in the ultraviolet and visible range of the electromagnetic spectrum. It is also known as gelbstoff, gilvin, and yellow substance (Coble, 1996; Del Vecchio and Blough, 2004; Kirk, 1994). CDOM together as humic and fulvic acids, represents 70% of the total dissolved organic material which contribute to light absorption and fluorescence by non-chlorophyllous material in a coastal region (Nieke et al., 1997). Changes in the CDOM absorption and fluorescence reflect the variations in CDOM composition from several autochthonous or allochthonous sources resulting from physical, biological, and chemical processes that occur in the water column (Coble, 1996; McKnight et al., 2001; Stedmon et al., 2007). CDOM is measured based on the intensity of absorption of light or fluorescence emission as a function of wavelength. Moreover, it shows a featureless absorption spectrum that increases exponentially from visible to UV with decreasing wavelength. Spatial and temporal distribution of CDOM in aquatic ecosystems can negatively affect ecosystem productivity. Since CDOM absorbs light, it positively impacts secondary productivity by providing a substitute for microbial respiration via photo-degraded CDOM (Del Vecchio & Blough, 2006). Spectral measurements of CDOM absorption and fluorescence provides useful information of CDOM source and have been used to study water-mass mixing in the bays (D'Sa et al., 1999; Rochelle-Newall and Fisher, 2002), estuaries (Stedmon et al., 2006), rivers (Spencer et al., 2007), coastal waters (D'Sa and Miller, 2003; D'Sa et al., 2006; D'Sa, 2008) and oceans (Coble et al., 1998) as CDOM serves as a tracer to examine transport and mixing processes.

Fluorescence spectroscopy technique using excitation-emission matrices (EEMs) (Coble et al., 1990) has been widely used to characterize and identify DOM in various natural waters in oceans and dynamic estuarine environments (Coble 1996, 1998; McKnight et al. 2001). To overcome the difficulty in identifying individual fluorescent components in a water sample and to compare dissolved organic matter characteristics in different regions, statistical tools such as principal component analysis (PCA) (Boehme et al., 2004) and parallel factor analysis (PARAFAC) (Cory and McKnight, 2005; Kowalczuk et al., 2009; Stedmon et al., 2003) have been widely used.

The EEMs in conjunction with PARAFAC have been used to trace photochemical and microbial reactions with organic matter (Cory and McKnight, 2005; Stedmon and Markager, 2005b), in water source categorization (Hua et al., 2007), and correlation with water quality parameters (Holbrook et al, 2006). It has recently been applied to characterize colored dissolved organic matter in lakes (Cory and McKnight, 2005; Hiriart-Baer et al., 2008; Zhi-gang et al., 2007), estuaries (Stedmon et al., 2003, 2005a), rivers (Hua et al., 2007), bays (Luciani et al., 2008; Yamashita et al., 2008), wetlands (Fellman et al., 2008; Holbrook et al., 2006), and in oceans (Murphy et al., 2008; Wedborg et al., 2007). PARAFAC modeling provides unique solution to dissolved organic matter EEM dataset and is argued as an important analytical tool to characterize the CDOM in complex coastal regimes. Two primary fluorescing groups in dissolved organic matter studies have been identified as humic-like and protein-like substances. Humics are complex mixture of aromatic and aliphatic compounds derived from decay of organic matter while protein-like substances are due to high biological activity. Humic substances are further characterized by humic acids and fulvic acids mainly differentiated on the basis of their solubility (Harvey et al., 1985). Humic acids are dominated by aromatic compounds whereas fulvic acids are characterized by the dominance of aliphatic content. The presence of protein-like substances generally implies autochthonous production of CDOM and

presence of microbial activity (Stedmon et al., 2007). PARAFAC modeling aids to resolve these two classes of fluorophores efficiently and indicates the dominance of particular class in an environment.

The Barataria Basin is a complex, well-mixed, and turbid water system characterized by high input of fresh water from different water bodies such as large lakes, streams and artificial water diversions. The Barataria Basin is located east of Bayou Lafourche and west of the Mississippi River delta and is separated from the Gulf of Mexico in the south by the Grande Terre Islands and bounded by the Mississippi River in the north. Swamp forests and marshes characterize the nature of the Barataria Basin which is isolated from the Mississippi River due to levee construction since the 1930s (Mossa, 1996), reconnected later by Davis Pond Diversion. Previous studies of naturally occurring wetlands in the Barataria Basin have shown the impacts of modifications by artificial diversions (Swenson et al., 2006), discharge from Mississippi River responsible for algal derived organic matter (Wissel et al., 2005) and canal dredging (Sasser et al., 1986) which is altering the natural habitat (Craig et al., 1989; Jones et al., 2002) as well as water quality (Conner and Day Jr., 1987; Happ et al., 1977; Wissel et al., 2005) of the region. A few studies have examined carbon and nitrogen flow in the Barataria Basin in order to estimate the carbon and nitrogen inputs through the basin to the Gulf of Mexico (Castro et al., 2003; Feijtel et al., 1985; Happ et al., 1977). Recent modeling of estuarine shelf exchanges in the Barataria Basin has however shown that it is a very small source of total organic carbon to the northern Gulf of Mexico (Das et al., 2009). Marsh derived soil organic matter from the Barataria Basin is also estimated to contribute to the total organic carbon pool through resuspension of unconsolidated sediments that is then exported towards adjacent Louisiana shelf waters (Sampere et al., 2008).

The objective of the present study is to characterize the fluorescent portion of CDOM in the Barataria Basin using field data during a high flow season (Fig. 1.3) and examine effects from different water bodies such as lakes and local runoff, and contribution from wetlands and agricultural sources. To our knowledge, this is the first detailed study on the spatio-temporal variability of CDOM, and its spectro-chemical characteristics identified using EEM and PARAFAC approach. We have reported here the compositional distribution and variation of CDOM in the Barataria Basin, the causative factors for the observed distributions and the possible sources of CDOM. Sample scores obtained from PARAFAC analysis have been used for tracing the probable sources along an axial transect in the Barataria Basin.

4.2. The PARAFAC Model

PARAFAC statistically decomposes the three-way data into individual fluorescence components or moieties. Bro (1997) has demonstrated the uniqueness of PARAFAC decomposition method to reduce an EEM into trilinear term and a residual array.

$$X_{ijk} = \sum_{n=1}^{F} a_{in} b_{jn} c_{kn} + \varepsilon_{ijk}$$

where, for EEM fluorescence data, X_{ijk} is the fluorescence intensity of the i^{th} sample at the kth excitation and jth emission wavelength. a_{in} is directly proportional to the concentration (e.g., moles C; here defined as scores) of the nth fluorophore in the ith sample. b_{jn} and c_{kn} are estimates of emission and excitation spectra (loadings) of nth fluorophore at wavelength j and k respectively. Also b_{jn} and c_{kn} are linearly related to the fluorescence quantum efficiency and

specific absorption coefficient respectively (Kowalczuk et al., 2009). F is the number of components (fluorophores) and ε_{ijk} the residual matrix of the model which represents unexplained variability by the model. Holbrook et al. (2006) suggested that individual components from a large complex EEM dataset can be identified provided the correct number of components was chosen after outliers were removed with preliminary examination of dataset. PARAFAC model identifies the number of components as well quantifies the scores for each component that is directly proportional to the component's (fluorophore) concentration in the sample. This score can be converted into actual concentration provided specific absorption coefficient of each fluorophore is known. The other method to obtain actual concentration of a component could be a calibration approach based on a known concentration (Stedmon et al., 2003).

4.3. Methods

4.3.1. Sampling Site

The Barataria Basin system is made up of biologically rich and productive habitats including swamps, fresh, brackish, and saline marshes, bayous, bays, and barrier islands. Barataria Basin is an irregular shaped basin covering 1,673 km^2 surface area and 5,700 km^2 of drainage area with an average depth of 2.0 meter (Fig. 1.3). The average daily fresh water inflow into the basin is approximately 156 $m^3 s^{-1}$ with an average salinity of 13. The main freshwater sources for the Barataria Basin includes rainfall, local run-off, Intracoastal waterway that delivers water from Atchafalaya river during high flow conditions to Mississippi River, and diversions from Davis Pond with a design-pumping rate of 300 $m^3 s^{-1}$, Naomi and West Pointe A la Hache with a maximum pumping rate of 60 $m^3 s^{-1}$ at each site, and Port Sulphur. Apart from these freshwater sources, numerous major and minor point discharges, septic tanks, sewage/storm water overflow, unsewered communities, pasturelands, and marshes contribute to changes in water quality of the basin (Conner and Day Jr., 1987). Although the salinity signals are highly coherent with Mississippi River discharge, these point sources can significantly contribute to a decrease in the average salinity of the basin region as reported in previous literature (Inoue et al., 2008; Swenson et al., 2006). The period of high river flow in spring, and high water residence time, typically 12 to 35 days (Wissel et al., 2005) could account for the variable CDOM concentrations in the study area. A detail description of the Barataria Basin system is reported by Das et al., (2009).

4.3.2. Collection of Water Samples

Surface water samples were collected at 36 stations (Fig. 1.3) located along a 124 km transect (South-East to North-West) from the mouth of the Barataria Basin (station 1) in the Gulf of Mexico to the north-west end of the upper Barataria Basin (station 36) during monthly field trips in March, April, and May 2008. These samples were brought back to the laboratory and immediately filtered using pre-rinsed 0.2 micron nucleopore membrane filters. The filtered samples were kept in a refrigerator for optical absorption and fluorescence analyses. The tap water was treated by a Barnstead Nanopure® Model D-50280 purification system with purity of 18.2 MΩ Milli-Q. Salinity profiles were recorded using a handheld YSI. Distribution of surface salinity, CDOM absorption (measured at 355 nm), and CDOM fluorescence (measured as maximum emission fluorescence intensity obtained at excitation wavelength, λ_{ex} = 355 nm) was also measured. Humification Index (HIX) (Zsolnay et al., 1999) was calculated by dividing the

integrated area of fluorescence intensity measured between emission wavelength of 435 and 480 nm by the integrated area of fluorescence intensity measured between emission wavelength of 300 and 345 nm with excitation at 254 nm.

4.3.3. Absorption Spectroscopy

The surface water samples were allowed to reach room temperature and the instrument was kept on for 30 minutes before the sample analysis. Absorption spectra were obtained between 190 and 750 nm at 2-nm intervals using Perkin Elmer Lambda 850 double-beam spectrophotometer equipped with 1 cm path-length quartz cuvette (volume of 4 ml) and 150 mm spectralon coated integrating sphere. The data were corrected for scattering and baseline fluctuations by subtracting the average value of absorption between 700 and 750 nm from each spectrum (Green and Blough, 1994). The absorption coefficients (a) were calculated from the absorbance (A) obtained from the spectrophotometer using:

$$a(\lambda) = 2.303 \times \frac{A(\lambda)}{l}$$

where A (λ) is the absorbance at a wavelength, λ, calculated as (Log (I_0/I), I is the intensity, and l is the path-length in meters.

4.3.4. Fluorescence Spectroscopy

Surface water samples were treated in a similar manner as those from absorption measurements along an axial transect from the Barataria Basin. Samples having absorbance greater than 0.02 at 350 nm (A_{350} > 0.02 for 1 cm pathlength) were diluted with particle free Nanopure Milli-Q water (also used as a blank) to account for the inner filter effects. Excitation Emission matrices (EEMs) were generated using a Horiba Jobin Yvon Fluromax-4 spectrofluorometer equipped with a 50 W ozone-free Xe arc lamp and a R928P photomultiplier tube as a detector. The spectrofluorometer was set to collect the signal in ratio mode with dark offsets using a 5 nm bandpass on the excitation as well as emission monochromators. Factory supplied correction factors were applied to the scans to correct for instrument configuration which were not valid for emission wavelength less than 290 nm. Since we have not observed any inconsistency of correction factors applying for 290 to 600 nm by factory supplied correction files for the range of 280 to 600 nm, we have used the same for our analysis in this study. The EEM spectra were recorded for excitation spectra from 250 to 500 nm at every 5 nm intervals (Kowalczuk et al., 2005; Zepp et al., 2004) while the emission spectra ranged between 280 – 600 nm, with data saved for every 5 nm over an integration time of 0.1s. Milli-Q water blank EEM's were subtracted from the sample EEM's to eliminate Raman peaks and then EEM's were normalized to daily-determined water Raman integrated area maximum fluorescence intensity (350 ex/397 em, 5 nm bandpass) (Colin Stedmon, Pers. Comm.). Finally, the EEM's were multiplied with a dilution factor derived from the fluorescence intensity at Ex/Em = 350/397 nm of water Raman scan to obtain the intensity for the original, undiluted sample (Coble et al., 1998). The fluorescence intensities measured were reported in Raman Units (RU) in this study. A 5% agreement was noted between replicate scans in terms of intensity and within bandpass resolution in terms of peak location using Milli-Q water scans. FLToolbox (ver. 2.10b; February, 2007) developed by Wade Sheldon (University of Georgia) for MATLAB® (Zepp et al., 2004) was utilized for EEM plots. Four samples for May (Station 31, 32, 34, and 35) could not be run because of unavailability of the instrument.

4.3.5. Chlorophyll-*a* and Total Organic Carbon (TOC) Measurements

Phytoplankton chlorophyll-*a* (Chl-*a*) were measured using EPA method 445.0 (Arar and Collins, 1992). The planktons were concentrated from a volume of water by filtering at a low vacuum through a glass fiber filter (GF/F). The pigments were extracted from the phytoplankton using a solution of 90% acetone and 10% dimethyl sulfoxide (DMSO). The use of the DMSO improves the extraction efficiency (Shoaf and Lium, 1976). The samples were allowed to steep for 2 to 24 hours (maximum) to extract the Chlorophyll-*a*. The samples were then centrifuged to clarify the solution. The fluorescence values were measured before and after acidification with 0.1 N HCl. The fluorescence readings were then used to calculate the concentrations (in mg m^{-3}) of chlorophyll-*a* in the sample extracts.

Total carbon (TC) was measured by employing High Temperature Catalytic Oxidation (HTCO) using a Shimadzu® TOC-5000A Analyzer. The machine operates by combusting the water sample (at 680^{o} centigrade) in a combustion tube filled with a platinum-alumina catalyst. The carbon in the sample is combusted to become CO_2 which is detected by a non-dispersive infrared gas analyzer (NDIR) to give the total amount of carbon in the sample. Inorganic carbon (IC) is analyzed by first treating the sample with Phosphoric acid to obtain the total amount of inorganic carbon in the sample. Total Organic Carbon (TOC) is obtained by subtracting the IC value from the TC value.

4.3.6. PARAFAC Analyses

PARAFAC Analyses were performed in MATLAB ver., 7a using the DOMFluor toolbox (ver., 1.7; Feb., 2009) developed for MATLAB® by Colin Stedmon (NERI, Aarhus University, Denmark). PARAFAC constraints, such as nonnegativity, and model initialization values derived from singular value decomposition (SVD) were used following the method of Stedmon et al. (2003, 2008). PARAFAC was applied to our EEM dataset (104 samples x 65 emissions x 51 excitations) with some analytical and statistical assumptions as reported by Stedmon et al. (2008). Determination of the number of components (i.e., model validation) was done by split half analysis and analysis of residuals and loadings (Stedmon et al., 2003). Also, the number of components was verified by CORCONDIA (Core Consistency Diagnostic) and Jackknifing Techniques (Riu and Bro, 2003) that shows similar explained variability (Table 4.1). Although we attempted to validate the PARAFAC model with larger number of components, but only four components were identified for a successful PARAFAC model for this dataset along with some variability remaining in the residuals. A typical example of the measured, modeled and residual EEM data is given in Fig. 4.1. It appears from Fig. 4.1 that the four-component PARAFAC model captured the bulk features in the measured EEM as indicated by the low residual (difference between measured and modeled data). However, some small peaks seen near first order Rayleigh scattering trough could not be modeled. This could be attributed to the size of the dataset or to the proximity of missing value settings done prior to running the PARAFAC model. This may also indicate the presence of weak fluorescing components due to noise, trivial quenching effects, inner filter or scattering effects. F_{max} was identified for each water sample collected over the Barataria Basin transect for the three months – March, April, and May, 2008. Table 4.2 shows the mean F_{max} values determined over the three month period for each component identified by PARAFAC model in this study using the peak (maximum) emission and excitation wavelengths. We have used leverage and loading technique (Stedmon et al., 2008) to identify the outliers and verified them using Jack-Knife technique (Riu and Bro, 2003). The

observed outliers by this analysis were seven samples (March: stations 5, 31, 33; April: station 31; May: stations 19, 33, and 36) and three emission wavelengths (280, 285, and 290 nm) which were removed before running the final PARAFAC model for four individual components from the whole EEM dataset resulting in final dataset (97 samples x 62 emissions x 51 excitations).

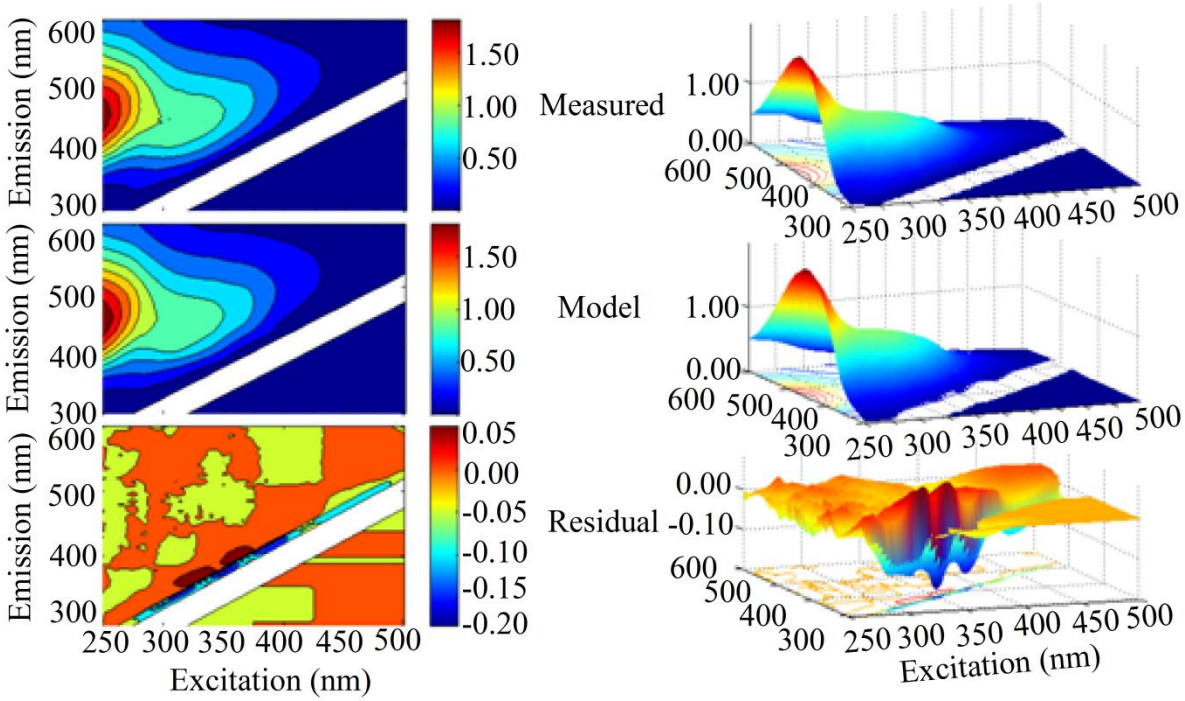

Figure 4.1 Typical example of surface and contour plot of a measured EEM and PARAFAC modeling result for station 15 (a middle basin station) as measured, model, and residual EEM. Note the change in z-axis representing fluorescence intensity reported in Raman Units (RU).

Table 4.1 Explained variance as a percentage against the PARAFAC analysis of excitation emission matrices (EEM) fluorescence for components 1 to 5.

	Number of Components			
Explained Variance (%)	2	3	4	5
Split Half Analysis	99.25	99.61	99.71	99.76
Core Consistency Diagnostic (CORCONDIA)	88.73	88.89	84.65	40.03
Jack-Knifing	88.71	88.83	82.64	22.58

Table 4.2 Positions of fluorescence maxima and fluorescence intensities, F_{max}, (scores) in Raman Units (R.U.) of the four components identified by PARAFAC analysis in this study. SD = Standard Deviation.

Component	Excitation Maxima (nm)	Emission Maxima (nm)	F_{max} (RU ± SD)
Component 1	< 250	440	1.16 ± 0.65
Component 2	270 (370)	460	0.78 ± 0.41
Component 3	< 250 (285)	395	0.78 ± 0.40
Component 4	< 250 (410)	520	0.40 ± 0.18

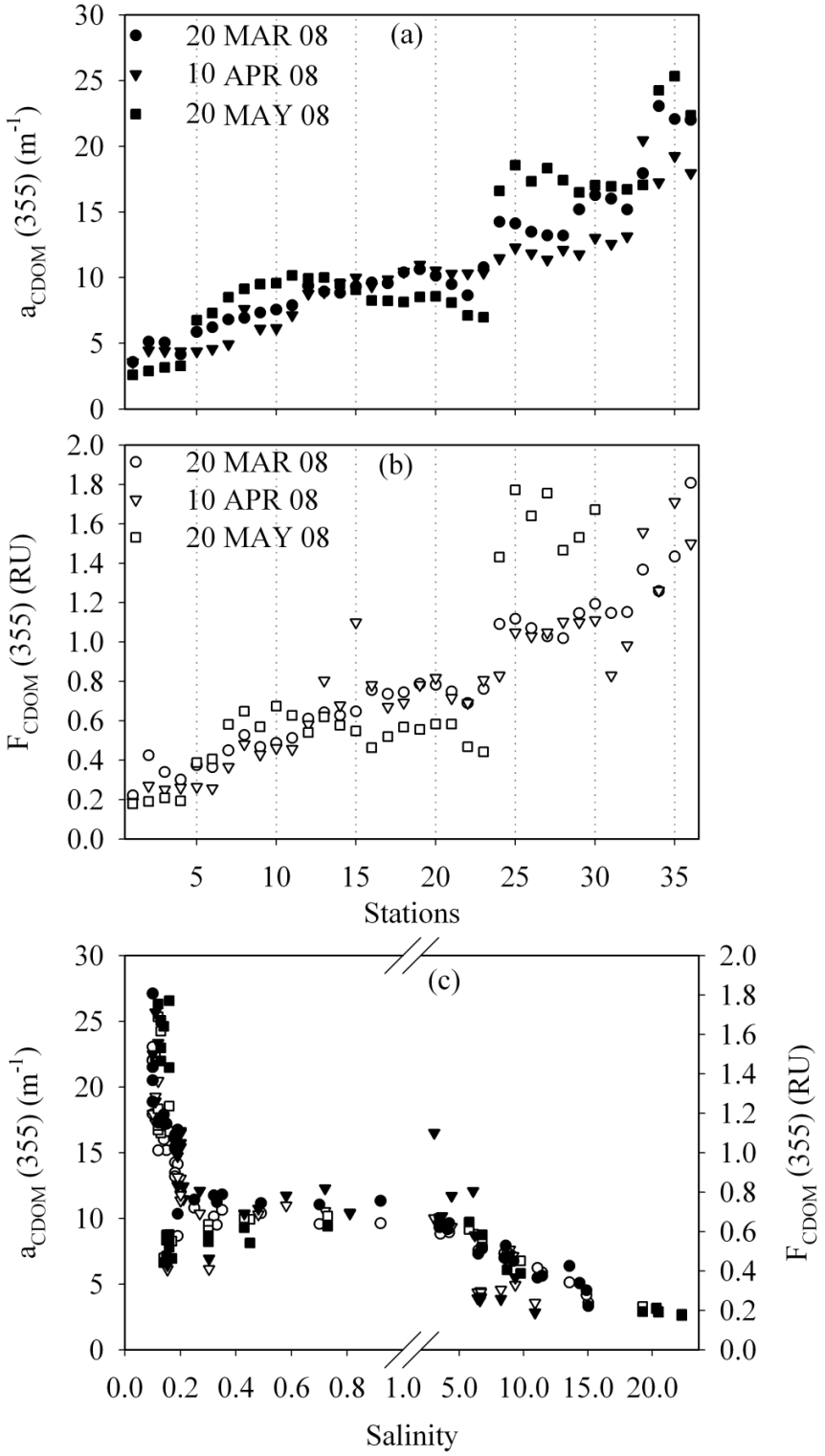

Figure 4.2 Spatial distributions of (a) absorption coefficient of CDOM at 355 nm, (b) CDOM fluorescence at 355 nm, and (c) variation of CDOM absorption and fluorescence with salinity, along the axial transect over three months sampling period (March, April, and May, 2008). Empty circles, triangles, and squares represent CDOM absorption for March, April, and May respectively, while filled circles, triangles, and squares represent CDOM fluorescence for similar months.

4.4. Results and Discussion

4.4.1. CDOM Absorption and Fluorescence Variability in the Transect

The monthly variation of CDOM absorption and fluorescence is shown in Figs. 4.2a and 4.2b along the Barataria Basin transect for this study measured at 355 nm. Also, the variation of CDOM absorption and fluorescence with salinity is shown in Fig. 4.2c. CDOM absorption and fluorescence demonstrate similar increasing trends for March, April, and May from the mouth of the basin (station 1-marine end member) to the end of the transect at upper basin (station 36-terrestrial end member) with few exception in May. The observed exceptions in May mostly lie between station 24 to 30, where point discharges from nearby living communities and runoff from fresh marshes into the narrow bayou channel could be responsible for observed variability in this part of the transect (discussed later). An unexplained variability of CDOM has been found in absorption data for March at stations 34 to 36. CDOM fluorescence seems to follow the increasing trend from stations 34 to 36 whereas the negative trend is observed for the absorption data. Mean values for CDOM absorption have been recorded as 11.06±5.01, 10.05±4.23, 11.67±6.03 (m^{-1}) and for fluorescence 0.80±0.37, 0.78±0.39, 0.75±0.51 (RU) for March, April, and May, respectively along the transect.

CDOM absorption and fluorescence show a similar relation with salinity along the transect. A negative relationship of CDOM absorption and fluorescence with salinity is shown in Fig. 4.2c. A conservative relationship of CDOM optical properties (absorption and fluorescence) with salinity occur in middle part of the transect from station 5 to station 17 with salinity ranges from 11.4 to 0.7 and 6.7 to 3.5 for March and April, respectively and 9.8 to 1.2 for May from station 5 to station 10. Few exceptions from the general trend can be seen for April with high salinity and low CDOM optical property values (Fig. 4.2c). The intrusion of high salinity sea water into the basin area due to tidal or wind effects probably caused a change in salinity dynamics thereby affecting the CDOM variability in this part of the transect for April. The non-conservative behaviour of salinity with CDOM optical properties has been observed in other parts of the transect.

4.4.2. Component Variability along the Transect

Four individual components were determined for this dataset using the PARAFAC model but this does not suggest that only four types of fluorophores were present in these samples (Fig. 4.3). It also does not suggest that all the four components are present in each sample of the transect. However, it does suggests that these four components were present in majority of the transect samples. Since, the size of the dataset (number of samples), heteorogeneity of the sampling locations, and the character of the component end members are critical to identify the number of fluorophores in a dataset, it hinders the ability of PARAFAC model to decompose EEMs into distinguishable components with underlying inherent variability of the dataset.

Figure 4.4 explains the excitation and emission loadings identified for four component PARAFAC model possessing excitation spectra with two maxima and emission spectra with single maxima. A small peak observed in emission spectra for component 2 can be attributed to artifacts (Fig. 4.4b). We attempted to remove this by increasing the missing value region (Colin Stedmon, Pers. Comm.), but with no success. Component 1 has a primary (and secondary) fluorescence peak at an excitation/emission wavelength of 250 (340) nm/440 nm. The primary and secondary fluorescence peaks for component 2 were red shifted compared to component 1,

occuring at 270 (370) nm/460 nm. The blue shift for component 3 with respect to component 1 and component 2, flourescing at a primary (secondary) excitation/emission wavelength pair of 250 (285) nm/395 nm, is also observed. This component is similar to a non-humic and lie in between tryptophan and N-peak (Table 4.3). Component 4 possessed a primary (secondary) excitation/emission wavelength pair of 240 (410) nm/520 nm. This component seems to be derived from agricultural catchments as have been reported in other estuarine environments (e.g., Stedmon et al., 2005a), and known to be rapidly produced and removed making it difficult to identify its presence. Also, the close proximity of the component 4 peak with the terrestrially derived organic material makes it difficult to identify distinctly (Stedmon et al., 2005b).

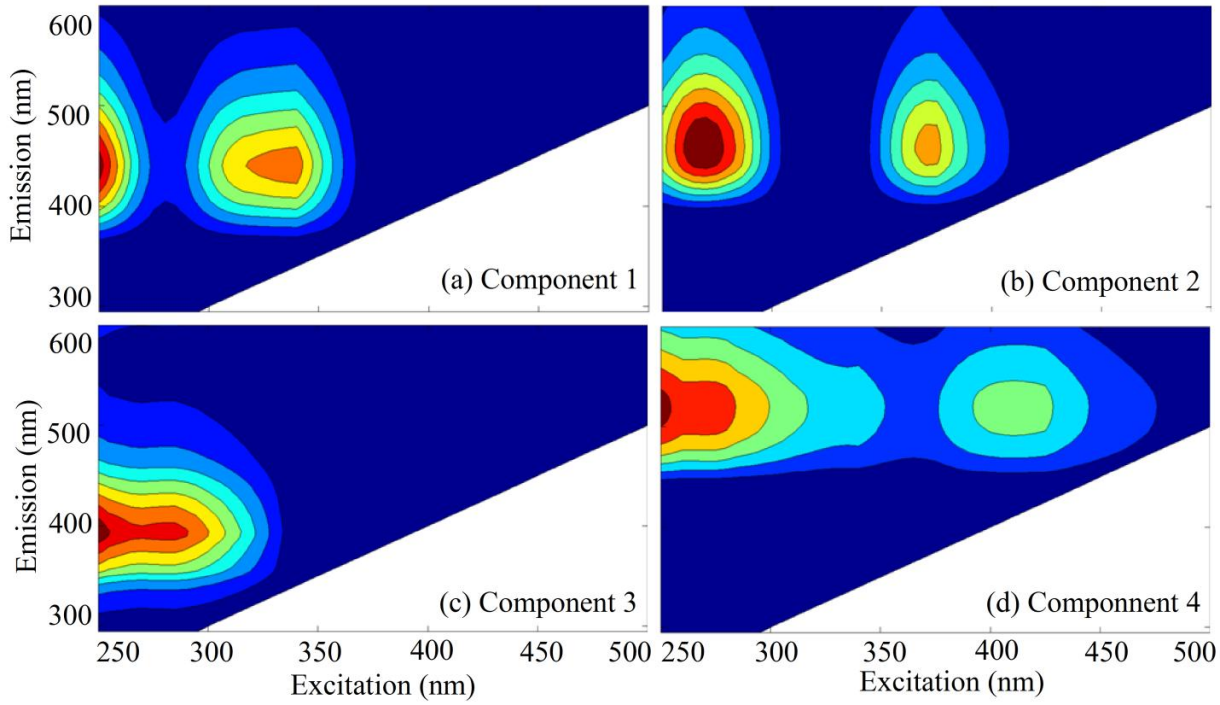

Figure 4.3 The four different fluorescent components found by the PARAFAC model. Positions of their maxima are given in Table 4.2.

Components 1 and 2 are similar to humic-like peaks identified and reported in previous literature (Coble et al., 1996; Stedmon et al., 2003, 2007). Barataria Basin is surrounded by swamps, marshes, forested and wetland regions and the acquired EEMs reflect their influence. Component 1 thought to be A-peak has maximum emission at 440 nm, whereas component 2 is found to be similar to previously reported C-peak using traditional "peak picking" technique with maximum emission intensity at 460 nm (Figs. 4.3 and 4.4; Tables 4.2 and 4.3) (Coble et al., 1996). Component 3 reported as N-peak (Coble et al., 1998), could be a combination of tryptophan (T-peak) and biologically labile matter produced in the surface water. Recently, it is reported as a non-humic component from freshly produced biologically labile material (e.g., Yamashita et al., 2008) and protein or amino-acid like component (Hua et al., 2007) (Figs. 4.3and 4.4; Table 4.3). Kowalczuk et al. (2009) reported this component as red shifted tryptophan peak associated with amino acids and included a fraction of autochthonous dissolved organic matter. Component 4 is found to be similar as soil derived humic acid originating from wetlands and marshes with a primary (secondary) excitation wavelength at 250 (410) and emission wavelength at 520 nm. This component is very similar to that found by Lochmuller and

Saavedra (1986) in study done for soil derived fulvic acid formally known as "Contech" FA (ex/em = 390/509 nm), but with a red shift in excitation emission maxima which suggests high aromatic contents and higher degree of humification in our study (Figs. 4.3 and 4.4; Tables 4.2 and 4.3). Later, Coble (1990) defined this component as D-region of dissolved organic matter study in the Black Sea. This component is common to several fresh water regimes and microbial degradation could be a source of this component when exposed to visible light (Stedmon et al., 2005b). Spectral signature of the soil derived humic acid component (component 4) could also be attributed to the leaching processes from agricultural catchments given the long residence time of water in these catchments (Stedmon et al., 2005a).

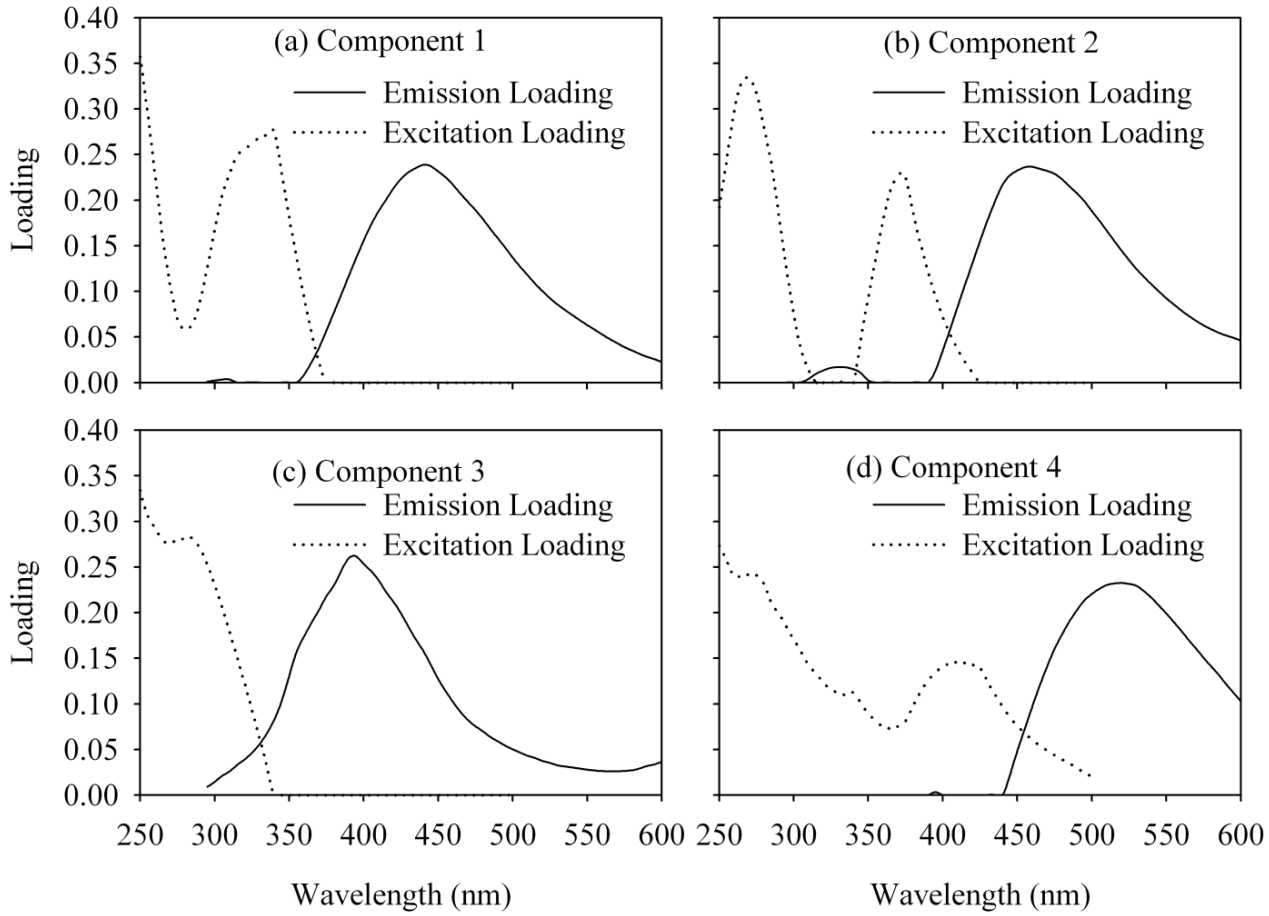

Figure 4.4 Excitation and emission loadings derived from the four-component PARAFAC model using split half validation technique. Solid lines represent emission loadings and dashed lines represent excitation loadings.

Table 4.3 Descriptions of the four components identified by PARAFAC analysis of excitation emission matrices (EEM) fluorescence data in this study and their comparison with previously identified components.

Component (This study)	Ex/Em (nm)	Description and References
Component 1	< 250 (340)/440	Humic-like; Terrestrial origin A-peak (Coble, 1996) Component 1 (Stedmon et al., 2003) Component 1 (Cory and McKnight, 2005) Component 4 (Stedmon & Markager, 2005a) Component 5 (Stedmon & Markager, 2005b) Component 1 (Holbrook et al., 2006) Component 3 (Ohno and Bro., 2006) Component 1 (Hua et al., 2007) Component 1 (Stedmon et al., 2007) Component 2 (Zhi-gang et al., 2007) Component 1 (Hiruiart-Baer et al., 2008) Component 1(Luciani et al., 2008) Component 2 (Yamashita et al., 2008) Component 2 (Kowalczuk et al., 2009)
Component 2	270 (370)/460	Humic-like; Terrestrial origin; related to terrestrial particulate organic matter C-peak (Coble, 1996) Component 3 (Stedmon et al., 2003) Component SQ1 (Cory and McKnight, 2005) Component 1 (Stedmon & Markager, 2005b) Component 1(Ohno and Bro., 2006) Component 2 (Hua et al., 2007) Component 3 (Yamashita et al., 2008) Component 1 (Kowalczuk et al., 2009)
Component 3	<250 (285)/395	Non-Humic-like; Labile matter; Biological production in the water column N-peak (Coble, 1998) Component 5(Stedmon et al., 2003) Component 3 (Stedmon & Markager, 2005b) Component 2 (Holbrook et al., 2006) Component 4(Hua et al., 2007) Component 5 (Yamashita et al., 2008) Component 6 (Kowalczuk et al., 2009)
Component 4	<250 (410)/520	Soil Fulvic-like; derived from agricultural catchments and exists in fresh water environments Soil-fulvic-acid (Lochmuller and Saavedra, 1986) D-region (Coble, 1990) Component 2 (Stedmon & Markager, 2005a) Component 7 (Stedmon & Markager, 2005b) Component 2 (Stedmon et al., 2007) Component 3 (Hiruiart-Baer et al., 2008) Component 4 (Kowalczuk et al., 2009)

4.4.3. Spatio-temporal Variability of Components

The spatial distribution of component 1, 2, 3, and 4 is shown in Fig. 4.5 for the three months. Component 1, 2, and 4 shows similar trends as of F_{CDOM} (355 nm) along the transect. Component 3 is also showing the similar trend for most part of the transect, except at stations 24 to 30 for May. This difference in behaviour of specific component from the general trend could only be achieved by the use of PARAFAC technique. The presence of component 3 at these locations is complemented by the increased Chl-*a* and TOC values suggesting the production of biologically labile organic material (discussed later). The biological production of labile organic matter in this part of the transect could be associated with periphytons (mainly in streams) or macrophytes (mainly in lakes or ponds) (Kortelainen et al., 2004). The presence of autochthonous dissolved organic matter could principally be derived from the production by periphytons and macrophytes and is usually not associated with terrestrially originated organic matter.

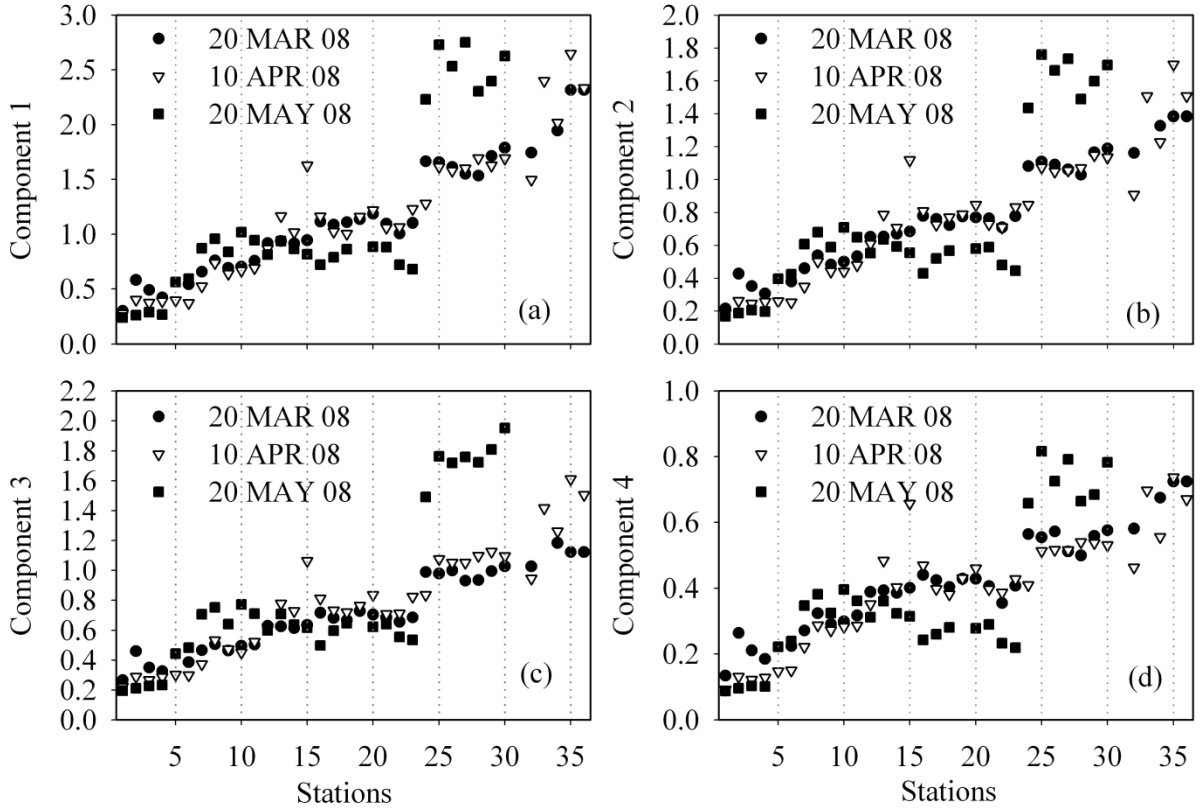

Figure 4.5 Spatial distributions of each PARAFAC component (a) component 1, (b) component 2, (c) component 3, and (d) component 4, over the three month period (March, April, and May, 2008). Filled circles and squares represent March and May respectively, while empty triangles represent April.

Figure 4.6 explains the temporal variation of four components identified in this study using PARAFAC model for the three months (March, April, and May) period. Mean values of component 1 and component 4 are found to be constant for the three month period with slight decrease in May. The mean values for component 1 are 1.16±0.53, 1.17±0.61, and 1.15±0.8, whereas for component 4, mean values recorded as 0.42±0.15, 0.40±0.17, and 0.38±0.22 for March, April, and May respectively. Component 2 and component 3 shows a very good

complementing relationship between each other, that is when component 2 is higher component 3 is lower and vice-versa. Mean value for component 2 is found as high (0.78±0.33) in comparison to mean value recorded for component 3 (0.71±0.26) for March. In April, component 2 and component 3 both have similar mean values, i.e. , 0.78±0.39 and 0.78±0.38 respectively. Component 3 recorded a higher mean value (0.84±0.55) in comparison to the mean component 2 for May (0.76±0.52). This increased component 3 value suggests autochthonous production occurred in the month of May, mostly between stations 24 to 30. The biological activity, presence of component 3, at these locations (Fig. 4.5) could be due to the longer residence time of water in the narrow Lac Des Allemands bayou (Fig. 1.3), or sources coming from agricultural catchments mainly practiced by nearby communities in the region. The presence of component 1 and 4 during the three month period is significant at the same level and could be associated with the presence of allocthonous dissolved organic matter derived from terrestrial sources and leaching from soil derived humic acid which as reported in previous literature (e.g., Holbrook et al., 2006; Kowalczuk et al., 2009; Stedmon et al., 2005b) is widespread in streams, lakes, and wetlands region.

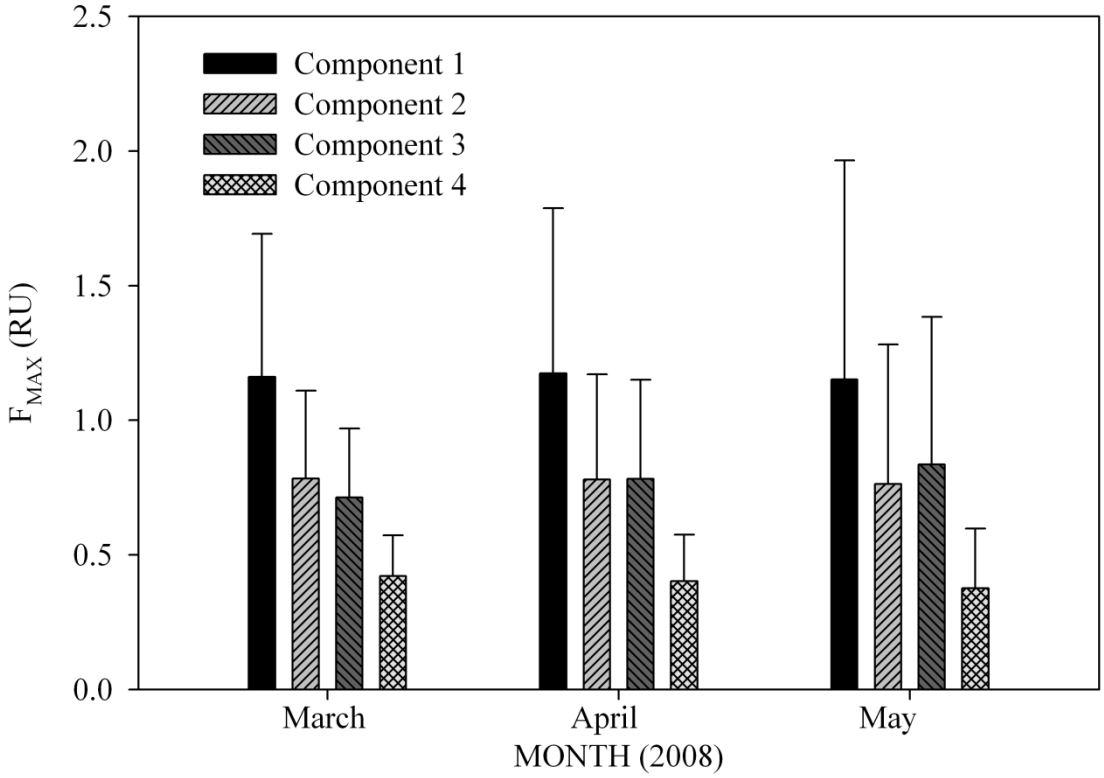

Figure 4.6 Mean values for temporal distributions of each PARAFAC component (a) component 1, (b) component 2, (c) component 3, and (d) component 4, along sampling stations identified by PARAFAC modeling results. Error bars represent standard deviations from mean values.

4.4.4. Component Variability with Salinity, Chl-*a*, and TOC

The behavior of four components identified in this study was studied with changes in salinity gradient (Fig. 4.7). All the four components show similar trend as observed for a_{CDOM} (355) and F_{CDOM} (355) with salinity (Fig. 4.2c). The fluorescence intensity of all the four components

decreased along the salinity gradient in the middle part of the transect and remained non-conservative in the remaining part of the transect. However, the four components decreased to lowest values in April (from stations 6 to 12) with a subsequent change in salinity. The argument of high salinity sea water intrusion seems to conclude the observed component variability in this part of the transect. Component 1, 2, 3, and 4 showed a similar trend of higher values at low salinity range (stations 18 to 36) and a gradual increase in fluorescence intensities along the salinity gradient from marine end member to terrestrial end member (station 17). No significant change in fluorescence intensities were observed for first four stations (stations 1, 2, 3, and 4) for all the components. In terms of fluorescence intensity, component 3, a combination of N-peak and tryptophan, indicated the presence of freshly produced biological material which was ready to be used up by microbial colonies and thus removed from the system (Coble et al., 1998; Stedmon et al., 2003; Yamashita et al., 2008). Although the salinity were small in May (0.1) in comparison to April (0.2), the marked difference in fluorescence intensity of component 3 at stations 25 to 30 in comparison to component 1, 2, and 4 for April and May (Fig. 4.7c) could indicate the presence of freshly produced organic matter at these locations during May.

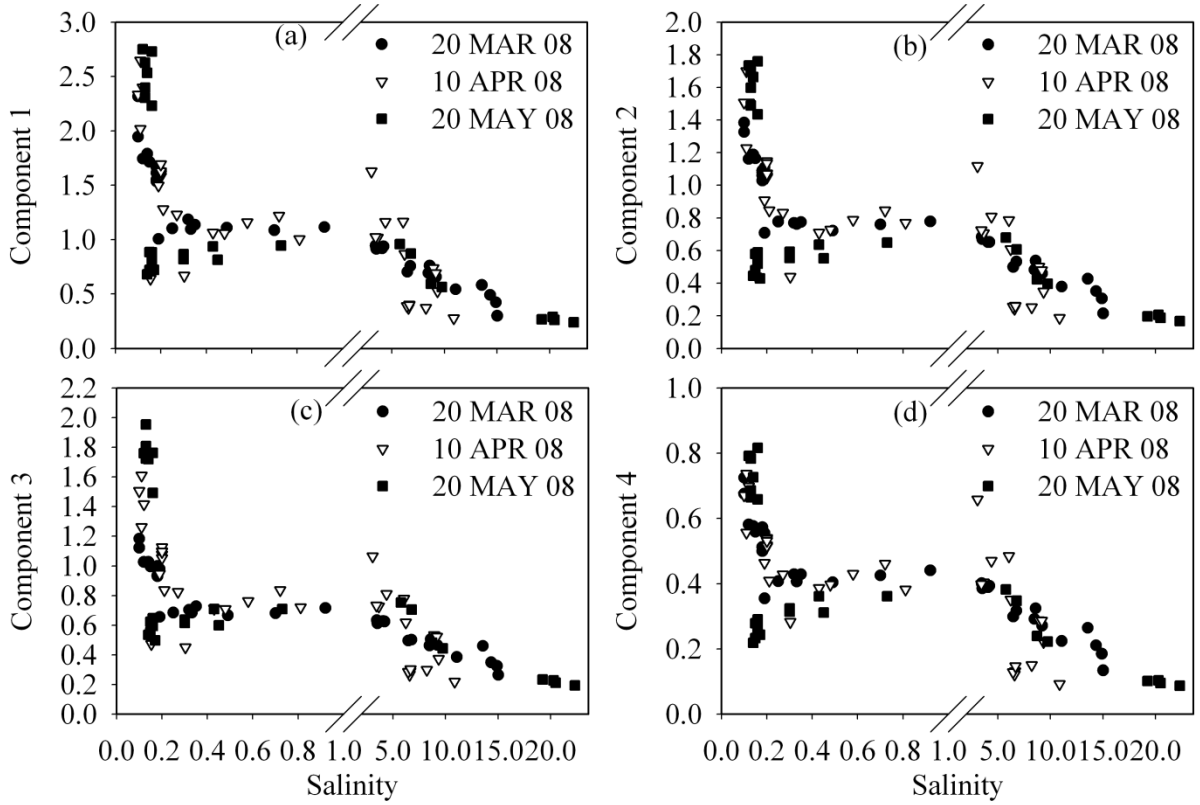

Figure 4.7 Fluorescence intensities of each PARAFAC component (a) component 1, (b) component 2, (c) component 3, and (d) component 4, with salinity gradient are plotted. Fluorescence intensities, F_{max} are in Raman Units (RU), and filled circles and squares represent March and May respectively, while empty triangles represent April. Breaks in plots are done to visualize the variability at low salinity values.

Figures 4.8 and 4.9 shows the variability of four components with Chl-*a* and TOC measurements for three months in the area of interest. Chl-*a* seems to have highest mean values in May with a gradual increase from March to April. The distribution of mean values for Chl-*a*

was found as 15.65 ± 8.57 (March), 17.11 ± 9.89 (April), and 26.74 ± 26.41 mg m^{-3} (May) with highest observed variability in May. But, TOC mean values decreased from March (10.98 ± 4.60) to April (8.61 ± 3.68) and later increased in May (9.37 ± 6.44). The increased Chl-*a* supports the case of autochthonous production of biologically labile dissolved organic matter in the transect, mostly prominent between stations 25 to 30. This could be attributed to slow runoffs and drainage of nutrient supply from agricultural catchments nearby. Three fold increase from station 24 (8.00 mg m^{-3}) to 25 (24.96 mg m^{-3}) was observed for Chl-*a* in May, that increased to 90.15 mg m^{-3} at station 30, an almost a ten-fold increase in comparison to station 24. This implies algal bloom like condition at these locations likely due to proximity of these stations to cultivated crops and associated runoffs containing high nutrients. Summer time low flow and calm conditions (Swenson, Pers. Comm.) and increased light exposure could be another source for this increased Chl-*a* associated with phytoplankton blooms, a potential source of autochthonous DOM at these locations (Stedmon et al., 2006). The Chl-*a* variability for March and April were not significant at these locations, in fact, lower values of Chl-*a* were observed at these location in comparison to first few stations (station 1 to 4) for March and April. Chl-*a* values have been found to be minimum at station 1 to 4 in May suggesting strong mixing or tidal flows as indicated by high salinity at these locations. Although measured TOC values have not shown as large a variation as Chl-*a* during May at stations 25 to 30, it however remained high at these locations supporting the argument of autochthonous production of biological material (Fig. 4.9c). Components 1, 2, and 4 have shown similar trend with Chl-*a* variation for May at stations 25 to 30, but fluorescence intensity of component 3 was higher indicating the biological matter production (Fig. 4.8c). Similarily, from Fig. 4.9c, a significant increase in concentrations of total organic carbon can be seen for component 3 at these locations (stations 25 to 30) in comparison to other components found in this study for the month of May.

4.4.5. Humification Indices along the Transect

The humification indices have been calculated as described in methods section and plotted in Fig. 4.10. The humification index (HIX), an indicator of dissolved organic matter bioavailability within a natural system, is used to investigate the degree of humification because highly humified organic material is expected to be less labile in comparison to that of low degree humified organic substance (Ohno, 2002; Zsolnay et al., 1999). This also indicate the higher degree humified organic matter should persist longer than lower degree humified substance in an environment. Our results here for HIX show similar results as obtained by (Justin Birdwell, pers. comm.) in a study done for terrestrial and microbial contributions to dissolved organic matter fluorescence in an aquifer in Central Texas, USA.

A positive relationship is obtained for humification indices for most part of the transect along the station locations as shown in Fig. 4.10a and a negative relationship is observed with salinity in Fig. 4.10b. In general, humification was increased along the transect as terrestrial derived organic matter increased from lower to upper basin (from station 1 to station 36). However, a decrease in humification indices were noticed with salinity gradient which implies reduced degree of humification with increasing salinity which can be clearly seen for first four stations (station 1 to 4) in Fig. 4.10b.

We have calculated the total normalized fluorescence intensity as suggested by Kowalczuk et al., (2009) by summing fluorescence intensities of all the four identified components in each month and plotted them against HIX in Fig. 4.10c. The variation for HIX was interesting to observe showing a decrease in HIX values from station 25 onwards. The inflection shown by HIX and

total normalized fluorescence intensity near station 25 onwards again suggested some *in situ* phytoplankton production at these locations which could also be seen by reduced humification values in later part of the transect with increasing total normalized fluorescence intensity, especially for May 2008 (Fig. 4.10c).

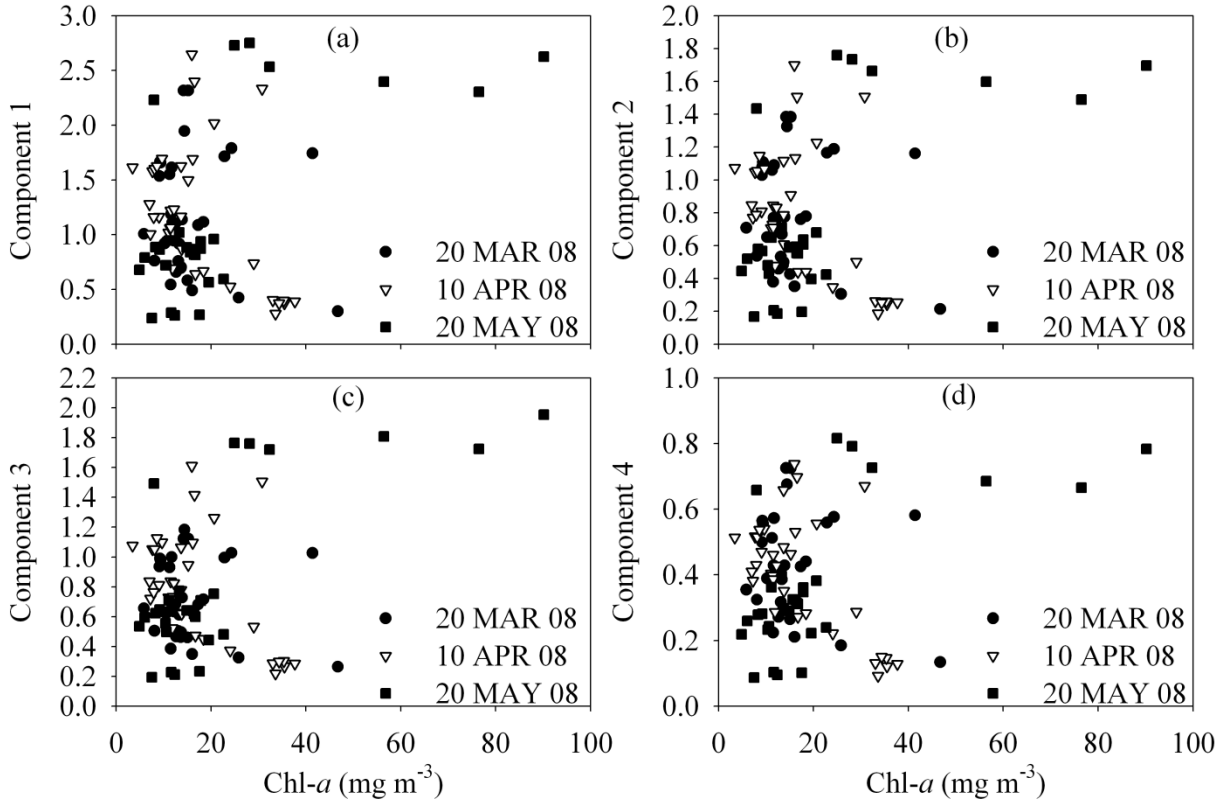

Figure 4.8 Fluorescence intensities of each PARAFAC component (a) component 1, (b) component 2, (c) component 3, and (d) component 4, with Chlorophyll-*a* (Chl-*a*) are plotted. Fluorescence intensities, F_{max} are in Raman Units (RU), and Chl-*a* values are in mg m^{-3}. Filled circles and squares represent March and May respectively, while empty triangles represent April.

The monthly variability in mean values of total normalized fluorescence intensity was observed as 3.08±1.26 (March), 3.14±1.83 (April), and 3.13±0.02 (May) in Raman Units (RU). Similarly, mean values of HIX were obtained as 13.33±2.14 (March), 11.98±1.83 (April), and 10.25±1.44 (May). HIX values were found decreasing over the monthly mean suggesting increased microbial activity and decreased humification the study period. It could also imply an increase in autochthonous production later in spring. Long term monitoring would improve an understanding of the seasonal variability. Student's t-test (two-tailed, type 2) performed (MATLAB® at a significance level, p-value = 0.05) to assess whether HIX values determined for this study were found to be significantly correlated with months. P-values obtained from these analyses showed significant differences in HIX calculated for March and April (p-value = 0.0025), while for HIX calculated during April and May sampling period noted a significant difference of p-value = 0.0016.The observed level of significant difference for March and May sampling period yielded p-value < 0.001. These results indicated that the HIX values were significantly different over the sampling periods. These results suggest that HIX was

significantly different over the period of study for three months and variability in HIX is pronounced along the transect.

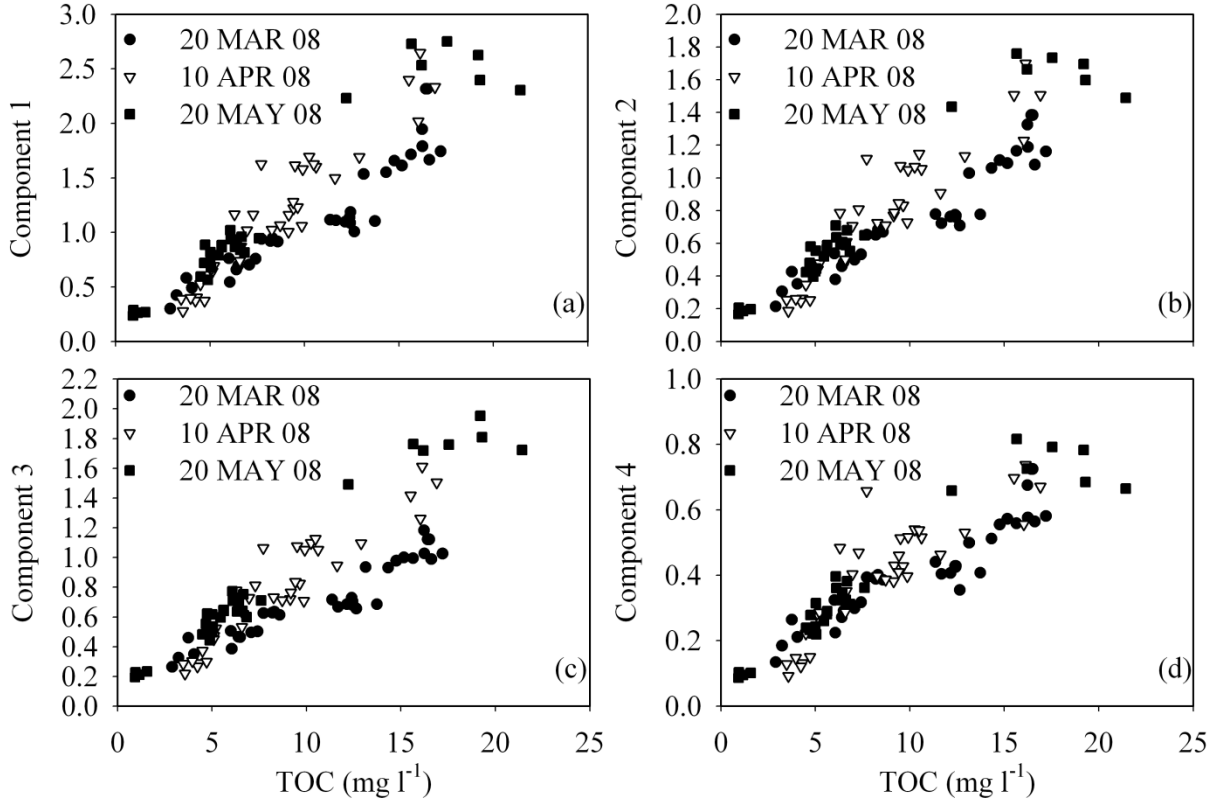

Figure 4.9 Fluorescence intensities of each PARAFAC component (a) component 1, (b) component 2, (c) component 3, and (d) component 4, with total organic carbon (TOC) are plotted. Fluorescence intensities, F_{max} are in Raman Units (RU), and TOC values are in mg l^{-1}. Filled circles and squares represent March and May respectively, while empty triangles represent April.

4.5. Conclusions

Fluorescence spectroscopy applied with the PARAFAC technique to study CDOM dynamics in the Barataria Basin revealed unique results. This study enabled us to quantify the compositional contributions by different fluorophores in the study area. The fluorescence intensities obtained for identified components showed their distribution along the transect and helped in identifying the potential autochthonous dissolved organic material in a part of the transect. It also suggested the need to focus on the discharge properties of this particular transect in terms of nutrient supplies. Conservative and non-conservative mixing have been observed in different parts of the transect suggesting the influence of point discharges. Major humic-like fluorescence intensities were expected but *in situ* production of dissolved organic matter on a small part of the transect was found to be quite revealing. In all, we have identified four components using PARAFAC model: two humic-like, one non-humic like, and one soil-humic like. The dominance of humic-like fluorophores in an estuarine region has already been established, but studies dealing with non-humic components and soil derived humic acids are limited. This study provides an opportunity to look forward with more plausible explanations for the compositional and

conformational pattern in CDOM study in the Barataria Basin. We not only identified the number of components, but presented their relationships with salinity, Chl-*a*, and total organic carbon measured on the transect.

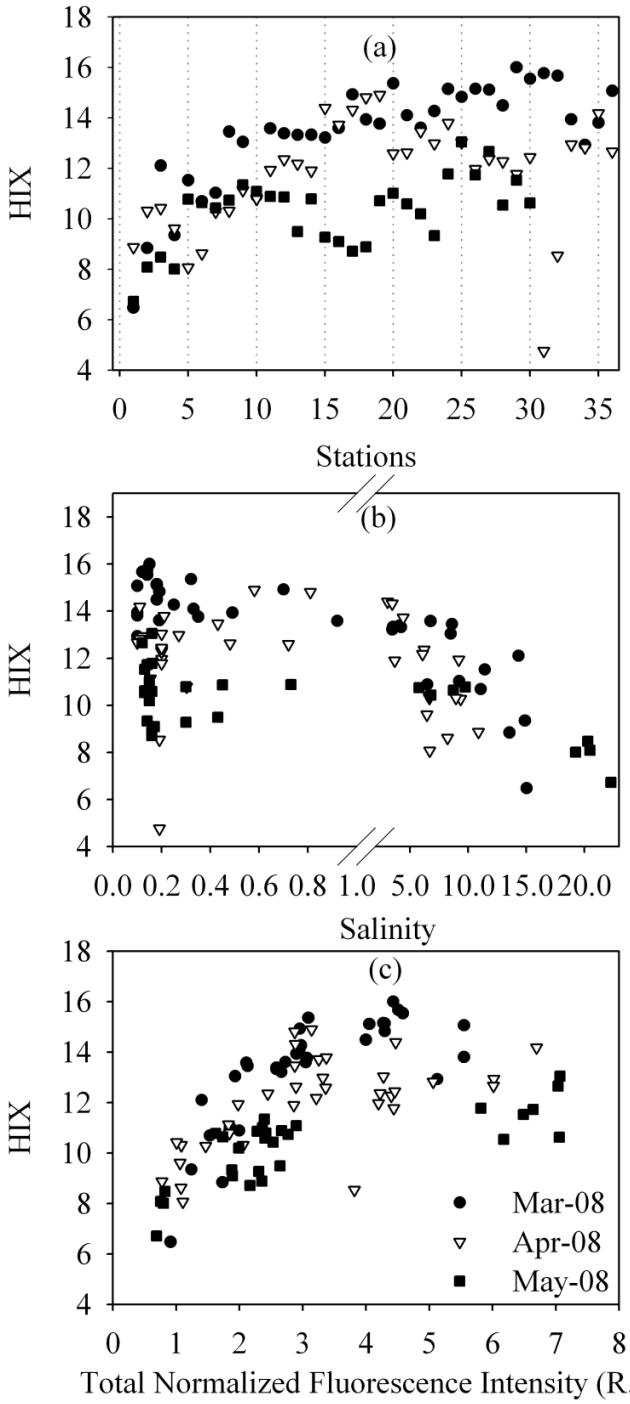

Figure 4.10 Distributions of Humification Indices (HIX) (a) against the sampling stations, (b) against the salinity gradients, and (c) against the total normalized fluorescence intensity. Total Normalized Fluorescence Intensities, calculated from summation of identified PARAFAC components, are in Raman Units (RU). Filled circles, empty triangles, and filled squares represent March, April, and May respectively for Humification Indices (HIX).

HIX can serve as identification tools for CDOM origination and fate in an estuarine environment. However, HIX showed a greater range of variability and could be considered as a more useful index than the earlier defined Fluorescence Index (FI) by McKnight et al. (2001) to study CDOM dynamics, especially in a complex coastal and estuarine regions like the Barataria Basin. We have tested for variability in HIX and FI for our study and have found HIX as more acceptable parameter to study regions with complex optical properties such as the Barataria Basin (plots not shown here). This study supported the use of excitation emission matrix fluorescence in combination with parallel factor analysis to distinguish between different sources of dissolved organic matter. Its applicability in estuarine regions such as the Barataria Basin could serve as a useful tool to evaluate the dynamics of dissolved organic matter in similar complex coastal regimes.

Chapter 5

General Conclusions and Future Scope

Absorption and fluorescence spectroscopy in conjunction with parallel factor analysis have been used in this thesis to study CDOM behavior in the Barataria Basin. This work focused on CDOM distribution, its variability in the Barataria Basin, and spectrochemical properties. The results of this study support the need to use EEMs and PARAFAC to monitor CDOM changes in the Barataria Basin. The major findings of this study are:

- Humic substances were a major contributor to the CDOM pool in the Barataria Basin, primarily derived from terrigeneous sources (in Chapter 2).
- Strong influence of freshwater input from point sources caused changes in CDOM optical properties (in Chapter 2).
- Increased sources of terrestrially derived organic matter have been found with salinity and absorption-fluorescence relationships (in Chapter 2).
- Conservative mixing was found to occur on a small portion of transect, mainly near saline and brackish marshes during March 2008 study (in Chapter 2).
- Resuspension of bottom sediments might be observed near the mouth of basin (stations 1 to 4) during study period showed a non-conservative mixing in this part of transect (in Chapter 2).
- Absorption and fluorescence were significantly and positively correlated (r^2 = 0.98; measured at 355 nm) demonstrating that fluorescence should be used in place of absorption for CDOM characterization in Barataria Basin (in Chapter 2).
- Seasonal variability in hydrographic variables is evident, but no correlations with season have been observed for absorption and fluorescence characteristics studied during high and low flow conditions (in Chapter 3).
- Fluorescence peak ratios performed better for low flow conditions than high flow conditions to trace terrestrial derived humic matter influences in the Barataria basin over the period of study (in Chapter 3).
- Allochthonous production was encountered in the basin during the study period along most of transect, but in May, an autochthonous production was observed in a small portion of the transect (in Chapter 4).
- Fluorescence would help in identifying the individual contribution of particular components in CDOM pool when used along with PARAFAC (in Chapter 4).
- PARAFAC in this study helped in identifying four components in all; two humic, one non-humic, and one soil-derived humic. The existence of non-humic component and pedogenic contribution was not visible when fluorescence spectroscopy was alone used as in results from Chapter 2 & Chapter 3 (in Chapter 4).
- Relationship between an identified non-humic component (representing autochthonous production) and chlorophyll-*a* suggested that short duration bloom conditions in the basin are influenced by nutrient supply through agricultural runoff from nearby catchments (in Chapter 4).
- Also, the use of humification and fluorescence indices supported a terrestrially derived organic matter source in the Barataria Basin. Humification indices were found to be more suitable than fluorescence indices for this wetland and should be used in future studies (in Chapter 4).

Fluorescence studies coupled with PARAFAC have proven to be valuable for CDOM characterization and to monitor changes in CDOM composition; however to establish a working model for CDOM using PARAFAC, a large dataset is required, so a continuation of this kind of

study is strongly recommended for the Barataria Basin. Since Barataria Basin has been exploited for years by humans for its resources, it is necessary to monitor changes not only for water quality but to maintain a balanced ecosystem. The anthropogenic inputs, such as nutrient supply, agricultural and industrial wastes, and municipal discharges also contribute to CDOM. These inputs should be monitored regularly to check the variability in organic matter concentration in the basin.

References

Ågren A., I. Buffam, M. Berggren, K. Bishop, M. Jansson, H. Laudon. 2008. Dissolved organic carbon characteristics in boreal streams in a forest-wetland gradient during the transition between winter and summer. Journal of Geophysical Research 113: G03031; doi: 10.1029/2007JG000674.

Arar, E.J., and G.B. Collins. 1992. Method 445.0: In vitro determination of Chlorophyll-a in marine and freshwater phytoplankton by fluorescence. Environmental Monitoring Systems Laboratory, Office of Research and Development, U.S. Environmental Protection Agency, Cincinnati, OH 45268; Reprinted by Turner Designs, Sunnyvale, CA 94086.

Baker, A., D. Ward, S.H. Lieten, R. Periera, E.C. Simpson, M. Slater. 2004. Measurement of protein-like fluorescence in river and waste water using a handheld spectrophotometer. Water Research 38: 2934-2938.

Boehme, J, Coble, PG, Conmy, R, Stovall-Leonard, A. Examining CDOM fluorescence variability using principal component analysis: seasonal and regional modeling of three-dimensional fluorescence in the Gulf of Mexico. Marine Chemistry 2004; 89: 3-14.

Boyd, T.J., and C.L. Osburn. 2004. Changes in CDOM fluorescence from allochthonous and autochthonous sources during tidal mixing and bacterial degradation in two coastal estuaries. Marine Chemistry 89: 189-210.

Bricaud, A., A. Morel, L. Prieur. 1981. Absorption by dissolved organic matter of the sea (yellow substance) in the UV and visible domains. Limnology and Oceanography 26 (1): 43-53.

Bro, R. PARAFAC. Tutorial and applications. Chemometrics and Intelligent Laboratory Systems 1997; 38 (2): 149-171.

Burdige, D.J., S.W. Kline, W. Chen, Fluorescent dissolved organic matter in marine sediment pore waters. Marine chemistry 2004, 89: 289-311.

Cahoon, D.R. 1994. Recent Accretion in Two Managed Marsh Impoundments in Coastal Louisiana. Ecological Applications 4 (1): 166-176.

Castro, M.S., C.T. Driscoll, T.E. Jordan, W.G. Reay, W.R. Boynton. 2003. Sources of Nitrogen to Estuaries in the United States. Estuaries 26 (3): 803-814.

Chen, Z., Y. Li, J. Pan. 2004. Distributions of color dissolved organic matter and dissolved organic carbon in the Pearl River Estuary, China. Continental Shelf Research 24: 1845-1856.

Chen, Z., C. Hu, R.N. Conmy, F. Muller-Karger, P. Swarzenski. 2007. Colored dissolved organic matter in Tampa bay, Florida. Marine Chemistry 104: 98-109.

Clark, C.D., J. Jimenez-Morais, G. Jones II,E. Zanardi-Lamardo, C.A. Moore, R.G. Zika. 2002. A time-resolved fluorescence study of dissolved organic matter in a riverine to marine transition zone. Marine Chemistry 78: 121-135.

Clark, C.D., L.P. Litz, S.B. Grant. 2008. Salt marshes as a source of chromophoric dissolved organic matter (CDOM) to Southern California coastal waters. Limnology and Oceanography 53 (5): 1923-1933.

Coble, P.G., S.A. Green, N.V. Blough, R.B. Gagosian. 1990. Characterization of dissolved organic matter in the Black Sea by fluorescence spectroscopy. Nature (348): 432-435.

Coble, P.G. 1996. Characterization of marine and terrestrial DOM in seawater using excitation-emission matrix spectroscopy. Marine Chemistry 51 (4): 325-346.

Coble, P.G., C.E. Del Castillo, B. Avril. 1998. Distribution and optical properties of CDOM in the Arabian Sea during the 1995 Southwest Monsoon. Deep-Sea Research II 45: 2195–2223.

Coble, P. G. 2007. Marine Optical Biogeochemistry: The Chemistry of Ocean Color. Chemical Reviews 107: 402-418.

Conner, W.H., J.W. Day Jr. 1987. The Ecology of Barataria Basin, Louisiana: An Estuarine Profile. Fish and Wildlife Service, U.S. Department of the Interior. Biological Report 85 (7.13).

Conner, W.H., J.W. Day Jr. 1992. Water Level Variability and Litterfall Productivity of Forested Freshwater Wetlands in Louisiana. American Midland Naturalist 128 (2): 237-245.

Cory, R.M., and D.M. McKnight. 2005. Fluorescence Spectroscopy Reveals Ubiquitous Presence of Oxidized and Reduced Quinones in Dissolved Organic Matter. Environmental Science and Technology 39: 8142-8149.

Craig, A., E.N. Powell, R.R. Fay, J.M. Brooks. 1989. Distribution of *Perkinsus marinus* in Gulf Coast Oyster Populations. Estuaries 12 (2): 82-91.

D'Sa, E.J., R.G. Steward, A. Vodacek, N.V. Blough, D. Phinney. 1999. Determining optical absorption of colored dissolved organic matter in seawater with a liquid capillary waveguide. Limnology and Oceanography 44 (4): 1142-1148.

D'Sa, E.J., and R.L. Miller. 2003. Bio-optical properties in waters influenced by the Mississippi River during low flow conditions. Remote Sensing of Environment 84: 538-549.

D'Sa, E.J., R.L. Miller, C. Del Castillo. 2006. Bio-optical properties and ocean color algorithms for coastal waters influenced by the Mississippi River during a cold front. Applied Optics 45 (28): 7410-7428.

D'Sa, E.J. 2008. Colored dissolved organic matter in coastal waters influenced by the Atchafalaya River, USA: effects of an algal bloom. Journal of Applied Remote Sensing 2: 023502.

Das, A., D. Justić, E. Swenson. 2009. Modeling estuarine-shelf exchanges in a deltaic estuary: Implications for coastal carbon budgets and hypoxia. Ecological Modelling; doi: 10.1016/j.ecolmodel.2009.01.023.

Del Castillo, C.E., P.G. Coble, J.M. Morel, J.M. Lopez, and J.E. Corredor. 1999. Analysis of the optical properties of the Orinoco River Plume by absorption and fluorescence spectroscopy. Marine Chemistry 66: 35-51.

Del Castillo, C.E., and P.G. Coble. 2000. Seasonal variability of the colored dissolved organic matter during the 1994–95 NE and SW monsoons in the Arabian Sea. Deep-Sea Research 47: 1563–1579.

Del Castillo, C.E. 2005. Remote Sensing of Organic Matter in Coastal Waters. In Remote Sensing of Coastal Aquatic Environments, eds. R.L. Miller, Chapter 7, 157-180. Printed in the Netherlands: Springer Publications.

Del Vecchio, R., and N.V. Blough, 2002. Photobleaching of chromophoric dissolved organic matter in natural waters: kinetics and modeling. Marine chemistry 78, 231-253.

Del Vecchio, R., and N.V. Blough. 2004. On the origin of the optical properties of humic substances. Environmental Science and Technology 38: 3885–3891.

Del Vecchio., R., and N.V. Blough. 2006. Influence of Ultraviolet Radiation on the Chromophoric Dissolved Organic Matter in Natural Waters. In Environmental UV Radiation: Impact on Ecosystems and Human Health and Predictive Models, eds. F. Ghetti, G. Checcucci, and J.F. Bornman, 203-216, Springer, printed in the Netherlands.

Feijtel, T.C., R.D. DeLaune, W.H. Patrick Jr. 1985. Carbon flow in coastal Louisiana. Marine Ecology Progress Series 24: 255-260.

Fellman, JB, D'Amore, DV, Hood, E, Boone, RD. Fluorescence characteristics and biodegradability of dissolved organic matter in forest and wetland soils from coastal temperate watersheds in southeast Alaska. Biogeochemistry 2008; 88: 169-184.

Ferrari, G.M., and M.D. Dowell. 1998. CDOM Absorption Characteristics with Relation to Fluorescence and Salinity in Coastal Areas of the Southern Baltic Sea. Estuarine, Coastal and Shelf Science 47: 91–105.

Ferrari, G.M. 2000. The relationship between chromophoric dissolved organic matter and dissolved organic carbon in the European Atlantic coastal area and in the west Mediterranean Sea (Gulf of Lions). Marine Chemistry, 70: 339-357.

Gonsior, M., B.M. Peake, W.J. Cooper, R. Jaffe, H. Young, A.E. Kahn, P. Kowalczuk. 2008. Spectral characterization of chromophoric dissolved organic matter (CDOM) in a fjord (Doubtful Sound, New Zealand). Aquatic Sciences, doi: 10.1007/s00027-008-8067-4.

Green, S.A., and N.V. Blough. 1994. Optical absorption and fluorescence properties of chromophoric dissolved organic matter in natural waters. Limnology and Oceanography 39: 1903–1916.

Happ, G., J.G. Gosselink, J.W. Day Jr. 1977. The Seasonal Distribution of Organic Carbon in a Louisiana Estuary. Estuarine and Coastal Marine Science 5: 695-705.

Harvey, G.R., and D.A. Boran. 1985. The geochemistry of humic substances in seawater. In Humic substances in Soil, Sediment, and Water, eds. G.R. Aiken, D.M. McKnight, R.L. Wershaw, P. MacCarthy. 233-247. Wiley-Interscience.

Hatton, R.S., R.D. DeLaune, W.H. Patrick Jr. 1983. Sedimentation, accretion, and subsidence in marshes of Barataria Basin, Louisiana. Limnology and Oceanography 28(3): 494-502.

Hiriart-Baer, V.P., N. Diep, R.E.H. Smith. 2008. Dissolved Organic Matter in the Great Lakes: Role and Nature of Allochthonous Material. Journal of Great Lakes Research 34: 383-394.

Hoge, F.E., A. Vodacek, N.V. Blough. 1993. Inherent optical properties of the ocean: Retrieval of the absorption coefficient of chromophoric dissolved organic matter from fluorescence measurements. Limnology and Oceanography 38: 1394-1402.

Holbrook, R.D., J.H. Yen, T.J. Grizzard. 2006. Characterizing natural organic material from the Occoquan Watershed (Northern Virginia, US) using fluorescence spectroscopy and PARAFAC. Science of the Total Environment 361: 249-266.

Hong, H., J. Wu, S. Shang, C. Hu. 2005. Absorption and fluorescence of chromophoric dissolved organic matter in the Pearl River Estuary, South China. Marine Chemistry 97: 78–89.

Hopkinson, C.S., J.G. Gosselink, R.T. Parrando. 1978. Aboveground Production of Seven Marsh Plant Species in Coastal Louisiana. Ecology 59 (4): 760-769.

Hua, B, Dolan, F, McGhee, C, Clevenger, TE, Deng, B. Water-source characterization with fluorescence EEM spectroscopy: PARAFAC analysis. International Journal of Environmental Analytical Chemistry 2007; 87 (2): 135-147.

Inoue, M., D. Park, D. Justić, W.J. Wiseman Jr. 2008. A high-resolution integrated hydrology-hydrodynamic model of the Barataria Basin system. Environmental Modelling & Software 23: 1122-1132.

Jones, R.F., D.M. Baltz, R.L. Allen. 2002. Patterns of resource use by fishes and macroinvertebrates in Barataria Bay, Louisiana. Marine Ecology Progress Series 237: 271-289.

Kirby, C.J., and J.G. Gosselink. 1976. Primary Production in a Louisiana Golf Coast Spartina Alterniflora Marsh. Ecology 57 (5): 1052-1059.

Kirk, J.T.O. 1994. Light and Photosynthesis in Aquatic Ecosystems. Second Edition. Cambridge University Press, New York: 509 pp.

Komada, T., O.M.E. Schofield, C.E. Reimers. 2002. Fluorescence characteristics of organic matter released from coastal sediments during resuspension. Marine Chemistry 79: 81-97.

Kortelainen, P, Mattsson, T, Laubel, A, Evans, D, Cauwet, G, Räike, A. Sources of dissolved organic matter from land. In: Søndergaard, M, Thomas, DN [eds.] Dissolved Organic Matter (DOM) in Aquatic Ecosystems: A Study of European Catchments and Coastal Waters. A publication by the EU project DOMAINE (EVK3-CT-2000-00034) 2004; Chap. 2: 15-22.

Kowalczuk, P., J. Ston-Egiert, W.J. Cooper, R.F. Whitehead, M.J. Durako. 2005. Characterization of chromophoric dissolved organic matter (CDOM) in the Baltic Sea by excitation emission matrix fluorescence spectroscopy. Marine Chemistry 96: 273-292.

Kowalczuk, P., M.J. Durako, H. Young, A.E. Kahn, W.J. Cooper, M. Gonsior. 2009. Characterization of dissolved organic matter fluorescence in the South Atlantic Bight with use of PARAFAC model: Interannual variability. Marine Chemistry; doi: 10.1016/j/marchem.2009.01.015.

Lakowicz, J.R. 2006. Principles of Fluorescence Spectroscopy. Third Edition, pp 954. Printed in New York: Springer Publications.

Lochmuller, C.H., and S.S. Saavedra. 1986. Conformational changes in a soil fulvic acid measured by time dependent fluorescence depolarization. Analytical Chemistry 38: 1978-1981.

Luciani, X., S. Mounier, H.H.M. Paraquetti, R. Redon, Y. Lucas, A. Bois, L.D. Lacerda, M. Raynaud, M. Ripert. 2008. Tracing of dissolved organic matter from the SEPETIBA Bay (Brazil) by PARAFAC analysis of total luminescence matrices. Marine Environmental Research 65: 148-157.

Madden, C.J., J.W. Day Jr., J.M. Randall. 1988. Freshwater and marine coupling in estuaries of the Mississippi River deltaic plain. Limnology and Oceanography, 33(4, part 2): 982-1004.

Markager, S., and W.F. Vincent. 2000. Spectral light attenuation and the absorption of UV and blue light in natural waters. Limnology and Oceanography 45: 642-650.

McKnight, D.M., E.W. Boyer, P.K. Westerhoff, P.T. Doran, T. Kulbe, D.T. Andersen. 2001. Spectrofluorometric characterization of dissolved organic matter for indication of precursor organic material and aromaticity. Limnology and Oceanography 46 (1): 38-48.

Mossa, J. 1996. Sediment dynamics in the lowermost Mississippi River. Engineering Geology 45: 457-479.

Murphy, K.R., C.A. Stedmon, T. D. Waite, G.M. Ruiz. 2008. Distinguishing between terrestrial and autochthonous organic matter sources in marine environments using fluorescence spectroscopy. Marine Chemistry 108 1-2: 40-58.

Nieke, B., R. Reuter, R. Heuermann, H. Wang, M. Babin, J.C. Therriault. 1997. Light absorption and fluorescence properties of chromophoric dissolved organic matter (CDOM), in the St. Lawrence estuary (Case 2 waters). Continental Shelf Research 17: 235-252.

Nyman, J.A., R.D. DeLaune. 1991. Emission and Soil Eh Responses to Different Hydrological Conditions in Fresh, Brackish, and Saline Marsh Soils. Limnology and Oceanography 36 (7): 1406-1414.

Ohno, T. 2002. Fluorescence Inner-Filtering Correction for Determining the Humification Index of Dissolved Organic Matter. Environmental Science and Technology 36: 742-746.

Parlanti, E., K. Worz, L. Geoffroy, M. Lamotte. 2000. Dissolved organic matter fluorescence spectroscopy as a tool to estimate biological activity in a coastal zone submitted to anthropogenic inputs. Organic Geochemistry 31: 1765-1781.

Reddy, K.R., and R.D. DeLaune. 2008. Biogeochemistry of Wetlands: Science and Applications. Printed in New York, pp 806: CRC press.

Riu, J, and R. Bro. 2003. Jack-knife technique for outlier detection and estimation of standard error in PARAFAC models. Chemometrics and Intelligent Laboratory Systems 65 (1): 35-49.

Rochelle-Newall, E.J., and T.R. Fisher. 2002. Chromophoric dissolved organic matter and dissolved organic carbon in Chesapeake Bay. Marine Chemistry 77: 23– 41.

Sampere, TP, Bianchi, TS, Wakeham, SG, Allison, MA. Sources of organic matter in surface sediments of the Louisiana Continental margin: Effects of major depositional/transport pathways and Hurricane Ivan. Continental Shelf Research 2008; 28: 2472-2487.

Sasaki, H., T. Miyamura, S. Saitoh, J. Ishizaka. 2005. Seasonal variation of absorption by particles and colored dissolved organic matter (CDOM) in Funka Bay, southwestern Hokkaido, Japan. Estuarine, Coastal and Shelf Science 64: 447-458.

Sasser, C.E., M.D. Dozier, J.G. Gosselink, J.M. Hill. 1986. Spatial and Temporal Changes in Louisiana's Barataria Basin Marshes, 1945-1980. Environmental Management 10 (5): 671-680.

Shoaf, W.T., and B.W. Lium. 1976. Improved extraction of Chlorophyll a and b from algae using dimethyl sulfoxide. Limnology and Oceanography 21 (6): 926-928.

Sierra, M.M.D., M. Giovanela, E. Parlanti, E.J. Soriano-Sierra. 2005. Fluorescence fingerprint of fulvic and humic acids from varied origins as viewed by single-scan and excitation-emission matrix techniques. Chemosphere 58; 715-733.

Spencer, R.G.M., B.A. Pellerin, B.A. Bergamaschi, B.D. Downing, T.E.C. Kraus, D.R. Smart, R.A. Dahlgren, P.J. Hernes. 2007. Diurnal variability in riverine dissolved organic matter composition determined by in situ optical measurement in the San Joaquin River (California, USA). Hydrological Processes 21 (23): 3181-3189.

Stedmon, C.A., and S. Markager. 2003. Behaviour of the optical properties of coloured dissolved organic matter under conservative mixing. Estuarine, Coastal and Shelf Science 57: 973-979.

Stedmon, C.A., S. Markager, R. Bro. 2003. Tracing dissolved organic matter in aquatic environments using a new approach to fluorescence spectroscopy. Marine Chemistry 82: 239-254.

Stedmon, C.A., and S. Markager. 2005a. Resolving the variability in dissolved organic matter fluorescence in a temperate estuary and its catchment using PARAFAC analysis. Limnology and Oceanography 50 (2): 686-697.

Stedmon, C.A., and S. Markager. 2005b. Tracing the production and degradation of autochthonous fractions of dissolved organic matter using fluorescence analysis. Limnology and Oceanography 50 (5): 1415-1426.

Stedmon, CA, Markager, S, Søndergaard, M, Vang, T, Laubel, A, Borch, NH, Windelin, A. 2006. Dissolved Organic Matter (DOM) Export to a Temperate Estuary: Seasonal Variations and Implications of Land Use. Estuaries and Coasts 29 (3): 388-400.

Stedmon, C.A., D.N. Thomas, M. Granskog, H. Kaartokallio, S. Papadimitriou, H. Kuosa. 2007. Characteristics of Dissolved Organic Matter in Baltic Coastal Sea ice: Allochthonoous or Autochthonous Origins ?. Environmental Science and Technology 41: 7273-7279.

Stedmon, C.A., and R. Bro. 2008. Characterizing dissolved organic matter fluorescence with parallel factor analysis: a tutorial. Limnology and Oceanography: Methods 6: 572-579.

Swenson, E.M., J.E. Cable, B. Fry, D. Justić, A. Das, G. Snedden, C. Swarzenski. 2006. Estuarine Flushing Times Influenced by Freshwater Diversions. In Coastal Hydrology and Process,eds. V.P. Singh and Y.J. Xu, 403-412. CO, USA: Water Resource Publications.

Tzortziou, M., C.L. Osburn, P.J. Neale. 2007. Photobleaching of Dissolved Organic Material from a Tidal March-Estuarine System of the Chesapeake Bay. Photochemistry and Photobiology 83: 782-792.

Tzortziou, M., P.J. Neale, C.L. Osburn, J.P. Megonigal, N. Maie, R. Jaffé. 2008. Tidal marshes as a source of optically and chemically distinctive colored dissolved organic matter in the Chesapeake Bay. Limnology and Oceanography 53 (1): 148-159.

Uher, G., C. Hughes, G. Henry, R.C. Upstill-Goddard. 2001. Non-conservative mixing behavior of colored dissolved organic matter in a humic-rich, turbid estuary. Geophysical Research Letters 28 (17): 3309-3312.

Vodacek, A., N.V. Blough, M.D. DeGrandpre, E.T. Peltzer, R.K. Nelson. 1997. Seasonal Variation of CDOM and DOC in the Middle Atlantic Bight: Terrestrial Inputs and Photooxidation. Limnology and Oceanography 42 (4). 674-686.

Wedborg, M., T. Persson, T. Larsson. 2007. On the distribution of UV-blue fluorescent organic matter in the Southern Ocean. Deep-Sea Research I 54: 1957-1971.

Wissel, B., A. Gace, B. Fry. 2005. Tracing River Influences on Phytoplankton Dynamics in Two Louisiana Estuaries. Ecology 86 (10): 2751-2762.

Yamashita, Y., R. Jaffé, N. Maie, E. Tanoue. 2008. Assessing the dynamics of dissolved organic matter (DOM) in coastal environments by excitation emission matrix fluorescence and parallel factor analysis (EEM-PARAFAC). Limnology and Oceanography 53 (5): 1900-1908.

Zepp, R.G., W.M. Sheldon, M.A. Moran. 2004. Dissolved organic fluorophores in southeastern US coastal waters: correction method for eliminating Rayleigh and Raman scattering peaks in excitation–emission matrices. Marine Chemistry 89: 15–36.

Zhang, Y., B. Quin, G. Zhu, L. Zhang, L. Yang. 2007. Chromophoric dissolved organic matter (CDOM) absorption characteristics in relation to fluorescence in Lake Taihu, China, a large shallow subtropical lake. Hydrobiologia 581: 43–52.

Zhi-gang, W., L. Wen-qing, Z. Nan-jing, L. Hong-bin, Z. Yu-jun, S. Wei-cang, L. Jian-guo. 2007. Compositional analysis of colored dissolved organic matter in Taihu Lake based on three dimension excitation-emission fluorescence matrix and PARAFAC model, and the potential application in water quality monitoring. Journal of Environmental Sciences 19: 787-791.

Zsolnay, A., E. Baigar, M. Jimenez, B. Steinweg, F. Saccomandi. 1999. Differentiating with fluorescence spectroscopy the sources of dissolved organic matter in soils subjected to drying. Chemosphere 38 (1): 45-50.

Appendix: Acronyms

a_{CDOM}: Absorption Coefficient of CDOM
CDOM: Chromophoric Dissolved Organic Matter
Chl-*a*: Chlorophyll-*a*
DOM: Dissolved Organic Matter
F_{CDOM}: Fluorescent Portion of CDOM
FI: Fluorescence Index
HIX: Humification Index
Insolation: Incoming Solar Radiation
nm: Nanometers
RU: Raman Units
S: Spectral Slope Coefficients
TOC: Total Organic Carbon
UV: Ultraviolet (radiations)
[UVA: Ranges from 315-400 nm
UVB: Ranges from 280-315 nm
UVC: Ranges from 200-280 nm]
λ: Wavelength

Vita

Shatrughan Singh was born in November, 1980, in Deoria, India. He was brought up in Allahabad, a holy city in India. After completing his formal school, he joined the University of Allahabad, India, in 1999 for his under graduation of three years to obtain a Bachelor in Science degree. In 2002, after completing his undergraduate degree, he was accepted into the graduate school of the prestigious Banaras Hindu University, Varanasi, India, for Master of Science (Technology) degree in geophysics with specialization in meteorology which he completed in 2005. He then joined Indian Institute of Technology, Kanpur, India, as a Research Associate in the Department of Civil Engineering and served there for one and half years before joining Louisiana State University, USA in Spring, 2007. Presently, he is a candidate for the degree of Master in Science in the Department of Oceanography and Coastal Sciences, Louisiana State University, Louisiana, USA. His career interests lie in using absorption and fluorescence spectroscopy coupled with mathematical skills (or statistical analyses techniques) to monitor water quality and help in managing better environmental practices to reduce negative human induced impacts on the environment.